Université de Lille 1 SCIENCES ET TECHNOLOGIES

THESIS

Université des Sciences et Technologies de Lille

For obtaining a title of

DOCTOR IN CHEMISTRY

Spécialité: Molécule et Matière Condensée

by

Mengdie Cai

Design of novel hybrid catalysts for direct synthesis of Dimethyl ether from syngas

The thesis will be defended publicly on the 09th of October, 2015

Reviewers

Dr Cuong Pham Huu, ICPEES, University of Strasbourg

Dr Valentin Valtchev, LCS, ENSICAEN

Members

Prof. Guy Marin, University of Gent, Belgium

Dr Ekkehard Schwab, BASF, Germany

Prof. Ovidiu Ersen, IPCMS, University of Strasbourg

Director

Dr Andrei Khodakov, UCCS, EC Lille, ENSCL, University Lille 1

Co-director

Dr Vitaly Ordomsky, UCCS, EC Lille, ENSCL, University Lille 1

Contents

Contents

Contents

Contents

Abstract

Dimethyl ether (DME) has been receiving great attention as an environment-friendly clean alternative fuel due to its low NO_x, SO_x emission, good burning characteristics and high cetane number. Two possible pathways have been proposed for DME production. One of these routes is DME synthesis through dehydration of methanol, which is produced from syngas by methanol synthesis in a separate reactor. Another route is direct DME synthesis from syngas in one single step, which can break the thermodynamic limitation on the overall CO conversion. Consequently, the CO conversion in the direct DME synthesis can be significantly higher than that of the two-steps process. Bi-functional catalysts composed of metallic function for methanol synthesis and acidic function for methanol dehydration are required for direct DME synthesis from synthesis gas.

In the first part of this thesis, conventional bi-functional catalyst Cu–ZnO–Al_2O_3/ZSM-5 was prepared by physical mixing method and its activity was tested in the fixed bed reactor for DME synthesis at different composition and reaction conditions. The results showed that the acid property of the dehydration component plays a crucial role in determining the overall CO conversion rate, DME selectivity, and catalyst durability. The presence of strong acid sites in HZSM-5 zeolite is the reason of lower selectivity to DME due to the production of hydrocarbons.

In chapter 4, direct synthesis of dimethyl ether (DME) from syngas was investigated on a series of hybrid Cu–ZnO–Al_2O_3/ZSM-5 catalysts with different zeolite crystallite sizes and Si/Al ratio. The activity of the hybrid catalysts gradually decreased with time on stream because of simultaneous copper sintering, copper oxidation and ion exchange with zeolite hydroxyl groups. This process can be suppressed by selective neutralisation of the acid sites on the external surface of zeolite by silylation. Both catalyst stability and dimethyl ether productivity were significantly improved after the TEOS modification.

The effects of crystal size and mesoporosity on the performance of various synthesized ZSM-5 zeolites in dimethyl ether synthesis from syngas have been investigated in chapter 5. The relationship between zeolite particle size, acidity and catalytic performance of the bi-functional catalysts in DME synthesis has been studied. The reaction rate in direct DME synthesis is strongly affected by the sizes of zeolite particles. The bi-functional catalysts containing small individual zeolite crystallites (60-100 nm) were more active in dimethyl

ether synthesis than the counterparts containing micron-sized zeolite crystal agglomerates. Moreover, the catalyst deactivation was related to the acid sites on the external surface of zeolites. It is established that the catalyst deactivation is less significant with the catalysts containing ZSM-5 zeolites with lower concentration of acid sites on the zeolite external surface.

CO_2 is the major byproduct formed by water gas shift reaction in direct DME synthesis. Tin-promoted bi-functional Cu-Zn-Al/HZSM-5 catalysts were prepared in chapter 6 to suppress WGS reaction with the increase in the selectivity to dimethyl ether. The characterization revealed that the electronic properties and surface distribution of Cu in the catalysts were significantly changed by tin addition leading to the decrease in the fraction of positively charged Cu sites. Addition of tin suppressed the water gas shift reaction and decreased the selectivity to undesired CO_2. As a result, the selectivity to valuable DME and methanol noticeably increased over mildly promoted catalysts. Further increase in Sn loading led to the decrease in the rate of carbon monoxide conversion.

Keywords: Bifunctional Catalyst, DME, Synthesis Gas, Direct Synthesis; Deactivation, Silylation, Tin effect, Crystal size

Chapter1. Literature Review

1.1 General Introduction

The energy is of utmost importance for the development of modern society. There are two sources of energy [1]: renewable (such as solar, wind, geothermal and hydropower) and nonrenewable energy (such as fossil fuels; coal, natural gas, oil) (Figure 1-1). The current demand of energy is almost completely fulfilled by fossil fuels, especially oil based liquid fuels, which is limited i.e. not renewable on the human time scale [2]. The fossil resoures are the major source to fulfill the current energy needs through their diversity [3]: petrol, diesel (for transportation), liquefied petroleum gas (for cooking and heating) and several key building block chemicals for industry such as ethylene, propylene and butylene (obtained via steam cracking).

Growing demand for fuels and value added chemicals need to be addressed as there is a drastic depletion of oil resources and sever environmental concerns related to that, such as the massive carbon dioxide emission, caused to the global warming [4]. Hence, there is an immense need to find an alternate to the oil based fuels.

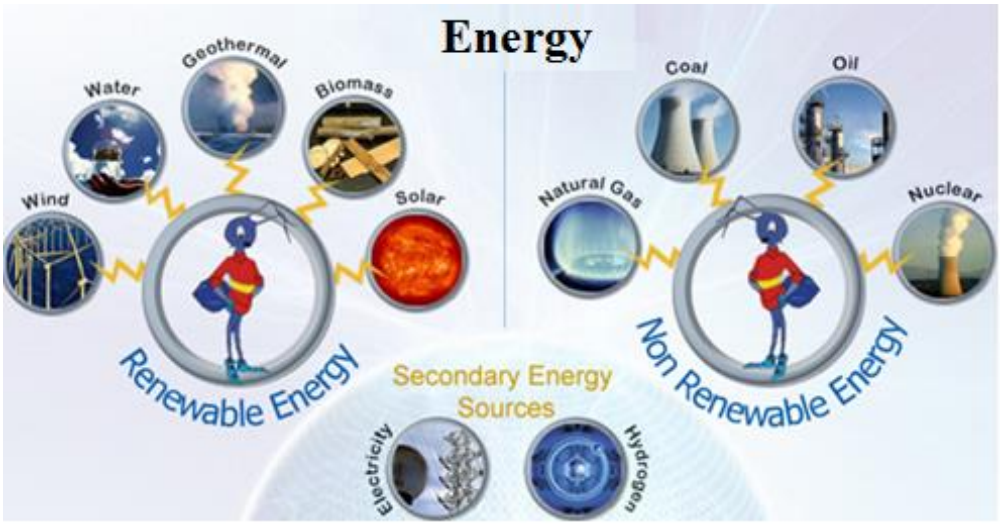

Figure 1-1. Types of energy

A great deal of research is being conducted to meet the rising demand for energy by developing new and more sustainable technologies that use available raw materials like coal, natural gas or biomass instead of petroleum [3, 5-8]. Synthesis gas [8], can be produced from

these potential energy source (like coal, natural gas, biomass and even municipal waste). It is a versatile intermediate for production of chemicals and fuels. Moreover it is considered to be a practical way of utilizing vast available sources since as such the direct conversion of aforesaid sources into fuels and value added chemicals are not practically feasible [9, 10]. Well-known examples of technologies that convert synthesis gas to liquid fuel are the Fisher-Tropsch synthesis [9] and methanol synthesis processes [11]. These technologies produce fuel containing fewer pollutants than that obtained from the traditional methods using petroleum. This is an advantage, because the 'cleaner' the fuel is, the less damage it can do to the environment. Another key issue to be addressed considering the alternate fuel is the usage of existing infrastructure, which includes transportation, storage, handling and distribution. This is rather important to meet the economic viability. Among the alternate fuels, dimethyl ether (DME) can be considered as one of potential candidate.

1.2 Dimethyl ether (DME) as an alternative fuel

1.2.1 Physical properties of DME

Dimethyl ether, also known as methoxy methane, having a chemical formula of CH_3OCH_3, without a C−C bond, is the simplest ether. DME is in the gaseous form at standard temperature and pressure and can be liquefied at 6 atm or -25 ^oC, which allows its storage and transportation just like LPG, with small changes in the current LPG storage and distribution technologies. DME is a volatile organic compound. Unlike petroleum based fuels, DME is non-carcinogenic, non-teratogenic, non-mutagenic, and non-toxic.

The potentiality of DME lies on its comparable physical properties with those of petroleum based fuels (e.g. LPG; propane and butane). The physical properties of DME and other commonly used fuels are given in table 1-1. DME has a high cetane number (around 60), which indicates the combustion quality of a diesel fuel, higher than diesel oil and other alternative fuels. Ignition point of DME is also very close to the ignition point of diesel fuel. Herein, high cetane number, low boiling point of DME (-25 ^oC) and high oxygen content (35 wt.%) are important fuel characteristics allowing fast vaporization and smokeless operation. This property makes DME so attractive for compression ignition engines.

Table 1-1. Comparison of Dimethyl Ether and Other Alternative Fuels' Physical Properties

Properties	DME	Methanol	Ethanol	Propane	Butane	Gasoline	Diesel
Formula	**CH_3OCH_3**	CH_3OH	C_2H_5OH	C_3H_8	C_4H_{10}	-	-
Molecular weight, g/mol	**46**	32	46	44	58	-	-
Liquid density, g/cm^3	**0.67**	0.79	0.79	0.49	0.57	0.73-0.76	0.86
Cetane number	**55-60**	5	40,50	5	10	5-20	40-55
Boiling point, ℃	**-24.9**	64	78	-42	-0.5	38-204	125-400
LHV (kJ g^{-1})	**28.62**	19.99	26.87	46.35	45.75	43.47	41.66
Cetane number	**55-60**	5	8	5	10	5-20	40-55
Sulfur content, ppm	**0**	0	0	-	-	~200	~250
Carbon Content, wt.%	**30.8**	37.5	29.4	81.8	82.8	85.5	87

1.2.2 Applications of DME:

Dimethyl ether can be synthesized from a variety of feed-stock including natural gas, coal, biomass, crude oil and waste products and it can be used for various important commercial applications (Figure 1-2) due to its suitable physicochemical properties and benefits (see Table 1-2).

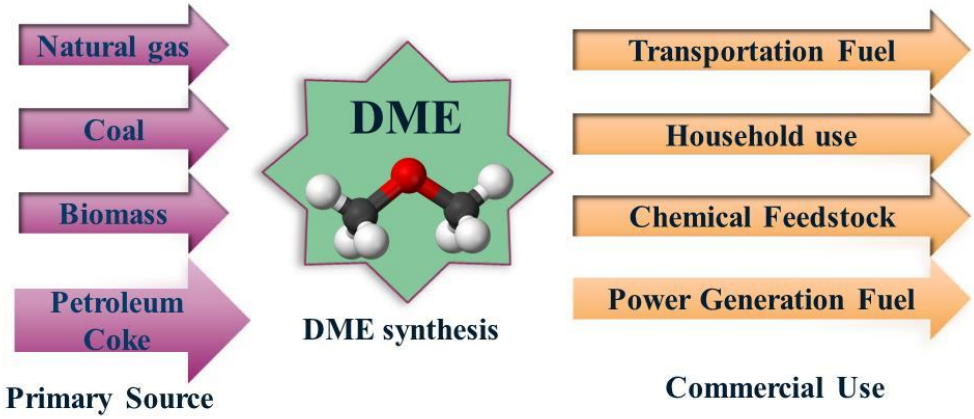

Figure 1-2. Schema of Dimethyl ether as an energy carrier for a sustainable development

Table 1-2. DME properties and benefits

Liquefies at -25℃ or under 6 atmospheres	▶	Can be stored and transported just like LPG
Higher cetane number than diesel	▶	Can be used in diesel engines
Completely safe with no adverse impact on health Hazard equivalent to LPG	▶	No problems expanding use
Decomposes in the atmosphere in several ten of hours	▶	No concern over ozone layer depletion (alternative to CFCs)
No sulfur content No direct carbon bonds (CH_3-O-CH_3)	▶	No particulate matter (PM) or soot emission from combustion
Lower temperature catalytic reforming than gasoline	▶	Better fuel for fuel cells

Transportation fuel

DME has very promising uses as an ultra-clean transportation fuel to replace diesel, for its usability in compression ignition engines and its liquefaction characteristics (i.e., DME liquefies easily at relatively low pressures) which makes the handling and loading of fuel into vehicles easy, with the absence of sulfur and black smoke generation. DME engine development and DME vehicle development have been completed, and the durability of DME vehicle was confirmed by road running test for 100,000 km or longer. Moreover, a technical development of DME filling equipment to DME vehicle has been completed, too. Serious efforts in these areas are seen in Japan, Europe and China.

The Japanese performed a number of tests of DME for transportation from 2003 to 2007 with 4 DME filling stations. At this period, they made 1,000 km with DME-fueled trucks. From 2009, they manufactured DME trucks for commercial uses. A representative DME production plant (Mitsubishi Gas Chemical's) is shown in Figure 1-3 (a). The Volvo Group was the first truck manufacturer in Europe to test BioDME as a vehicle fuel on a large scale. The tests show that BioDME trucks function very well on the road, the technology is reliable and the entire process is energy efficient, from production and distribution all the way to the vehicles themselves. In 2013, Volvo has conducted extensive customer field tests of the DME-powered trucks in real-world applications, both in the U.S. and in Europe, resulting in 650,000 on-highway miles. (Figure 1-3 (b)). First DME bus developed in 2005 in China. DME fuel stations for powering taxis and buses are successfully tested and implemented in China (Figure 1-3 (c)).

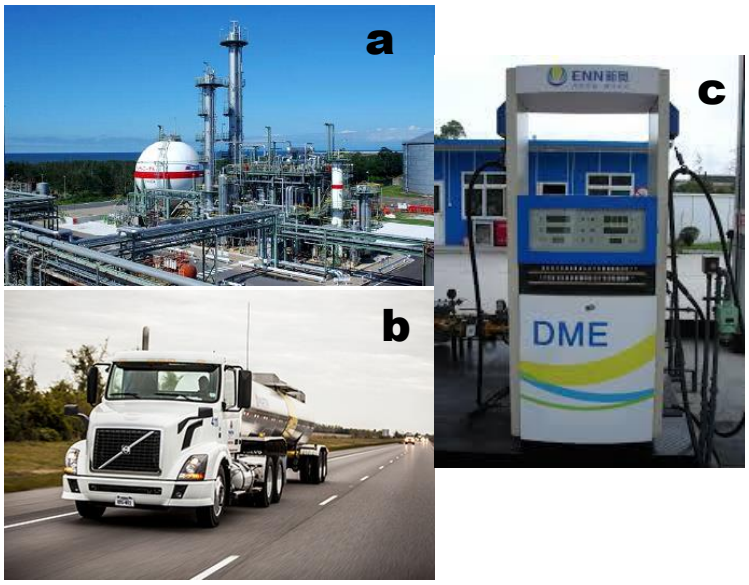

Figure 1-3. Representative images of (a) DME production plant, (b) DME powered Volvo truck and (c) DME fuel station in China.

Household use fuel

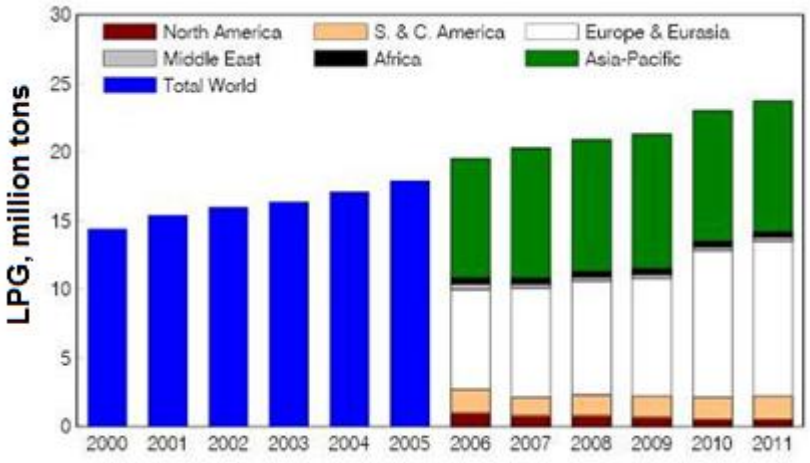

Figure 1-4. Increasing global demand of LPG consumption.

Petroleum based gas, LPG (propane and butane) is widely used for household applications such as cooking and heating. The consumption rapidly increases every year worldwide as depicted in Figure 1-4. The value-added DME has almost similar physicochemical properties of LPG and could potentially occupy the household applications. The largest market for DME is Asia where the capacity has steadily increased and will continue to grow with new plants constructed for the domestic fuel market.China has developed a large DME production base, which reportedly amounts to almost 9 million tons per annum in installed DME capacity.

Power generation fuel

DME can be also used as a boiler fuel and a gas turbine fuel. It was confirmed by demonstration tests that a thermal efficiency and an environmental characteristic of existing equipment with DME are similar to those with the natural gas. A large-scale diesel engine test with DME for power generation was executed. DME is reformed with steam at relatively lower temperature than natural gas and LPG, etc. and has some advantage on heat balance, therefore DME is a promising fuel for the fuel cell. Moreover, a compact reforming device has been developed for the fuel-cell car.

Chemical feedstock

The potential candidate DME can be employed as an useful intermediate to get many value-added chemicals as shown in the Figure 1-5. A technology producing lower olefins from DME has been developed as DMETO process. It is expected that the production cost is reduced compared with producing from the petroleum naphtha of which the price has soared. Methyl acetate produced by DME carbonylation is favorable from economic, safety and process engineering standpoints. It can be further carbonylated to acetic anhydride, which can be converted to acetic acid, a highly valuable chemical for the production of other petrochemicals. Methyl acetate may also be converted to ethylidene diacetate (EDA), a precursor to vinyl acetate and polyvinyl acetate. Dimethyl sulfate is an important commercial commodity as a solvent and also as an electrolyte in high energy density batteries.

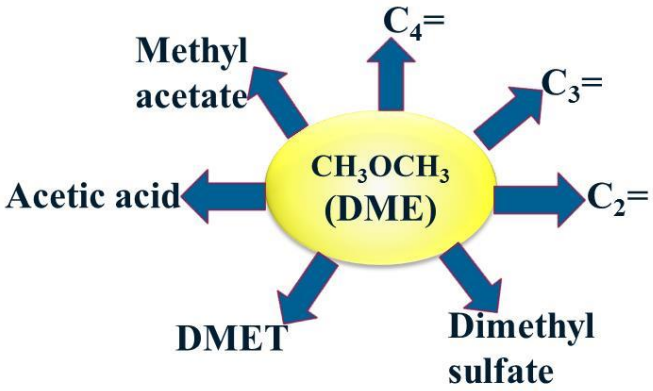

Figure 1-5. Schematic of Dimethyl ether as an intermediate for value-added products

As mentioned, DME can be used as liquefied petroleum gas (LPG) for heating and home cooking [12], transportation fuel [13] (diesel vehicles, fuel cell vehicles), power plant fuel (thermal plants, cogeneration plants, stationary fuel cells), and as a raw material for chemical products such as olefins [14]. The properties of DME, including a high oxygen

content, extremely low content of sulfur or other noxious compounds, and ultra clean combustion make DME a versatile and promising solution for manuufacturing of clean renewable and low-carbon fuels and chemicals worldwide.

1.3 Synthesis methods of Dimethyl ether (DME)

1.3.1 Routes of DME synthesis

The DME can be efficiently synthesized from various energy sources: natural gas, coal, biomass and even municipal waste. Two processes have been claimed so far for the production of DME (Figure 1-6) [15, 16]. The first one is the conventional two-step process of DME synthesis in which methanol is synthesized from synthesis gas, followed by methanol dehydration to DME at different reactor. This process is known as "indirect synthesis". The second way is dimethyl ether synthesis directly from synthesis gases (CO, CO_2 and H_2) which is also named as "direct synthesis". It has a higher economic value because of reducing the thermodynamic limitations applicable to methanol synthesis.

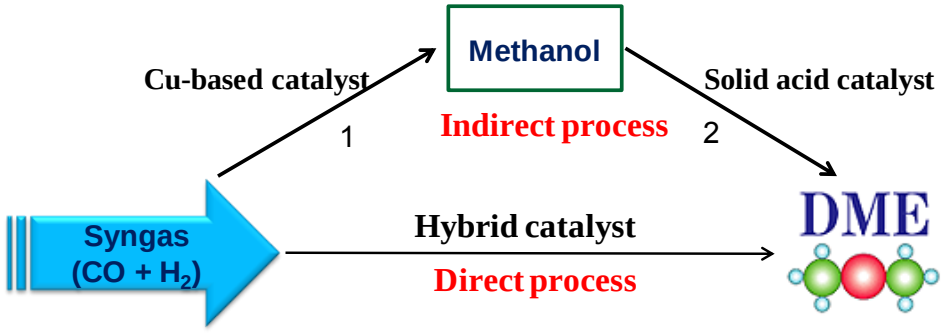

Figure 1-6. Dimethyl ether production diagram

The equilibrium conversions of syngas in methanol synthesis and direct DME synthesis reactions are compared in Figure 1-7 [20]. The direct DME synthesis has very high syngas conversion compared to the methanol synthesis. The ultimate result is economic viability by reducing the overall production cost (direct DME synthesis) and it is estimated as about two-thirds of the cost of DME production by the methanol dehydration process (two steps process) [6].

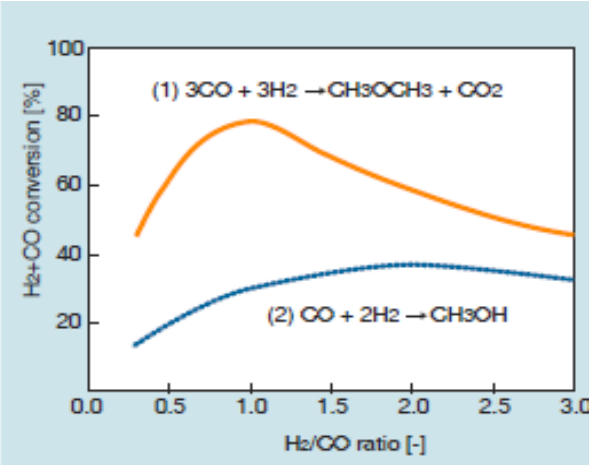

Figure 1-7. Equilibrium conversion of synthesis gas (280 ^{o}C, 5 MPa) [20]

1.3.1.1 Indirect synthesis of Dimethyl ether

Synthesis of DME by dehydration of methanol over several solid acid catalysts is the traditional route for DME synthesis. This route needs two sequential reactors; the first reactor is for methanol formation and the second reactor is for dehydration of methanol. The commercialized process reaction of DME production from methanol dehydration is shown in equation. (1):

$$2CH_3OH \rightarrow CH_3OCH_3 + H_2O \qquad \Delta H = -23.5\ kJ/mol \qquad (1)$$

Many investigations on the kinetics of DME synthesis by dehydration of methanol on solid-acid catalysts have been published. The majority of them agree that the mechanism follows the Langmuir–Hinshelwood [17] reaction mechanism, in which one methanol molecule adsorbs on a Brönsted acid site and another methanol molecule adsorbs at adjacent Lewis basic sites with formation of the two surface species $[CH_3OH_2]^+$ and $[CH_3O]^-$ which give DME and water during condensation [17, 18]. The proposed mechanism contains the following reaction steps and the reaction (5) is considering as the rate limiting step.

$$CH_3OH + H^+ \leftrightarrow [CH_3OH_2]^+ \qquad (2)$$

$$CH_3O\text{-}H + O^{2-} \leftrightarrow [CH_3O]^- + [OH]^+ \qquad (3)$$

$$[CH_3OH_2]^+ \leftrightarrow [CH_3] + + H_2O \qquad (4)$$

$$[CH_3]^+ + [CH_3O]^- \leftrightarrow CH_3OCH_3 \qquad (5)$$

Methanol dehydration to DME reaction occurs easily over solid acid catalyst at relatively low temperature ranges between 250 - 300 ^{o}C in vapor phase. The reaction is pressure insensitive [19]. Theoretically, methanol dehydration is favored at lower temperatures because it is an exothermic reaction and the formation of by-products such as olefins, and coke is significant at higher temperatures.

1.3.1.2 Direct synthesis of Dimethyl ether from syngas

Direct synthesis of DME from syngas involves the catalytic synthesis of methanol and in-situ dehydration to yield DME. The reaction proceeds in a single reactor. A combined one-step or direct DME synthesis has been recently developed [6, 16, 19]. The main advantage of direct DME synthesis is mitigating the thermodynamic limitation, which normally restricts CO conversion to methanol in indirect synthesis.

The direct syngas to DME (STD) process is composed of three reaction steps: hydrogenation of CO to methanol, methanol dehydration to DME, and water-gas-shift reaction (WGSR). The reactions proceed according to the chemical equations (6)-(8) as shown below:

$2\ CO + 4\ H_2 = 2\ CH_3OH \quad \triangle H = -182\ kJ$ (6)

$2CH_3OH = CH_3OCH_3 + H_2O \quad \triangle H = -23\ kJ$ (7)

$H_2O + CO = H_2 + CO_2 \quad \triangle H = -41\ kJ$ (8)

The combination of reactions (6)–(8) gives the overall reaction:

$3CO + 3H_2 = CH_3OCH_3 + CO_2 \quad \triangle H = -246\ kJ$ (9)

In the direct STD process, methanol formed by reaction (6) is consumed in the formation of DME and water in reaction (7). The water generated in reaction (7) can react with CO in the WGS reaction (8), forming carbon dioxide and hydrogen; the latter is a reactant for the methanol synthesis in reaction (6). Thus, one of the products of each step is a reactant for another. This creates a strong driving force for the overall reaction, allowing a very high syngas conversion in a single pass as a result of favorable thermodynamics. Besides that, the investment is relatively lower than the two-step reaction.

Typical reaction conditions of direct DME synthesis are listed in Table 1-3 [21]. Direct dimethyl ether synthesis reactors usually operate at a temperature range of 240 °C - 280 °C, a pressure range of 30 – 80 bar and the feed ratio of H_2/CO is 0.5-2.0.

Table 1-3. Reaction conditions of direct DME synthesis [21]

Reaction Conditions	
Temperature (℃)	240-280
Pressure (bar)	30-80
Feed (H_2 / CO) ratio	0.5-2.0
Catalyst loading ratio (W/F) [kg-cat.*h/ kg•mol]	3.0-8.0

1.4 Catalyst for Dimethyl ether synthesis from syngas

For Dimethyl ether (DME) synthesis either through a conventional two steps process or through direct DME synthesis. The ultimate goal is design the catalysts having better selectivity, stability and activity. As discussed earlier, the overall DME synthesis process is comprised of two key reactions: methanol synthesis and methanol dehydration. Both are catalytically driven reaction with different catalytic systems. For example, traditionally, $CuO\text{-}ZnO\text{-}Al_2O_3$ catalyst is deployed for methanol synthesis [22-25]. Likewise, a solid acid catalyst such as $\gamma\text{-}Al_2O_3$ [26-29], various zeolites [17, 30-34], and silica-alumina composite oxides [35, 36] are well known for dehydration of methanol to DME. On other hand, catalysts for the direct DME synthesis are bi-functional catalysts composed of a metallic function for methanol synthesis and a solid acid function for the methanol dehydration into DME. On both directions, extensive research has been deployed in designing active, selective and stable catalysts.

1.4.1 Catalyst for methanol synthesis from syngas

Methanol is an important industrial commodity. Methanol synthesis can be carried out via two different processes (Table 1-4). The first one is methanol synthesis through high-pressure operation, proposed by BASF [37, 38]. Operating parameters were in the range of 250 bar - 350 bar and 320 ℃ - 450 ℃. The catalyst was highly poison resistant, $ZnO\text{-}Cr_2O_3$ and this high pressure process was used for 45 years from the synthesis gas, which was obtained by German low quality coal/lignite.

Table 1-4. Catalyst type and operation condition for methanol synthesis

	Process	Catalyst	Pressure (bar)	Temperature(^oC)
BASF	High-pressure process	ZnO/Cr_2O_3	250-350	320-450
ICI	Low-pressure process	$Cu/ZnO/Al_2O_3$	50-100	200-300

In the 1960s, Imperial Chemical Industries (ICI) was used copper-based catalysts in methanol synthesis with Zn promoter, one of the roles of the promoter was to enhance the dispersion of copper and prevent agglomeration of it. By this catalyst, operating pressure was dropped to 50 bar - 100 bar, which is known as low-pressure process [39, 40]. The almost exclusively used methanol synthesis technology is the low-pressure, low-temperature process using the Cu-ZnO based catalyst.

The conversion of syngas to methanol over Cu-ZnO based catalyst is dependent upon the copper metal surface area and copper dispersion [22, 24, 41]. Copper particle size and its dispersion are found to be affected by preparation conditions such as Cu/Zn molar ratio, type of precipitant, the promoter (like Mn [22], Zr [42] and Pd [43].etc) and calcination temperature [24]. Especially, the importances of the palladium incorporated to the base Cu-ZnO catalyst in increasing the catalytic activity and stability are the spillover effect of hydrogen and the enhancement of CuO reduction. Hydrogen is dissociated on the Pd particles and then spilt over the Cu-ZnO phase of the base catalyst.

Supported palladium (Pd) catalysts have also demonstrated methanol synthesis activity, and that the nature of the support has a great influence on both the rate and selectivity of catalyst. As a major product, Pd/Al_2O_3 produces dimethyl ether, Pd/SiO_2 favors methanol formation, Pd/TiO_2 produces CH_4, and Pd/ZrO_2 yields methanol at 523 K and 20 bar. Higher CO conversions over Pd/ZrO_2 and Pd/TiO_2 were ascribed to the presence of cationic palladium species formed through the metal–support interaction [44].

Palladium supported on ceria has also been reported to be a good catalyst for methanol synthesis from CO hydrogenation due to the strong interaction between palladium and ceria. Tsubaki et al. [45] reported the promotional strong metal–support interaction (SMSI) effect on high-temperature-reduced Pd/CeO_2 catalysts for methanol synthesis. The SMSI effect improved remarkably the activity and selectivity of methanol synthesis from hydrogenation of carbon dioxide. By reduction at 773 K, the conversion at 503 K and 3 MPa with H_2/CO = 2 dropped to half of that at 673 K and, in addition to methane, significant amounts of higher hydrocarbons were formed.

Shen et al. [46] inverstigated the effect of palladium precursors on the catalytic performance of Pd/CeO_2 catalysts for methanol synthesis through hydrogenation of carbon monoxide. The palladium precursor, or more specifically its anion, had an effect on the final palladium particles, and therefore affected the interaction between Pd and ceria, which would cause different reaction results. Catalysts prepared from palladium chloride and palladium acetate showed much higher overall catalytic activities than those prepared using palladium nitrate.

For the methanol synthesis, the $CuO-ZnO-Al_2O_3$ catalyst is the optimal methanol synthesis catalyst. Since the methanol synthesis over Cu-based catalyst is a very established and quite optimized technology, much of the efforts in the research concerning DME synthesis have been devoted to the study of the methanol dehydration catalyst.

1.4.2 Catalyst for methanol dehydration

Solid acid type catalysts are responsible for the dehydration of methanol in vapor phase to DME by so called methanol to DME (MTD) process. Typical solid acids deployed in MTD are conventional γ-Al_2O_3 [26-29], acidic zeolite (HZSM-5 [30, 31], HY [47], FER [32], and H-SAPO [33], etc), heteropolyacid [48], and composite oxides (SiO_2−Al_2O_3 [36]; ZrO_2−TiO_2). Among this, generally, owing to low cost, favorable acidity and high mechanical resistance, γ-Al_2O_3 is the most commonly used catalyst. Considerable attention has been paid to improve the performance of methanol dehydration to DME on conventional γ- Al_2O_3 by optimizing the textural properties of Al_2O_3 or its modification with another oxide. For example, Chang et al. [29] studied the influence of Al_2O_3 structure on dehydration of methanol. Their studies showed η - Al_2O_3 exhibited better catalytic activity than γ- Al_2O_3. Larger number of active sites and enhancement in surface area were successfully achieved by promoting γ- Al_2O_3 with Nb_2O_5. The modified catalysts showed higher activity in the low temperature region when compared to unmodified γ- Al_2O_3 [49]. Kenan et al [50] explored different alumina based catalysts. When compared to commercial alumina catalysts, alumina impregnated SBA-15 possessed higher Brönsted acidity and facilitated the catalytic performance.

The performance of γ-alumina and aluminium phosphate modified catalysts was compared by Yaripour et al. [51]. The phosphate modified catalyst, with molar ratio of Al/P=1.5 exhibited better activity for methanol dehydration with almost 100 % DME selectivity and ~80 % conversion at reaction condition of 300 ℃ and 16 bar. In another studies [27], they reported enhancement in surface acidity in silica modified alumina as a function of silica content with a maximum at silica loading of 6 wt. %. Apart from better catalytic activity no by-product formed in the final product. In addition of the modification of γ- Al_2O_3, the effect of crystal size on the catalytic activity was explored by Hosseini et al. [52]. The results showed that samples with smaller crystallite size possessed higher concentration of medium acidic sites and responsible for higher catalytic activity, in terms of dehydration of methanol to DME.

Recently, ordered mesoporous materials as solid acid catalysts were used for various reactions because of their high surface areas, regular frameworks, and large pore size. According to the work of Sabour et al. [53], in the Al-HMS materials, Al incorporation into HMS framework enhanced number of surface acid sites as well as acidity strength, causing the increase in the methanol accessibility to active sites, and consequently enhanced the

catalyst activity with optimum yield of 89 % with 100 % selectivity and excellent stability of Al-HMS-10 catalyst.

The methanol dehydration reaction is performed at 300 – 350 ℃ and 10 – 20 bar [49-51] over an alumina based catalyst. One of major problem on methanol dehydration with γ-Al_2O_3 is rapid and irreversible deactivation [26]. Insufficient stability of alumina-based catalyst has motivated the research towards search and implementation of other solid acid catalysts such as zeolites, especially HZSM-5 owing to its hydrophobic character and abundant Brönsted-type acidity [54]. Zeolites also exhibit much higher activity and stability during the methanol dehydration reaction [30, 31].

It is widely accepted that DME synthesis occurs preferably on the weak and moderated acidic sites of solid acid catalyst [19, 27, 35]. Based on the research, it can be concluded that if the acidic sites are too weak, the dehydration rate will be suppressed. In another case, where if the acid strength is more than required, then the reaction will result in formation of by-products (hydrocarbons) and coke deposition and catalyst deactivation [33]. The latter case is more prone to zeolites based solid acid due to very high acidic strength. Hence, it is highly important to control the acidity of zeolites based solid acid catalysts before employing as methanol dehydration catalyst. Normally it has been achieved by adjusting and modifying the acidity of zeolite. The techniques involve diluting the strong acid sites by embedding other elements (such as alkali metals or rare earth metals) or optimizing the preparation method of zeolite to get the zeolite with suitable Si/Al ratio, hierarchical structure and small crystal size.

This phenomenon can be controlled by employing a suitable concentration of Na in the zeolite in order to moderate the number of Brönsted sites and to reduce the acid strength of the H-ZSM-5 zeolite. Ying et al [55] studied the alkaline treated ZSM-5 with different Si/Al ratio as a dehydration component. The alkaline treatment combined with partial activation created extra mesoporosity, moderated the acidity and improved diffusion capability of the HZSM-5. Thus, the alkain-treated catalyst exhibited improved catalytic performance with almost 100% DME selectivity, near 84 % methanol conversion and excellent stability in methanol dehydarion to DME reaction. The combination of micro-mesoporous H-ZSM-5/MCM-41 as a dehydration catalyst was evaluated by Li et al. [56]. The acid amount and required strength were controlled by varying the SiO_2/Al_2O_3 ratio. When compared to parent pure H-ZSM-5, uniformly dispersed nanoparticles of H-ZSM-5 in MCM-41 matrix exhibited 100 % DME selectivity in wide temperature range. Similarly micro-mesoporous ZSM-5 zeolite, prepared by desilication method was utilized for MTD by Rutkowska et al. [57].

A controlled modification of porous structure and acidity was correlated to the enhanced catalytic activity, selectivity and stability. The micro-mesoporous structure were claimed to be more resistant to coke poisoning in comparison to the parent ZSM-5 catalyst. The relationship between the crystallite size of ZSM-5 zeolites and the catalytic performance in MTD reaction was investigated in Ref [58]. Higher methanol conversion was observed on smaller zeolite crystallites during the catalytic reaction between the temperature range of 180 and 320 ℃. Uniform nanocrystal catalysts showed highest activity and stability for methanol dehydration to dimethyl ether due to smaller mass transport resistance. On the other hand, both the activity and selectivity of large crystals were low. Moreover, the DME selectivity depends on the uniformity of Al distribution, which determines acidity of external surface and low mass transport resistance of small crystal size. Therefore, a decrease in the number of acid sites on the external surface and reduction in crystal size are key ways to enhance catalytic selectivity and activity, respectively.

Yang et al. [59] synthesized a series of hierarchical mesoporous HZSM-5 using a cationic polymer as meso-structure directing agent to adjust the mesoporosity. The zeolites were used for the dehydration of methanol to DME. Compared to the conventional HZSM-5, the hierarchical mesoporous HZSM-5 zeolite showed the better stability and excellent DME selectivity due to the relative high weak/strong acid site ratio, suitable amount of total acidity, and large mesopore volume. These results suggest that a zeolite catalyst with the proper acidity and mesoporous structure can give excellent performance in the methanol dehydration process.

Silico-aluminophosphate (SAPO) molecular sieves having weaker acid site compared to aluminosilicate zeolites were utilized as methanol dehydration catalysts [60]. At low temperature (250 ^{o}C), SAPO-11 zeolite containing very low concentration of mostly weak acid sites exhibited high activity in methanol dehydration reaction. Yadollah et al. [61] modified HZSM-5 by coating with aluminophosphate to control the acidity strength and the modified HZSM-5 catalyst with mild acidity achieved 86 % conversion and 100 % selectivity to DME over the temperature range of 250–315 ℃ in methanol dehydration reaction.

Aiming to improve the thermal stability, Cuong et al. [62] successfully incorporated zeolites into the porous heat stable SiC support to produce a highly selective and stable catalyst for methanol dehydration reaction. The formation of zeolites on the SiC surface was confirmed by ^{29}Si magic-angle spinning NMR. The high stability was attributed to the presence of highly dispersed micrometer-sized zeolite particles, which make the active sites

more accessible to the reactants and promote the quick transfer of the desired product, DME, out of the catalyst bed, minimizing deactivation of the catalyst.

In conclusion, two types of catalysts are usually used for methanol dehydration to DME: alumina and zeolites based. The alumina based catalyst showed better DME selectivity because of the absence of stronger Brönsted acid sites compared to zeolite based solid acid catalyst. However, lower hydrothermal stability in the presence of water leads to deactivation. Most importantly, higher operation temperature required for direct DME synthesis could be a problem for alumina based catalyst. In this case, zeolite, especially HZSM-5 zeolites which have hydrophobic character and abundant moderate strength of Brönsted acid sites could possibly provide better performance in methanol dehydration.

1.4.3 Hybrid catalyst for direct DME synthesis

The bi-functional catalyst for direct DME synthesis is composed of metallic function for methanol synthesis catalyst and dehydration function for DME synthesis from methanol. The catalytic performance of the bi-functional catalyst mainly depends on the dispersion of copper particels and acidic properties of dehydration catalyst. In general, two kinds of active components in the bi-functional catalysts should be finely dispersed and maintain a closer contact but not react with each other. They often exhibit a high degree of 'synergistic effect', which will facilitate the formation of DME.

Researchers are trying to modify the catalyst structure and/or formulation in order to optimize the DME production as well as catalyst stability improvement. However, two key challenges lie in designing of efficient bi-functional catalyst for direct DME synthesis: the catalyst preparation method and optimized catalyst composition to bring the optimized active sites for methanol synthesis and acidic sites for dehydration of methanol. The preparation method of the bi-functional catalyst systems for direct DME synthesis has a significant effect on the performance of the process. The hybrid catalysts are prepared in different ways including physical mixing of methanol synthesis catalyst and solid-acid catalyst [33, 34], co-precipitation [63], impregnation, and combined co-precipitation-ultrasound [64]. During the preparation, extreme care should be taken not to suppress the individual functionalities such as active sites for methanol synthesis or acidic sites for methanol dehydration. The interaction between two different acitive sites is a very important factor to affect the direct DME synthesis performance.

Generally, two different methods of combining methanol synthesis function and solid acid function can be summarized as either composite or admixed catalysts (Figure 1-8). For

the former the methanol synthesis and methanol dehydration catalyst components exist together as a single entity [65]. Such catalysts are generally prepared by co-precipitation or mixing of the freshly precipitated precursors [65, 66]. While in the case of the admixed catalysts, each function is prepared separately and then the powders of both functions are mechanically blended [33, 34, 67] It is important that the contact between these functions does not cause blockage of active site. Contact between metallic and acidic functions depends on the preparation method of the bi-functional catalyst [68, 69]. In some cases [68-70], the interactions between two functions results in partial blockage of zeolite micropores by the methanol synthesis catalysts and/or migration of Cu^{2+} species through their exchange with protons of zeolites. This will result in deactivation and loss in acidity or unavailability of active copper species for methanol synthesis. In the open literatures, some of these key issues have been addressed with aiming to improve the overall performance of DME synthesis directly from syngas using hybrid catalyst.

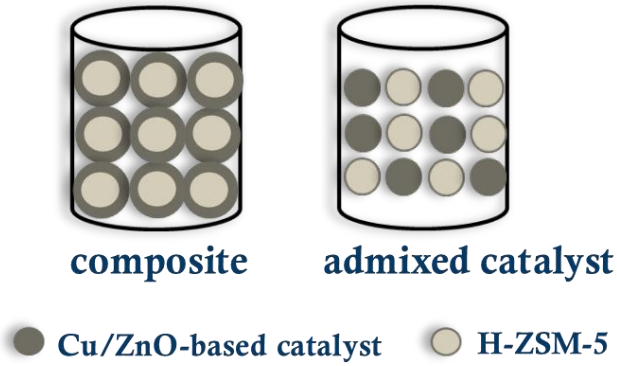

Figure 1-8. Schema for synthesis of bifunctional composite and admixed catalyst

The effect of different preparation methods on the performance of bi-functional catalyst for direct DME synthesis was investigated by Li et al [71]. Cu-La_2O_3-ZrO_2 and γ- Al_2O_3 were used as methanol synthesis and dehydration catalysts. Four different methodologies such as physical mixing of pre pelletized individual components; grinding followed by pelletizing; precipitation of methanol catalysts over the suspension of solid acid part and mixing of freshly precursor of individual components were investigated. Among those, mixing of freshly prepared precursors resulted in highest CO conversion (73 %) and DME yield (58 %). Both the higher dispersion of active copper species and the optimum acidic strength are required for the optimized catalytic performance. Naik et al. [72] investigated two strategies for the preparation of active dimethyl ether (DME) catalysts using CuO-ZnO-Al_2O_3 and silica-alumina (Si/Al ≈ 2) as model methanol synthesis and methanol dehydration catalytic components, respectively. The results showed that hybrid catalysts prepared by a mechanical

mixing of the two catalytic components showed a higher conversion of CO. However, the composite catalysts prepared by mixing the catalyst precursors before calcination or using co-precipitation methods were partially deactivated because the catalyst constituents reacted with each other during the catalyst preparation or calcination stages. Thus, the composite catalyst exhibited much lower activity, as compared to the hybrid catalysts toward syngas conversions.

Influence of mixing methods on the performance of hybrid CuZnAl/HZSM-5 catalysts was explored by Garc á et al. [68]. A series of catalyst were prepared using different mixing methods in order to analyze the possible existence of interactions between components and their influence in the STD process namely: grinding of catalysts powders and pelletizing, slurring of two solids in water (drying and pelletizing) and simple physical mixture of pre-pelletized catalysts particles (Figure 1-9). When compared to physical mixing, former two methods resulted in drastic reduction of the amount of Br önsted acid sited due to interaction of two active components, including blockage (partial) of micropores of zeolite, and Cu^{2+} species exchange, which confirmed by EPR spectroscopy. As a result, lower catalytic activity was observed compared to the catalyst prepared by physical mixture which holds the individual counterparts unaltered during the hybridization process.

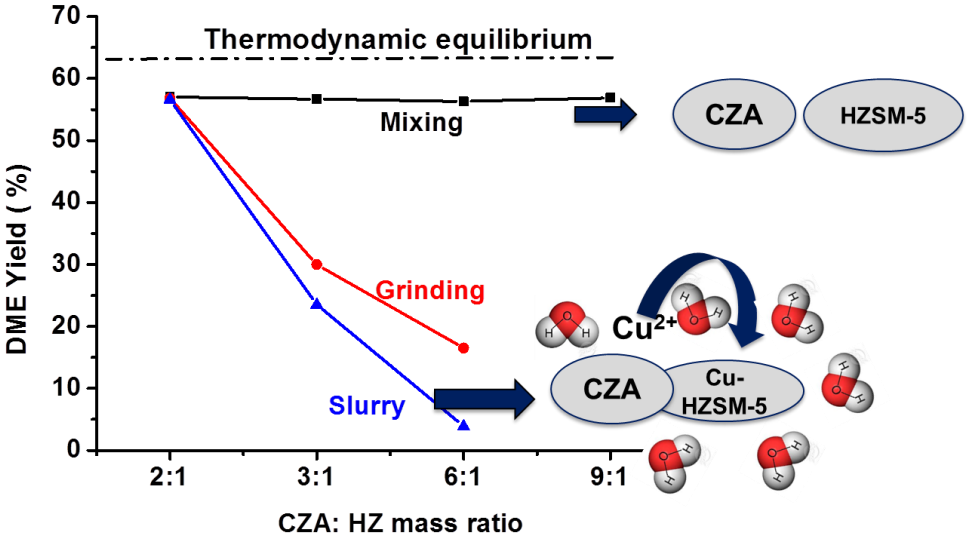

Figure 1-9. The different hybrid catalyst for DME synthesis [68]

In the same way, Bonura et al.[69] studied on different combination procedures between methanol synthesis catalyst and methanol dehydration catalyst. And the catalytic results showed a superior DME productivity obtained by using the bi-functional catalyst prepared with physical mixing. The combined effect of active sites located at metal/oxide(s)–acid interface was claimed as the main factor affecting the activity and DME selectivity.

Typically, the bi-functional catalyst was prepared by physically mixing method. The activity of catalysts prepared by physicalling mixing is higher than the activity of ones prepared by co-precipitation, impregnation, slurrying and grinding method.

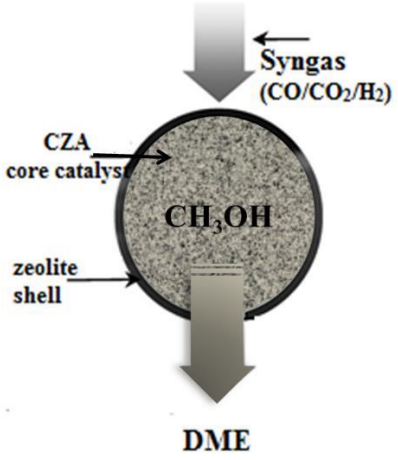

Figure 1-10 Schematic Diagram of DME Synthesis on a Single Zeolite Capsule Catalyst [73]

Aiming to enhance the selectivity by bringing the close proximity of individual active sites for the direct DME synthesis from syngas, Yang et al. [73] synthesized a novel bifunctional catalyst composed of millimeter-sized alumina pellets supported $Cu/ZnO/Al_2O_3$ components as a core and a micron-sized HZSM-5 layer in situ grown on the surface of the core, called a "capsule catalyst" (Figure.1-10). In this special structure, methanol can contact the active sites of the H-type zeolite shell and is converted into the expected DME product. Furthermore, the preliminary methanol synthesis reaction on the catalyst core and the following DME formation from methanol inside the catalyst shell occurred concertedly and promoted mutually. The catalytic results showed a very high selectivity to DME without any side products, but the CO conversion was only 5.59%. The lower catalytic activity should be attributed to some damage on the core CZA catalyst during catalyst preparation.

In another study [74], Cr/ZnO was used for methanol synthesis catalyst. A neutral silicate layer was deposed over it and conveted to zeolites (H-ZSM-5) membrane. By using Cr as metallic active site, the catalyst operated at high temperature performance showed higher selectivity to DME, without producing any by products like alkane/alkene.

Kang et al. [67] synthesized the composite catalysts, $Cu\text{-}ZnO\text{-}Al_2O_3$/Zr-modified zeolites (Ferrierite, ZSM-5 and Y) by co-precipitation of CZA precursors in the slurry of Zr-modified zeolites. The catalysts were tested in DME synthesis from syngas. Among these three samples, CZA-FER catalyst showed stable activity and the best DME selectivity. Apart from the easy reducibility of Cu species, the presence of appropriate acid sites of required

strength for methanol dehydration is proposed to be the reason for the superior performance of CZA/FER catalyst. It was also found that the Cu species in the case of CZA–Y were easily to be sintering, leading to change in product distribution.

Andrés et al. [75] localized the Cu-ZnO catalyst within the pores of SBA-15 silica. Zn and Cu were incorporated sequentially from their respective precursors through incipient impregnation followed by calcination. Further the confined catalyst was mixed with an acid catalyst H-ZSM-5. A maximum loading of 15 wt.% Cu was successfully achieved and displayed very high surface area resulting in higher methanol synthesis activity. Similarly, higher DME selectivity was also obtained when the catalyst was admixed with H-ZSM-5. It was suggested that an enhanced stability was due to the confinement of active species in a localized environment when compared to the reference catalyst.

Besides that, the acid property of the dehydration component also plays a crucial role in determining the overall CO conversion rate, DME selectivity, and catalyst durability. It is important to balance the acidity of zeolite by embedding other suitable basic oxides or optimal the topology and crystal size of zeolite.

Wang et al [76] used two kinds of HZSM-5 zeolite in the STD at different (SiO_2/Al_2O_3) ratio with $CuO/ZnO/Al_2O_3$. They found that the acidity of HZSM-5 played a critical role in the performance of STD catalyst, and that an optimal acidic amount was required to obtain the best activity of STD catalyst; more and less acidic amounts were both unfavourable for the selectivity to DME.

A detailed study was performed by Mao et al. [67] who prepared a hybrid catalyst for the STD reaction by physically mixing the $CuO{-}ZnO{-}Al_2O_3$ component and magnesium oxide modified HZSM-5 zeolite. With the suitable amount of MgO addition, the selectivities to undesired byproducts such as hydrocarbons and CO_2 were clearly decreased. As the unselective strong Brönsted acid sites were removed, the DME yield was improved from 49% to higher than 64%. The process for methanol dehydration was possibly realized on both acidic and basic sites on magnesium oxide modified HZSM-5. Similarly, Kim et al. [77] investigated NaZSM-5 and HZSM-5 with three Si/Al ratios (30, 50, and 100) and concluded that the acid strength of HZSM-5 increased with a decrease in the Si/Al ratios. The methanol dehydration rate was dependent on the acid strength of the ZSM-5, the difference of acid strength would change the optimal ratio of the two components, because the relative intrinstic rate of methanol synthesis and methanol dehydration were changed.

In other way, García-Trenco et al. [34] reported the impact of the zeolite topology on the performance of hybrid catalysts in syngas-to-DME conversion. They used 10 atom-ring bi-

and tri-dimensional structures (ZSM-5, FER, MCM-22, IM-5 and TNU-9) and the delaminated MWW structure, ITQ-2, all with Si/Al ratios around 10. The authors studied the direct dehydration of methanol over the zeolites alone at atmospheric pressure and found that deactivation was caused by carbonaceous deposits whose nature depended on the topology of the zeolite used. On the other hand, the loss of activity for the hybrids was found to be related mainly to the aluminium content in the exterior of the zeolite crystallites. This was explained by a detrimental interaction between the Cu/ZnO component and the proton-exchange positions located on the external surface of the acid catalyst.

The optimized composition of bi-functional catalyst is also very important for the activity and DME selectivity in direct DME synthesis. By changing the hybrid catalyst composition, the DME / MeOH ratio in the product mixture can be controlled. If the same amount of methanol catalyst is used, the reaction systems with higher content of methanol dehydration catalyst would lead to higher DME yield at the expense of methanol. For bi-functional catalyst CZA/γ-Al_2O_3, maximum values of DME selectivity (83.4 %) were obtained for a molar ratio of H_2/CO = 6/1, at 275 ^oC, 40 bar [78]. Under these reaction conditions, the use of NaHZSM-5 zeolite as an acid component allowed a DME selectivity of 77.6 % at a lower H_2/CO molar ratio (2/1) in the feed [79].

Another major issue to be addressed is catalyst deactivation in DME synthesis. The stability of various catalyst compositions (methanol synthesis and methanol dehydration), under different reaction conditions have been studied. Based on the available literature studies, the major causes for depletion in catalytic activity as a result of deactivation of catalyst could be loss in active surface area of copper, which is a key factor for methanol synthesis [80], coke / carbon deposition and decrease in the number of acid sites. The loss of active aopper generally occurs at higher reaction temperatures, especially when γ-Al_2O_3 is used an acid catalyst as it requires higher temperature get better activity causing sintering of active copper sites. In case of zeolites the scenario can be correlated higher acidic strength-causes formation of by-products and coke. The deposition of coke to active site of methanol synthesis catalyst has major influence in causing deactivation for the same [81, 82]. Another reason, as a result of intimate contact between copper species with zeolites, in presence of water forming during the course of reaction can result in Cu^{2+} exchange with protons of zeolites resulting in acidity loss, which, in turn, will decay in dehydration sites. As a result the formation of DME will be suppressed. In addition to this, if the catalyst is not properly designed, especially in case of hybrid catalysts for direct DME synthesis, the blockage of one active site over another will also result in poor over all activity. Hence, a balance is required

in terms of surface area, synergetic interaction between two active functionalities and architectural arrangement are require while designing the active, selective and stable bi-functional catalyst for selective synthesis of DME from syngas.

Several authors have reported more rapid catalyst deactivation with a higher acid strength and higher acid site density. Guisnet and co-workers [83] elegantly explained these effects of the acidity characteristics as follows : (i) the stronger are the acidic sites, the faster are the chemical steps and the more pronounced is the retention of coke precursors and coke molecules, hence the faster is the coking rate; (ii) the higher is the density of the acid sites, thus the closer these sites are to each other, the larger is the number of successive chemical steps undergone by reactant molecules along the diffusion path within the zeolite crystallites and the more favorable are the condensation reactions, hence the faster is the coking rate.

Furthermore, water in the reaction medium may also affect the deactivation rate. Aguayo et al. [84] proved that water presence in the catalyst system could depress the deactivation according to the effective coke deposition; however, it also decreased the activity of γ-Al_2O_3 acid function, due to its high adsorption capacity on the acid sites.

Wang et al. [85] studied the deactivation of composite catalyst for one-step dimethyl ether (DME) synthesis in slurry reactor under reaction conditions of 260 ^oC and 5.0 MPa. They found that instability of Cu-based methanol synthesis catalyst led to rapid deactivation of the composite catalyst. Compared with the deactivation rate of the hybrid catalyst in fixed-bed reactor, the harmfulness of water, which is formed in the synthesis of DME, caused the Cu-based catalyst to deactivate at a high rate in slurry reactor. Characterization results showed that carbon deposition and grain growth of Cu were important reasons for the rapid deactivation of the Cu-based catalyst.

Further studies of the deactivation and subsequent regeneration of the bi-functional catalyst system are, however, necessary in order to establish the deactivation mechanism (for instance, whether it occurred as a result of Cu crystallites sintering due to the lack of stabilizing CO/CO_2 or because of carbon deposition blocking the pores and the active sites of the system) and an optimal regeneration procedure.

1.5 The research objective of this thesis

DME is an efficient, cleaner and economically viable alternate fuel and can be produced from wide range of feedstock. Our analysis of the literature data shows that copper based catalyst is normally deployed for methanol synthesis and modified γ-Al_2O_3 or zeolites, are

mostly used for dehydration of methanol to DME. Considerable efforts have been directed toward the development of highly active, selective and stable hybrid bi-functional catalyst for the direct synthesis of DME from syngas.

As discussed before, key issues still need considerable effort in catalyst development for direct DME synthesis are (Scheme 1-11):

- Stabilizing the active metallic copper surface area against sintering, avoiding Cu^{2+} exchange with proton sites of zeolites to improve the catalytic activity and stability;
- Optimizing the acidic sites and their strength and density required for dehydration of methanol formed to suppress the subsequent dehydration of DME to unwanted side products such as alkanes/alkenes;
- Partial passivated Cu active site for water gas shift reaction to suppress the production of main byproduct CO_2 .

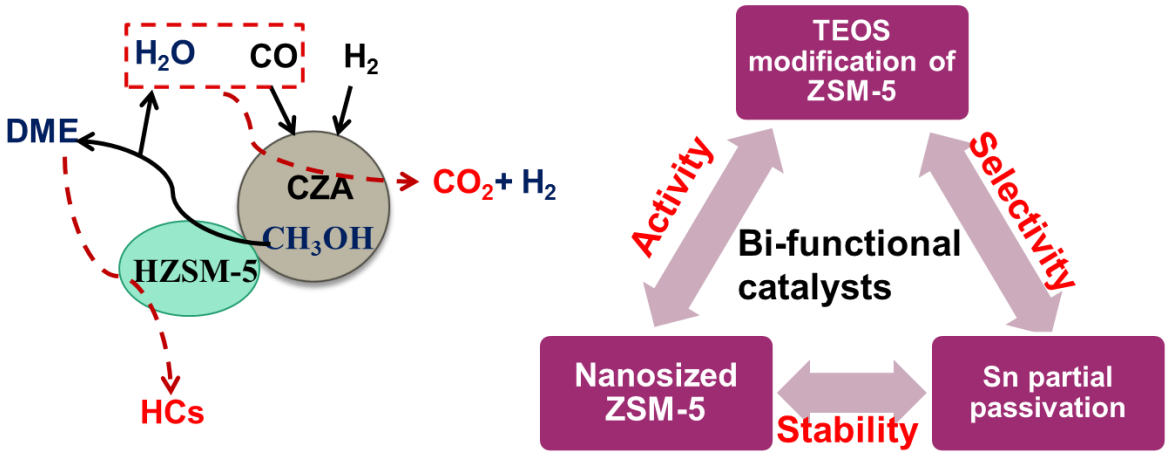

Scheme 1-11. Designing of highly active, stable and selective hybrid CZA/HZSM-5 catalyst

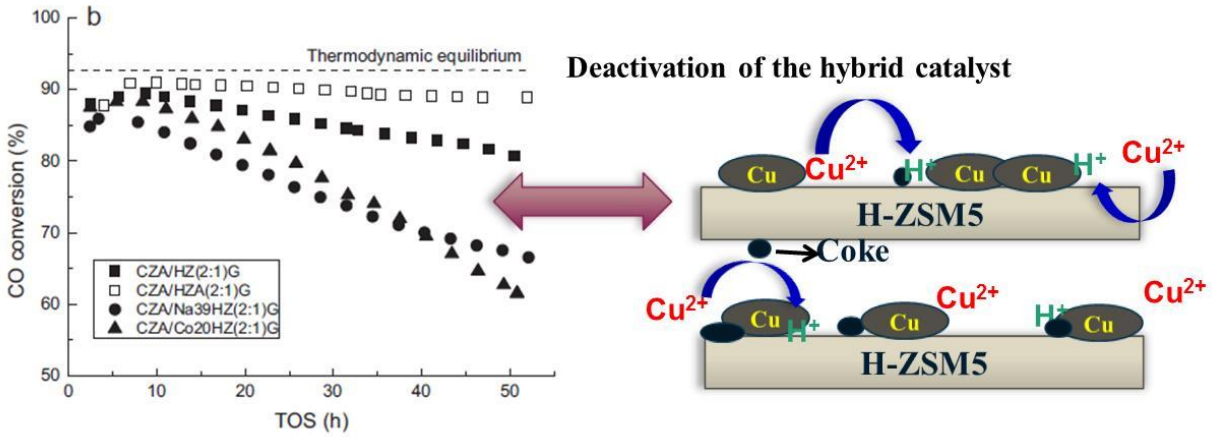

Scheme 1-12. Illustration of possible causes of deactivation of hybrid CZA/H-ZSM-5 catalyst [86]

An important challenge in the formulation of the bi-functional catalyst and the reactor design is the prevention or limitation of deactivating phenomena: copper sintering, coking of acidic components and metal ions migration (Scheme 1-12).

The research work performed in this thesis has been directed to addressing the aforesaid issues by architecture design and/or synthesis of bi-functional CuO-ZnO-Al_2O_3/HZSM-5 hybrid catalyst with high catalytic activity, selectivity of DME and better stability. The goals of this thesis are as follows:

To find out the mechanism of deactivation of hybrid catalyst during direct DME synthesis, which could be provided a new methodology for the improvements of the catalyst activity, selectivity and stability.

To improve the catalyst stability and DME productivity via modification of zeolite outer surface by silylation: Preventing/slowing down copper sintering and ion exchange.

To heighten the catalytic performance and stability of copper-zeolite hybrid catalysts for direct DME synthesis by optimizing the crystallite size of zeolite

To improve the selectivity to DME by suppressing the water gas shift reaction via partial passivation of active copper site.

1.6 References

[1] O. Tahvonen, S. Salo, European Economic Review, 45 (2001) 1379-1398.

[2] G.A. Olah, A. Goeppert, G.S. Prakash, The Journal of organic chemistry, 74 (2008) 487-498.

[3] T. Dogu, D. Varisli, Turkish Journal of Chemistry, 31 (2007) 551.

[4] M. Kampa, E. Castanas, Environmental pollution, 151 (2008) 362-367.

[5] G.A. Olah, A. Goeppert, G.S. Prakash, Beyond oil and gas: the methanol economy, John Wiley & Sons, 2011.

[6] T.A. Semelsberger, R.L. Borup, H.L. Greene, Journal of Power Sources, 156 (2006) 497-511.

[7] S. Lee, J.G. Speight, S.K. Loyalka, Handbook of alternative fuel technologies, crc Press, 2014.

[8] J. Kopyscinski, T.J. Schildhauer, S.M. Biollaz, Fuel, 89 (2010) 1763-1783.

[9] A.Y. Khodakov, W. Chu, P. Fongarland, Chemical Reviews, 107 (2007) 1692-1744.

[10] P.C. Munasinghe, S.K. Khanal, Bioresource technology, 101 (2010) 5013-5022.

[11] G. Farina, Hydrocarbon Processing;(United States), 71 (1992).

[12] T. Fleisch, A. Basu, R. Sills, Journal of Natural Gas Science and Engineering, 9 (2012) 94-107.

[13] Y. Kikkawa, I. Aoki, Oil and Gas Journal, 96 (1998) 55-59.

[14] T.-S. Zhao, T. Takemoto, N. Tsubaki, Catalysis Communications, 7 (2006) 647-650.

[15] Z. Azizi, M. Rezaeimanesh, T. Tohidian, M.R. Rahimpour, Chemical Engineering and Processing: Process Intensification, 82 (2014) 150-172.

[16] J. Sun, G. Yang, Y. Yoneyama, N. Tsubaki, ACS Catalysis, 4 (2014) 3346-3356.

[17] S.R. Blaszkowski, R.A. van Santen, Journal of the American Chemical Society, 118 (1996) 5152-5153.

[18] W.-H. Cheng, Methanol production and use, CRC Press, 1994.

[19] F. Ramos, A.D. de Farias, L.E.P. Borges, J. Monteiro, M.A. Fraga, E.F. Sousa-Aguiar, L.G. Appel, Catalysis Today, 101 (2005) 39-44.

[20] Y. Ohno, M. Omiya, 12th ICCS Coal Conversion in DME, (2003) 2-6.

[21] T. Ogawa, N. Inoue, T. Shikada, O. Inokoshi, Y. Ohno, Studies in surface science and catalysis, 147 (2004) 379-384.

[22] J. Li, W. Zhang, L. Gao, P. Gu, K. Sha, H. Wan, Applied Catalysis A: General, 165 (1997) 411-417.

[23] C. Busetto, G. Del Piero, G. Manara, F. Trifiro, A. Vaccari, Journal of Catalysis, 85 (1984) 260-266.

[24] C. Baltes, S. Vukojević, F. Schüth, Journal of Catalysis, 258 (2008) 334-344.

[25] M. Behrens, F. Studt, I. Kasatkin, S. Kühl, M. Hävecker, F. Abild-Pedersen, S. Zander, F. Girgsdies, P. Kurr, B.-L. Kniep, Science, 336 (2012) 893-897.

[26] K.W. Jun, H.S. Lee, H.S. Roh, S.E. Park, BULLETIN-KOREAN CHEMICAL SOCIETY, 23 (2002) 803-806.

[27] F. Yaripour, F. Baghaei, I. Schmidt, J. Perregaard, Catalysis Communications, 6 (2005) 147-152.

[28] E.-Y. Lee, Y.-K. Park, O.-S. Joo, K.-D. Jung, Reaction Kinetics and Catalysis Letters, 89 (2006) 115-121.

[29] C.W. Seo, K.D. Jung, K.Y. Lee, K.S. Yoo, Industrial & Engineering Chemistry Research, 47 (2008) 6573-6578.

[30] S. Jiang, J.-S. Hwang, T. Jin, T. Cai, W. Cho, Y.s. Baek, S.E. Park, Bulletin-Korean Chemical Society, 25 (2004) 185-189.

[31] V. Vishwanathan, K.-W. Jun, J.-W. Kim, H.-S. Roh, Applied Catalysis A: General, 276 (2004) 251-255.

[32] P.S. Prasad, J.W. Bae, S.-H. Kang, Y.-J. Lee, K.-W. Jun, Fuel Processing Technology, 89 (2008) 1281-1286.

[33] K.S. Yoo, J.-H. Kim, M.-J. Park, S.-J. Kim, O.-S. Joo, K.-D. Jung, Applied Catalysis A: General, 330 (2007) 57-62.

[34] A. García-Trenco, S. Valencia, A. Martínez, Applied Catalysis A: General, 468 (2013) 102-111.

[35] M. Xu, J.H. Lunsford, D.W. Goodman, A. Bhattacharyya, Applied Catalysis A: General, 149 (1997) 289-301.

[36] F. Zha, J. Ding, Y. Chang, J. Ding, J. Wang, J. Ma, Industrial & Engineering Chemistry Research, 51 (2011) 345-352.

[37] M.C. Bradford, M.V. Konduru, D.X. Fuentes, Fuel processing technology, 83 (2003) 11-25.

[38] S. Lee, Methanol synthesis technology, CRC Press, 1989.

[39] K. Waugh, Catalysis Today, 15 (1992) 51-75.

[40] J.-P. Lange, Catalysis Today, 64 (2001) 3-8.

[41] M.M. Günter, T. Ressler, B. Bems, C. Büscher, T. Genger, O. Hinrichsen, M. Muhler, R. Schlögl, Catalysis Letters, 71 (2001) 37-44.

[42] A. Xin, Z. Yizan, Q. Zhang, W. Jinfu, Chinese Journal of Chemical Engineering, 17 (2009) 88-94.

[43] I. Melian-Cabrera, M.L. Granados, J. Fierro, Journal of Catalysis, 210 (2002) 285-294.

[44] W.-J. Shen, M. Okumura, Y. Matsumura, M. Haruta, Applied Catalysis A: General, 213 (2001) 225-232.

[45] N. Tsubaki, K. Fujimoto, Topics in Catalysis, 22 (2003) 325-335.

[46] W.-J. Shen, Y. Ichihashi, H. Ando, M. Okumura, M. Haruta, Y. Matsumura, Applied Catalysis A: General, 217 (2001) 165-172.

[47] Y. Fu, T. Hong, J. Chen, A. Auroux, J. Shen, Thermochimica Acta, 434 (2005) 22-26.

[48] R.W. Wegman, J. Chem. Soc., Chem. Commun., (1994) 947-948.

[49] D. Liu, C. Yao, J. Zhang, D. Fang, D. Chen, Fuel, 90 (2011) 1738-1742.

[50] K.C. Tokay, T. Dogu, G. Dogu, Chemical Engineering Journal, 184 (2012) 278-285.

[51] F. Yaripour, M. Mollavali, S.M. Jam, H. Atashi, Energy & Fuels, 23 (2009) 1896-1900.

[52] S.Y.g. Hosseini, M.R.K. Nikou, Journal of American Science, 8 (2012).

[53] B. Sabour, M.H. Peyrovi, T. Hamoule, M. Rashidzadeh, Journal of Industrial and Engineering Chemistry, 20 (2014) 222-227.

[54] D.P. Serrano, G. Calleja, J.A. Botas, F.J. Gutierrez, Separation and purification technology, 54 (2007) 1-9.

[55] Y. Wei, P.E. de Jongh, M.L. Bonati, D.J. Law, G.J. Sunley, K.P. de Jong, Applied Catalysis A: General, (2014). doi:10.1016/j.apcata.2014.12.027

[56] H. Li, S. He, K. Ma, Q. Wu, Q. Jiao, K. Sun, Applied Catalysis A: General, 450 (2013) 152-159.

[57] M. Rutkowska, D. Macina, N. Mirocha-Kubień, Z. Piwowarska, L. Chmielarz, Applied Catalysis B: Environmental, 174 (2015) 336-343.

[58] A.A. Rownaghi, F. Rezaei, M. Stante, J. Hedlund, Applied Catalysis B: Environmental, 119 (2012) 56-61.

[59] Q. Yang, H. Zhang, M. Kong, X. Bao, J. Fei, X. Zheng, Chinese Journal of Catalysis, 34 (2013) 1576-1582.

[60] W. Dai, W. Kong, G. Wu, N. Li, L. Li, N. Guan, Catalysis Communications, 12 (2011) 535-538.

[61] Y. Tavan, M.R.K. Nikou, A. Shariati, Journal of Industrial and Engineering Chemistry, 20 (2014) 668-673.

[62] S. Ivanova, E. Vanhaecke, B. Louis, S. Libs, M.J. Ledoux, S. Rigolet, C. Marichal, C. Pham, F. Luck, C. Pham‐Huu, ChemSusChem, 1 (2008) 851-857.

[63] J.W. Jung, Y.J. Lee, S.H. Um, P.J. Yoo, D.H. Lee, K.-W. Jun, J.W. Bae, Applied Catalysis B: Environmental, 126 (2012) 1-8.

[64] R. Khoshbin, M. Haghighi, Catalysis Science & Technology, 4 (2014) 1779-1792.

[65] J.W. Bae, S.-H. Kang, Y.-J. Lee, K.-W. Jun, Applied Catalysis B: Environmental, 90 (2009) 426-435.

[66] S.-H. Kang, J.W. Bae, K.-W. Jun, H. Potdar, Catalysis Communications, 9 (2008) 2035-2039.

[67] D. Mao, W. Yang, J. Xia, B. Zhang, Q. Song, Q. Chen, Journal of Catalysis, 230 (2005) 140-149.

[68] A. Garc á-Trenco, A. Vidal-Moya, A. Mart ínez, Catalysis Today, 179 (2012) 43-51.

[69] G. Bonura, M. Cordaro, C. Cannilla, A. Mezzapica, L. Spadaro, F. Arena, F. Frusteri, Catalysis Today, 228 (2014) 51-57.

[70] V. Ordomsky, M. Cai, V. Sushkevich, S. Moldovan, O. Ersen, C. Lancelot, V. Valtchev, A. Khodakov, Applied Catalysis A: General, 486 (2014) 266-275.

[71] Z. Li, J. Li, M. Dai, Y. Liu, D. Han, J. Wu, Fuel, 121 (2014) 173-177.

[72] S.P. Naik, H. Du, H. Wan, V. Bui, J.D. Miller, W.W. Zmierczak, Industrial & Engineering Chemistry Research, 47 (2008) 9791-9794.

[73] G. Yang, N. Tsubaki, J. Shamoto, Y. Yoneyama, Y. Zhang, Journal of the American Chemical Society, 132 (2010) 8129-8136.

[74] G. Yang, M. Thongkam, T. Vitidsant, Y. Yoneyama, Y. Tan, N. Tsubaki, Catalysis Today, 171 (2011) 229-235.

[75] A. Garc á-Trenco, A. Mart ínez, Applied Catalysis A: General, 493 (2015) 40-49.

[76] L. Wang, Y. Qi, Y. Wei, D. Fang, S. Meng, Z. Liu, Catal Lett, 106 (2006) 61-66.

[77] J.-H. Kim, M.J. Park, S.J. Kim, O.-S. Joo, K.-D. Jung, Applied Catalysis A: General, 264 (2004) 37-41.

[78] J. Ere ña, R. Garo ña, J.M. Arandes, A.T. Aguayo, J. Bilbao, Catalysis Today, 107–108 (2005) 467-473.

[79] G. Bozga, I.T. Apan, R.E. Bozga, Recent Patents on Catalysis, 2 (2013) 68-81.

[80] J.T. Sun, I.S. Metcalfe, M. Sahibzada, Industrial & engineering chemistry research, 38 (1999) 3868-3872.

[81] A.G. Gayubo, J. Vicente, J. Ereña, L. Oar-Arteta, M.J. Azkoiti, M. Olazar, J. Bilbao, Applied Catalysis A: General, 483 (2014) 76-84.

[82] J. Ereña, I. Sierra, M. Olazar, A.G. Gayubo, A.T. Aguayo, Industrial & Engineering Chemistry Research, 47 (2008) 2238-2247.

[83] M. Guisnet, P. Magnoux, D. Martin, Studies in surface science and catalysis, 111 (1997) 1-19.

[84] A.T. Aguayo, J. Ereña, I. Sierra, M. Olazar, J. Bilbao, Catalysis Today, 106 (2005) 265-270.

[85] D.-S. Wang, Y.-S. Tan, Y.-Z. Han, T. Noritatsu, Journal of Fuel Chemistry and Technology, 36 (2008) 171-175.

[86] A Garcá-Trenco, A Martínez, Applied Catalysis A: General, 411– 412 (2012) 170–179

Chapter 2 Experimental

2.1 Catalyst preparation

Direct synthesis of DME from syngas requires bifunctional catalysts having two different active sites; one for methanol formation ($Cu/ZnO/Al_2O_3$ catalyst) and another one for methanol dehydration (HZSM-5 zeolite). As stated in Chapter 1, copper (Cu) is the active metal for methanol synthesis. In addition to this, the catalysts contain Zinc (Zn) and Aluminum (Al). On the other hand, HZSM-5 zeolites are commonly employed as methanol dehydration catalysts for DME synthesis owing to their high hydrothermal stability and low-temperature availability.

2.1.1 Preparation of a methanol synthesis catalyst

The chemicals used in the present study were all analytical grades and supplied by Sigma-Aldrich. The metal salts were in the form of nitrates such as copper nitrate [$Cu(NO_3)_2 \cdot 3H_2O$], zinc nitrate [$Zn(NO_3)_2 \cdot 6H_2O$], aluminum nitrate [$Al(NO_3)_3 \cdot 9H_2O$] and sodium carbonate Na_2CO_3.

The $CuO/ZnO/Al_2O_3$ catalyst was prepared by a conventional co-precipitation method with Cu: Zn: Al atomic ratio equal to 6:3:1 following the optimized methodology described in Ref. [1]. The mixed solutions of the metal nitrates copper nitrate (0.6 M), zinc nitrate (0.3 M), and aluminum nitrate (0.1 M)] and an aqueous solution of sodium carbonate (1 M) as precipitating agent were simultaneously added at a constant flow rate of 5 mL/min to a glass beaker kept under stirring at a temperature of 70 ^oC and a constant pH of 7.0. After precipitation, the precipitate was aged for 1 h at the same temperature under continuous stirring. Subsequently, the precipitate was then filtered and washed several times with deionized water to remove residual sodium ions, dried in an oven at 100 ℃ for 12 h, and finally calcined at 360 ℃ for 5 h under air flow (40 ml/min). For simplicity this catalyst is designated and labelled as CZA.

The xSn-CZA catalysts were prepared by sequential impregnation using incipient wetness method at different Sn loading, 0.1, 0.2, 0.5 and 1.0 wt. %, respectively. After the impregnation with a $SnCl_2$ solution, the promoted catalysts were dried at 90 ˚C for 12 h followed by calcination in air at 360 ˚C for 5 h.

2.1.2 Preparation of solid acid catalyst

2.1.2.1 Commercial ZSM-5

The commercial MFI type zeolites (ZSM-5) were supplied by Zeolyst International and Süd-Chemie. The samples characterized by three different silica to alumina ratios were used and denoted as ZSM-5(x), where x marks silica to alumina ratio: ZSM-5(13) (Zeolyst; Code: CBV 2314, Si/Al=13, NH_4^+ form), ZSM-5(25) (CBV 5524G, Si/Al=25, NH_4^+ form) and ZSM-5(45) (Süd-Chemie; Code: MFI 90, Si/Al = 45, H- form).

The ZSM-5 zeolites were converted from NH_4^+ into H-form by calcination in air at 550 ℃ for 6 h (at the heating rate of 2 ℃/min) (see Figure 2-1) and used as a solid acid catalyst

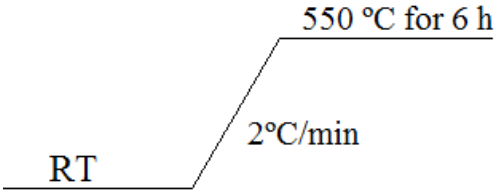

Figure 2-1. Calcination temperature programme used to obtain the HZSM-5 zeolite

2.1.2.2 Synthesis of silylated ZSM-5

The surface modified, silylated samples were prepared by the chemical liquid deposition using TEOS as a silica source. 5 g of dried zeolite in H-form was added to the solution of 1 g of TEOS in 50 cm^3 of n-hexane and refluxed for 24 h at 50 ℃. The modified sample was dried at 100 ℃ for 12 h and calcined at 550 ℃ (heating rate: 2 ℃/min) for 5 h in air. The calcined silylated zeolites are denoted as SiO_2/ZSM-5-I(13) and SiO_2/ZSM-5-II(45).

2.1.2.3 Synthesis of nano-sized ZSM-5

The chemicals used to prepare the nano-sized ZSM-5 crystallites were sodium aluminate (w (Al_2O_3) = 54 %, w (Na_2O) = 41 %), tetra-n-propylammonium hydroxide (TPAOH, Alfa Aesar, 20 wt.% water solution), tetraethyl orthosilicate (TEOS, Aldrich, 98%) and distilled water produced in our laboratory. Appropriate amounts of sodium aluminate, TPAOH and water were mixed and stirred with magnetic stirrer until the system gets clear. Thereafter, TEOS was added to the solution and hydrolyzed at 80 ℃ for 24 h. The final molar oxide composition of the reaction mixture was $1.23Na_2O$: 9.74TPAOH: $1.0Al_2O_3$: $43.2SiO_2$: $806H_2O$. Aliquots of clear solution was divided in four autoclaves and heated at 100, 120, 150 and 170 ℃. The synthesis duration at 120, 150 and 170 ℃ was 5 days. The synthesis at 100 ℃ was performed for 7 days. Recovered solid phases of the samples were washed with

distilled water until the pH of the supernatant was 7, dried at 80 ℃ and calcined at 550 ℃ for 5 h (heating rate 1.75 ℃/min).

After the first calcination, the zeolite was exchanged three times with a 2 M ammonium nitrate solution (NH_4NO_3), under reflux at 80 ℃ for 6 h. A ratio volume of solution/mass of catalyst of 100 mL g^{-1} was used. After exchange, the zeolite was filtered and washed with deionized water and dried overnight at 100 ℃. The zeolite in the NH_4^+ form was then calcined under dry air flow (80 cm^3 min^{-1} g^{-1}) at 550 ℃ for 6h with the ramp of 2 ℃/min to obtain its H- form.

The ZSM-5 samples are labeled according to average particle size which was calculated from the SEM images. For example, the sample labeled ZSM-5@65 is a ZSM-5 with an average individual crystallite size of 65 nm. The individual zeolite size of the laboratory synthetized samples increases with the crystallization temperature: ZSM-5@65 (100 ℃), ZSM-5@80 (120 ℃), ZSM-5@95 (150 ℃) and ZSM-5@110 (170 ℃).

2.1.3 Preparation of hybrid catalyst

The admixed catalyst was prepared by kneading the mixture of the as prepared CZA and H-form of zeolite powders (eg; CZA: ZSM-5(13) a mixture of CZA and zeolite converted to H-form with Si/Al =13) equal to 5:3 wt/wt) in an agate mortar to form homogenous mixture, the resultant powder was pressed into tablets and finally crushing them into granules before reaction.

2.2 Catalyst Characterization

2.2.1 Surface area and pore size distribution

The BET surface area, pore volume, average pore diameter and pore size distribution of the catalysts were determined by N_2 physisorption at 77 K using a Micromeritics ASAP 2010 apparatus. Prior to the experiments, the samples were outgassed at either 150 ℃ (for methanol synthesis catalysts) for 3 h or 300 ℃ (for zeolites) for 5 h. The specific surface area was calculated following the BET method, the t-plot method was used for determining the micropore volume (V_{micro}) and mesopore surface area (S_{meso}), the total pore volume was determined using the value at relative pressure (P/P_0) of 0.995, and the pore size distribution curves were calculated from the desorption branches of the isotherms using BJH formula [3].

2.2.2 X-ray diffraction measurements

The crystal structure of the catalysts were revealed by X-ray diffraction (XRD) on a Bruker D8 Advance diffractometer, using Cu-Kα radition (λ = 1.5506 Å) as X-ray source. For methanol synthesis catalyst, a 10 °< 2θ <80 °range was scanned with step of 0.02 °/ s and the 2 s acquisition time. The range of Bragg's angles 2θ = 5-50 °, step size of 0.0167 °, time per step of 99.68 s were used for zeolite sample analysis. The average size of CuO particle was calculated according to the Sherrer equation [4].

$$d = \frac{0.89\lambda}{B\cos\theta} \times \frac{180°}{\pi} \qquad (2\text{-}1)$$

where d is the average crystallite diameter, λ is the wave length of X-ray radiation, and B is the full width half in degrees.

2.2.3 H_2-temperature programmed reduction

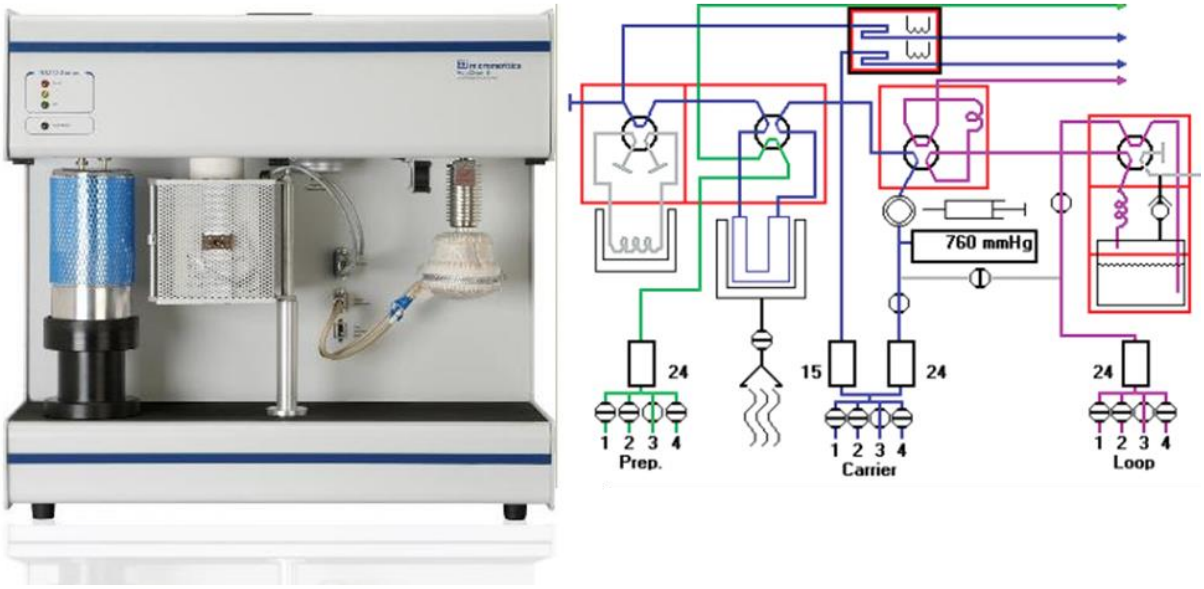

Figure 2-2. Micromeritics AutoChem 2920 equipment.

The temperature-programmed reduction (TPR) profiles were obtained by passing 10 % H_2/Ar gas mixture through the catalyst while increasing the temperature at a linear rate using the Micromeritics Autochem 2920 equipment (Figure 2-2). 100 mg of the samples were loaded into a quartz reactor and pretreated by a He flow (30 ml/min STP) at 100 ℃ for 2 h. Then He was replaced by the reductive gas H_2/He (5 mol.% H_2 in He) at the same flow-rate of 30 ml/min. The temperature was heated up to 800 ℃ at a ramp rate of 5 ℃/min. The effluent gas was analyzed by a thermal conductivity detector (TCD).

2.2.4 Temperature programmed desorption of ammonia

Ammonia temperature programme desorption (NH_3-TPD) was employed in order to measure the amount and strength of the acidic sites of the catalysts. A typical test was done as follows: 50 mg of the catalyst was pretreated at 500 ℃ for 90 min in a He flow in order to remove the physisorbed and crystal water. Then the sample was cooled down to the adsorption temperature (100 ℃) and NH_3 was absorbed on the surface by pulsed injections until saturation. After the saturation, the sample was purged with He for 45 min to remove physically adsorbed NH_3 from the surface of the catalyst. The TPD profiles were monitored by a thermal conductivity detector and recorded from 100 to 700 ℃ at a heating rate of 10 ℃/min.

2.2.5 X-photoelectron spectroscopy

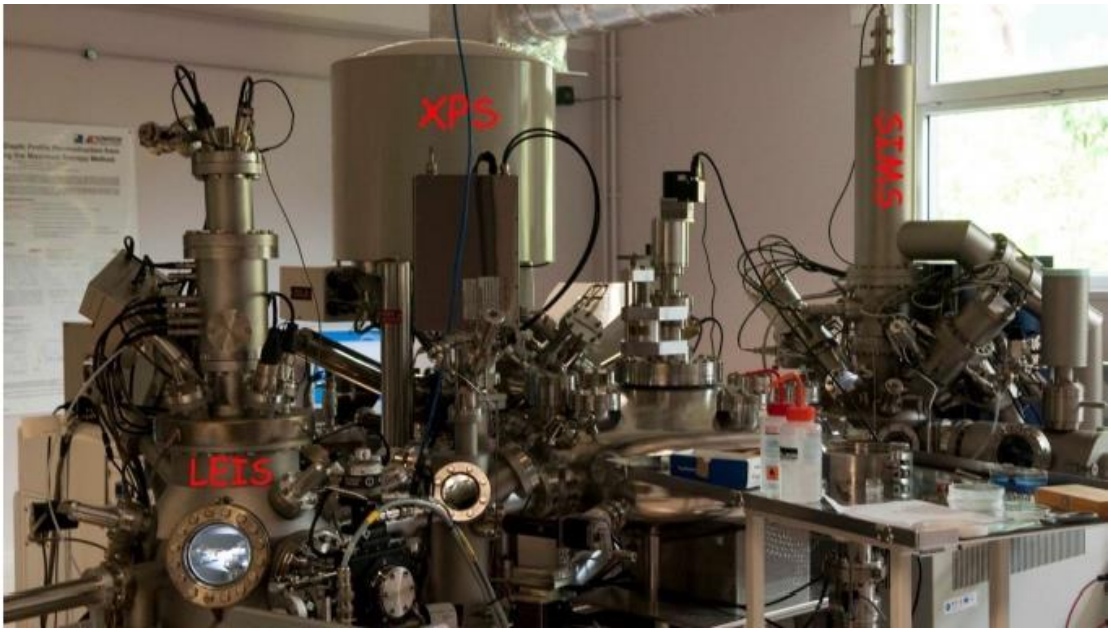

Figure 2-3. XPS Surface Analysis platform

X-ray photoelectron spectra (XPS) were acquired on a Kratos Axis Ultra DLD apparatus (see Figure 2-3) equipped with a hemispherical analysis and a delay line detector on calcined powder samples and after in situ reduction (at 290 ℃ for 6 h for the CZA catalysts). The reduction was carried out in the atmospheric pressure reaction cell attached to the preparation chamber of the spectrometer. The experiments were performed using an Al monochromatized X-ray source (10 kV, 15 mA) with a pass energy of 40 eV (0.1 eV/step) for high resolution spectra and a pass energy of 160 eV (1 eV/step) for the survey spectrum in hybrid mode and slot lens mode respectively.

2.2.6 IR spectroscopy analysis

2.2.6 1 CO-FTIR

FTIR of CO measurements are carried out on a Nicolet Protege 380 spectrometer equipped with a DTGS detector. Before the measurements all samples were diluted with calcined silica (1:3 by weight) to avoid the full adsorption of IR beam by the catalyst. About 20 mg of the samples were pressed in self-supported wafers. The sample was then introduced in a glass cells specially designed for in-situ FTIR spectroscopy at low temperature (-140 ℃) and enabling preliminary thermal treatments. The activation procedure started with a heating step (5 ℃/min) under a vacuum from ambient temperature to 400 ℃ with a 3 h plateau. When the activation procedure was completed, the sample was cooled down to -140 ℃. Carbon monoxide was then gradually introduced into the cell and FTIR spectra subsequently were recorded. The procedure was repeated until the evolution of adsorbed species indicated that CO saturation of the surface has been reached. The difference spectra were obtained by the subtraction of the reference spectra from the spectra of the samples with adsorbed CO.

2.2.6.2 FTIR combined with pyridine adsorption and 2,6-dimethylpyridine adsorption

One of the most commonly used techniques to determine the acidity of a zeolite is Fourier Transform IR spectroscopy (FTIR) (Figure 2-4) [5-7]. The acidity can be determined from the study of the hydroxyls (OH) vibration bands and from analysis of their interaction with suitable probe molecules. The OH bond stretching vibration originates bands in the range of 3500 cm^{-1} to 3800 cm^{-1}.

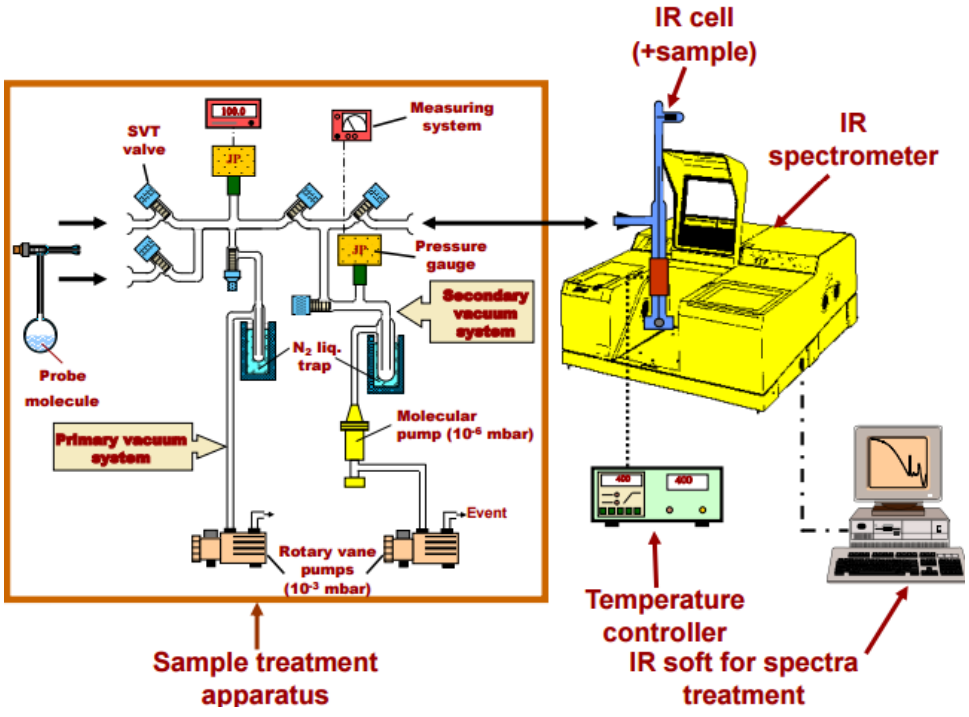

Figure 2-4. Scheme of the FTIR setup

When pyridine (Py, pK_b= 3.5) is chemisorbed on the catalyst, it can interact:

- with bridging hydroxyl groups (Brönsted acid sites) by protonation, forming pyridinium ions (PyH^+ , ~1545 cm^{-1} and 1640 cm^{-1}),
- with Lewis acid sites by coordination (PyL), giving rise to bands around 1445-1460 cm^{-1},
- with OH groups of low acid strength (~1445 cm^{-1} and 1595 cm^{-1}), as silanols and by hydrogen bond (Py….OH) [6].

Another band at ca. 1490 cm^{-1} is also present and corresponds to the interaction of pyridine both with Brönsted and Lewis acid sites and also through hydrogen bonding.

2, 6-dimethylpyridine (2,6-lutidine (Lu), or DMPy, pK_b = 8.7) which is a stronger base than pyridine, has been also used in the acidity study. LuH^+ Species (lutidinium) show IR bands in the 1630~1650 cm^{-1} range characteristic of DMPy adsorption on Brönsted active sites [8]. Moreover, the kinetic diameters of DMPy and pyridine are 0.67 nm and 0.54 nm, respectively. The size of DMPy is significantly larger than the channel diameter of zeolite ZSM-5, thus only Brönsted acid sites at the external surface of zeolite or in the pore mouth region can be reached by DMPy, while pyridine can reach all sites [6, 8, 9].

Pyridine and 2, 6-dimethylpyridine adsorption were performed on a Nicolet Magna 550-FT-IR spectrometer at 4 cm^{-1} optical resolution. Prior to the measurements, each sample was pressed into self-supporting disc (diameter: 2 cm, 13 mg) and pretreated in the IR cell attached to a vacuum line at 120 ℃ (0.33 ℃/min) for 1.5 h first and then at 500 ℃ (1.27 ℃/min) for 2 h under the pressure of 10^{-6} torr. The adsorption of pyridine and lutidine was performed at 150 ℃ temperature. After establishing a pressure of 1 Torr at equilibrium, the cell was evacuated at room temperature. In order to study the strength of the interactions between the zeolite and probe molecules, the samples were heated to 50- 400 ℃ (step 50 ℃) and the spectra were taken at each temperature. Then, the amount of Brönsted acid sites at each desorption temperature was calculated from the integrated area of the bands (after background subtraction) of adsorbed pyridine at ca. 1545 cm^{-1} and 1490 cm^{-1} or from the bands of adsorbed DMPy at 1610 and 1640 cm^{-1} using the extinction coefficients reported by Emeis [10] and Onfroy [11].

The concentration of Brönsted and Lewis acid sites was determined from the integrated areas of the bands at ca. 1545 and 1450 cm^{-1}, respectively, with the equation: $\varepsilon = AS/n$, where A (cm^{-1}) is the corresponding absorption band intensity, S (cm^2) is the surface area of a

pellet, and n (μmol) is the amount of the adsorbed substance. The outer surface acidity of the zeolites was determined by FTIR of adsorbed DMPy.

The extinction coefficients for MFI zeolites reported by Emeis [10] were the following: ε(B)1545 = 1.8 and ε(L)1454 = 1.5 cm/μmol for Pyridine; ε(B)1632–1648 = 6.8 cm/μmol for DMPyridine.

2.2.7 Solid-state ^{27}Al MAS NMR

Solid-state ^{27}Al MAS NMR spectra were recorded at room temperature in a Bruker AV-400 WB spectrometer operating at 104.2 MHz and equipped with a 4 mm Bruker BL4 mm probe. Fully hydrated samples were packed into zirconia rotors and spun at the magic angle spinning (MAS) at 10 kHz. The spectra were acquired with excitation pulses corresponding to a flip angle of $\pi/18$. Chemical shifts were referred to a 0.1 M aqueous solution of $Al(NO_3)_3$.

2.2.8. Transmission Electron Microscopy

The TEM analyses were carried out on a Jeol 2100F (field emission gun) microscope operating at 200 kV equipped with a probe corrector for the spherical aberrations. The point-to-point resolution reached was on the order of 2 Å under the parallel TEM mode and 1 Å under the STEM mode. For a better chemical resolution, the micrographs were also acquired in the HAADF mode by using a spot size of 1.1 Å with a current density of 0.5 pA $Å^{-1}$. The energy X-ray dispersive spectroscopic analyses have been performed by using a Li-Si EDS detector with an energy resolution of 0.03 eV. Prior to the analysis, the sample was dispersed by ultrasound in ethanol solution for 5 min, and a drop of solution was deposited onto a carbon membrane onto a 300 mesh-copper grid.

2.2.9. Scanning Electron Microscope

Scanning electron microscopy (SEM, Philips XL 30 ESEM-FEG) was used to explore the morphology and size of zeolite crystals.

2.2.10. N_2O decomposition method

Copper surface area and dispersion were measured using a N_2O decomposition method [12]. The catalysts (0.1 g) were first reduced upon heating to 290 ℃ in a 10% H_2/Ar mixture (40 mL/min) with a ramp of 5 ℃/min, and the temperature was maintained for 2 h. The amount of hydrogen consumed is denoted as n_1. Then, the reduced samples were cooled to 50 ℃ and purged with Ar for 30 min. The samples were exposed to 10% N_2O/Ar for 1 h to oxidize

surface copper to Cu_2O and then flushed with Ar to remove the N_2O. Finally, TPR was performed under a 10% H_2/Ar flow to reduce Cu_2O back to metallic Cu using a ramp rate of 5 ℃/min to 300 ℃. The amount of H_2 consumed is denoted as n_2. The Cu dispersion and exposed Cu surface area of the catalysts were calculated as by Eqs. (2-1) and (2-2), respectively:

$$D_{Cu} = 2\ n_2/n_1 * 100\%; \quad (2\text{-}1)$$

$$S_{Cu} = 2n_{2*}N/\ (W*14*10^{19}) \quad (2\text{-}2)$$

where D_{Cu} (%) is the dispersion of Cu, S_{Cu} (m^2/g) is the exposed copper surface area per gram catalyst, W (g) is the weight of the catalyst, N is the Avogadro's constant (6.02×10^{23} atoms/mol), and (1.4×10^{19}) is the number of copper atoms per square meter.

2.2.11. Combined time-resolved X-ray Absorption and in situ XRD analysis

Combined XRD and XAS can be regarded as complimentary techniques since XRD probes structures with long-range order whereas EXAFS is sensitive mainly to the local surroundings of the atoms in a material to obtain a more complete structural description of catalysts.

X-ray absorption spectroscopy provides the element specific structural information for crystalline and amorphous materials. With these high energy X-rays it is possible to probe the short range order (coordination sphere of about 6 Å) of crystallites, e.g. local disorder or strain in the solids. XAS with hard X-rays (> 5 keV) is insensitive to gas phase absorption and can therefore be used as an in situ technique. With these advantages it is very suitable to investigate heterogeneous catalysis under working conditions.

Figure 2-3 shows the copper metal spectra recorded at the Cu K-edge, the XAS spectrum can be divided into the two regions, XANES and EXAFS. X-ray absorption near-edge structure (XANES) provides information about valence state and local site symmetry of the absorber, while extended X-ray absorption fine structure (EXAFS) can yield atomic distances, number of surrounding atoms and identity of the nearest atoms. The position of the absorption edge is related to a specific atomic number and hence, to a certain quantum-mechanical transition that excites a particular atomic core-orbital electron to the free or unoccupied continuum levels. The nomenclature for X-ray absorption is related to this origin, for example K edges refer to transitions that excite the innermost 1s electron. The edge position can therefore, give information about valence states [13, 14]. The more oxidized the element, the higher lies the absorption edge and vice versa.

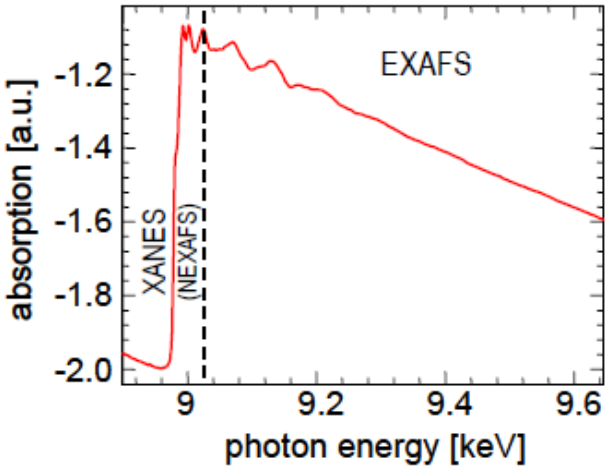

Figure 2-3. X-ray absorption spectra of copper metal at the Cu K-edge Absorption (The XAS spectrum is divided into the XANES region, before and around the absorption edge, and the EXAFS region, from the edge to the end of the spectrum [14].)

High-resolution X-ray powder diffraction (XRD) measurements were performed simultaneously with XAS measurements in the European Synchrotron Radiation Facility (ESRF, Grenoble) at the Swiss–Norwegian Beamlines (BM01B beam line). XAS spectra were acquired at the Cu and Zn K-edges in transmission mode by using a monochromatic X-ray beam (Si 111 channel-cut monochromato) and a high-resolution diffractometer.The beam current varied in a range of 100–200 mA at 6.0 GeV. A copper metal foil, and CuO powders were used as XAS references. The energy calibration was checked by measuring the spectrum of the Cu foil with the energy of the first inflection point being defined as the edge energy (8979.0 eV) [15]. XRD patterns were collected by using an Si(111) channel-cut monochromator set to a wavelength of 0.503.

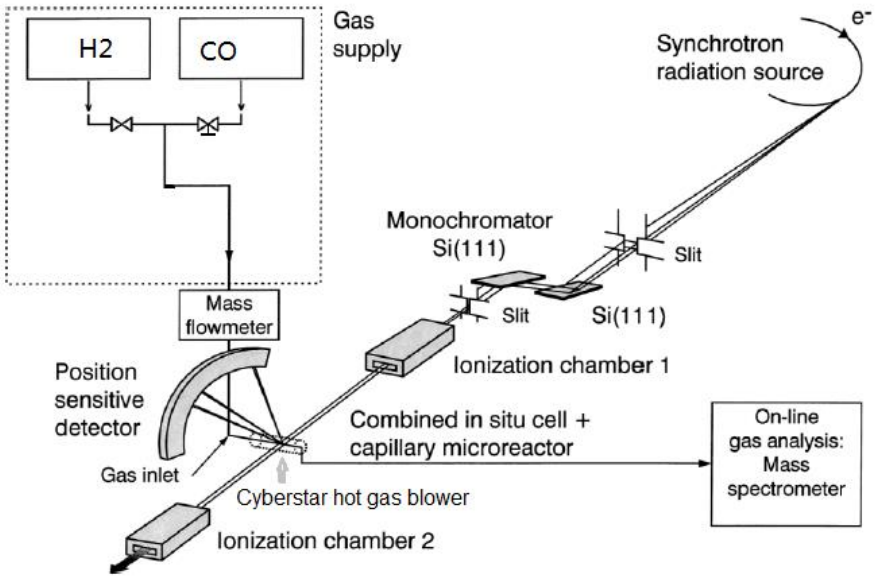

Figure 2-4. Schetch of the setup, time-resolved combined EXAFS/XRD experiments with on-line analytic analysis.

The combined in situ experiments (Figure 2-4 and Figure 2-5) were performed by using a quartz capillary micro-reactor originally developed by Clausen [16] for use with in situ XRD studies of catalysts, and further developed by Grunwaldt and co-workers at the Swiss-Norwegian Beamlines [17] (Figure 2-4). In a typical reduction or reaction process, about 5.0 mg of the catalyst together with 5.0 mg boron nitride (BN) were pressed into tablets and finally crushing them into granules (125-200 μm grain size), then loaded in a quartz capillary (OD=1 mm, wall thickness = 0.020 mm, Figure 2-6) and and pressed from both sides with quartz wool. A Cyberstar gas blower was used to control the reactor temperature.

The system was first purged with pure Helium gas, followed by reduction and reaction process. The experimental procedure was as follows:

1. XRD and XANES spectra of the fresh catalyst were acquired at room temperature.

2. The catalyst was reduced under H_2 flow (6 ml/min) heated from room temperature to 290 ℃ (dT = 5 ℃/min), then hold at 290 ℃ for 1 h. XANES scans and XRD spectra were measured until the temperature reached 290 ℃. After the temperature reached 290 ℃, EXAFS scans and XRD spectra were acquired.

3. Cooling down to 40 ℃, the gas feed was switched to the reaction mixture (CO: H_2 =2 ml/min: 4 ml/min), the pressure was increased to 20 bars.

4. The temperature was ramped up to reaction temperature 260 ℃ (dT = 5 ℃/min) while acquiring XANES spectra. When the temperature was stable at 260 ℃, XANES scans and XRD spectra were performed.

5. The temperature was reduced to room temperature .EXAFS scans was acquired.

XANES data analysis was performed by using the Athena and Artemis interfaces of the IFEFFIT software [18]. The spectra were energy calibrated, normalized and background-subtracted. The k^3-weighted EXAFS spectra were Fourier-transformed in the k-range of 2.5-12.0, with modified Hanning windows, dk = 1.0 $Å^{-1}$, and an R range from 1.2 to 2.7 Å using single path standards generated by FEFF (version 8.0) program [19].

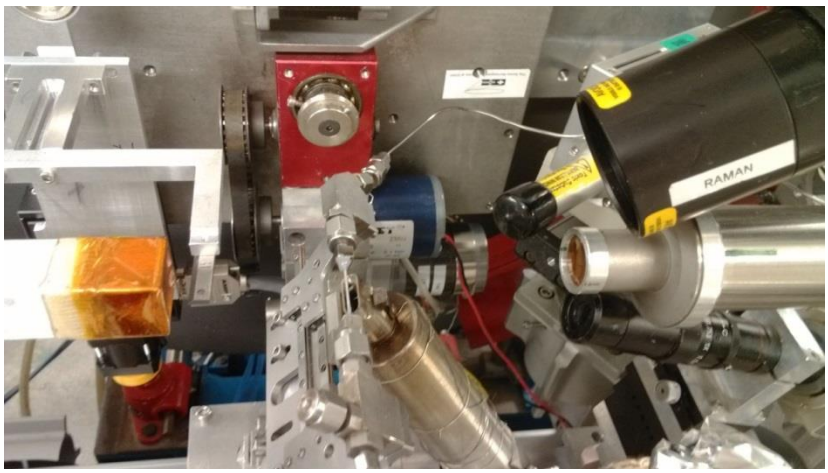

Figure 2-5. Setup used for the synchrotron measurements

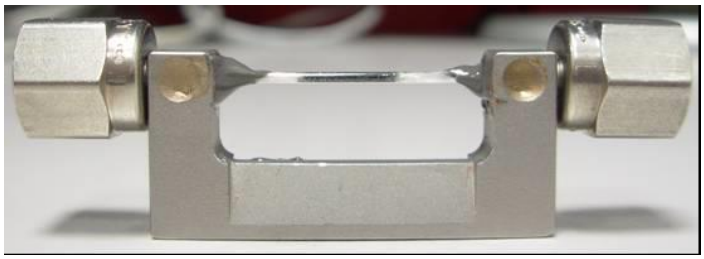

Figure 2-6. In situ XAS cell

2.2.12. Temperature programmed oxidation

Temperature programmed oxidation (TPO) was used to characterize and to quantify the coke deposited on spent catalysts. TPO were performed as follows. 50 mg of catalyst were placed in a plug flow reactor. The catalyst was first pretreated in pure He flow at 150 ℃ for 120 min with subsequent temperature increase to 800 ℃ with the ramp of 10 ℃/min in a He/O_2 (10% O_2) flow of 50 cm^3/min. CO_2 (m/e = 44) profiles were recorded using a Varian Saturn III mass spectrometer.

2.3 Catalytic measurements

2.3.1 Setup for DME synthesis reaction

The DME synthesis reaction was carried out in a fixed-bed stainless-steel tubular micro-reactor (d_{int} =8 mm) operating at high pressure. The schema for catalytic measurements is shown in **Figure 2-7**. The catalyst was crushed and sieved to obtain catalyst grains 63 - 200 μm in diameter. The hybrid catalyst loading was typically 0.5 g. Before reaction, the samples were reduced in hydrogen flow with the flow rate of 30 ml/min, and the temperature was

increased to 290 ^{o}C with a heating rate of 1 ^{o}C / min, then hold in this temperature for 6 h. The thermocouple was in direct contact with the catalyst, so that the thermocouple measurements could reflect the temperature inside the reactor. No temperature spike and temperature swings were observed during the whole catalytic testing. After reduction, the gas flow was switched to premix H_2/CO molar ratio of 2/1. The reaction was carried out at 260 ^{o}C under a pressure of 30 bar maintained using a back pressure regulator, and the gas hourly space velocity (GHSV) of 3600 ml/g/h. All experimental data were obtained under steady-state conditions that were usually maintained for 5 h. Carbon monoxide contained 5 % nitrogen, which was used as an internal standard for conversion and selectivity calculation purposes. Before any run the reactor system was first pressure- tested with inert gas (nitrogen or argon) under the planned operating conditions to check for any possible leak of gas along the reactor and piping.

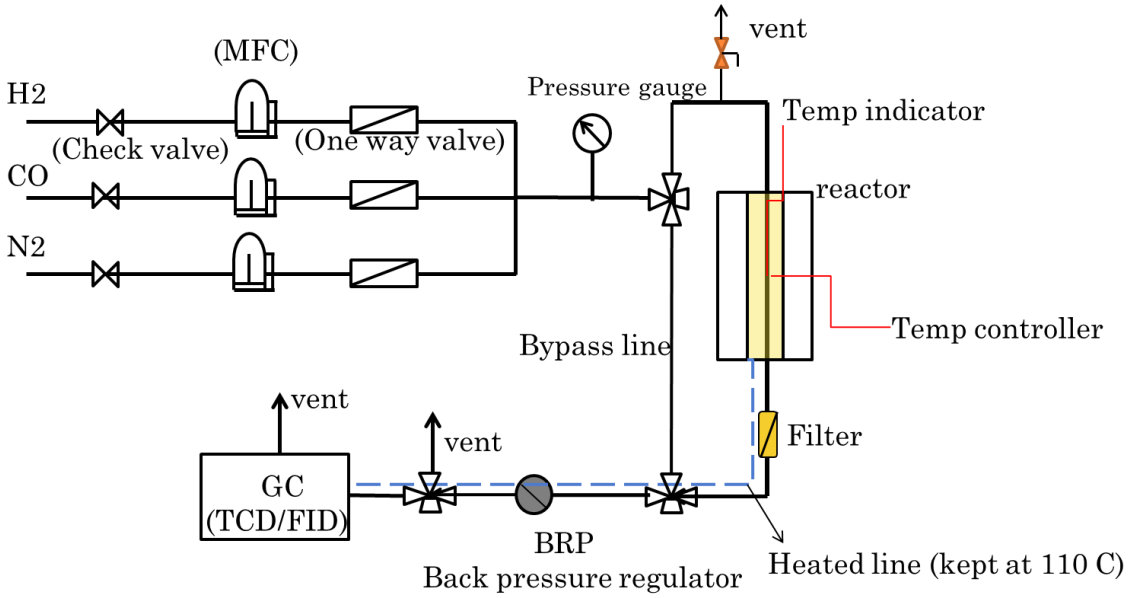

Figure. 2-7. Schematic diagram of the reaction system

The methanol synthesis reaction was carried out using the same setup. The reaction conditions were also maintained the same as DME synthesis.

The catalytic performance for methanol dehydration was investigated in the temperature range of 200-280 ^{o}C using a feed composition consisting of 30 % CH_3OH (in He). In a typical experiment, an amount of 250 mg of fresh catalyst was placed in the reactor, heated at 500 ^{o}C under He flow and left at that temperature for 1 hour. The flow was then switched to the reaction mixture, the catalyst was conditioned under reaction conditions at 200 ^{o}C for 3 hours, then the temperature was increased to 220 ^{o}C with the heating ramp of 1 ^{o}C/min, hold

at 220 ^{o}C for 3 hours to check the catalytic performances. The same procedures were repeated at 240, 260, and 280 ^{o}C, and the concentrations of reactants and products at the reactor effluent were determined using the analysis system described above. In all cases, the catalytic results were obtained after the system had reached steady state conditions and data points presented are averages of at least three injections. The experiments were conducted at pressure of 10 bars and under a total flow rate of 20 cm^3/ min, which corresponds to a gas hourly space velocity (GHSV) of 4800 ml/g_{cat}/h.

The water gas shift (WGS) reaction was carried out at 260 ^{o}C and atmospheric pressure in a continuous fixed-bed reactor packed with 0.5 g of the Cu-based catalyst. Prior to each experiment, the catalyst was reduced for 6 h at 290 ◦C in an H_2 flow of 30 mL/ min. Then He saturated by pure water (0.01 ml/min water in 20 ml/min He) was used as feed with the space velocity (GHSV) of 3600 ml/g_{cat}/h. Moreover, CO with the flow rate of 10 ml/min was introduced to the reactor for the water gas shift reaction. The performance of the catalysts was measured after 2 h time on stream (TOS) for each experiment. The analysis of the reaction products was carried out on-line using a gas chromatograph (Varian 450) equipped with a TCD detector.

2.3.2 Analytical method

The GC technique was used to determine the composition of reaction products. The gas product coming from the reactor flows through the GC column via an automatic dix-way sampling valve, which allows the gas to pass through the injector, which vaporizes the sample, after which the carrier gas conveys it to the column for separation into its components identifiable by the detector.

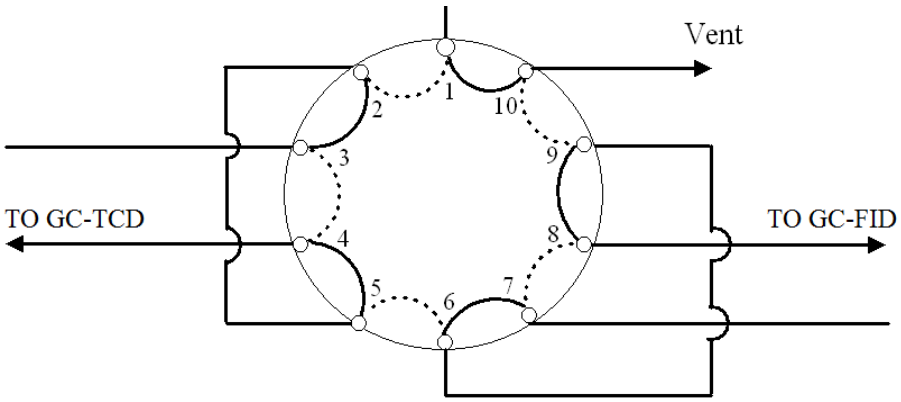

Figure 2-8 The dix-way sampling valve

The sampling valve operates as shown in Figure 2-8. In dotted line position, the sample enters the sampling loop and is then vented (sequence 1-2-5-6-9-10), while the carrier gas flows through to the column (sequence 3-4 and 7-8). The solid lines correspond to position of the valve when a portion of the sample is retained in the sample loop and transported by the carrier gas into the column for GC-TCD analysis (sequence 3-2-5-4) and GC-FID analysis (sequence 7-6-9-8), whereas the fresh sample is vented (sequence 1-10).

The gaseous products are identified while they pass through the detector at a specific rate. The gas that moves most rapidly is the first to be detected, while the others are identified in a sequence dictated by the amount of time that elapses between injection and their becoming detectable (retention time). The detector is connected to a digital read-out that transforms the signal generated by the contact gas detector into a chromatogram that is shown on the computer screen. The area of the peaks on the chromatogram indicates the amount of the gas that is being analyzed.

The retention time of the products depends on the type of column used for the analysis and the operating conditions of the GC. A capillary column WCOT fused silica CP-Sil5CB (30 M × 0.53 mm, CP8735) was used on the FID for the detection of oxygenate and hydrocarbon compounds, while a CTR-1 column on the TCD enabled the researcher to identify the components of the synthesis gas, CO, CO_2, CH_4 and N_2. The carrier gas used was Helium.

2.3.3 Calculation of conversion and selectivities

2.3.3.1 Calculation of CO conversion

The mass flow controllers placed in the inlet stream before it reached the reactor measured the inlet volumetric flow rate and from this the molar flow rates F_{in}, were determine. The bubble meter placed in the outlet stream after it left the reactor was used to calibrate the flow meter.

The outlet molar flow rate was established by applying the following equation:

$$F_{in} * (Q_{N2,\,in}) = F_{out} * (Q_{N2,out}) \qquad (2\text{-}3)$$

Where F_{in} is the total molar flow rate (moles/min) of the inlet stream of the reactor; F_{out} is the total molar flow rate (moles/min) of the reactor outlet gas stream; ($Q_{N2,\,in}$) is the mole fraction of nitrogen in the inlet stream of the reactor; and ($Q_{N2,\,out}$) is the mole fraction of nitrogen in the outlet gas stream of the reactor.

The molar flow rate of CO in the feed stream F_{CO}, in and molar flow rate of CO in the product stream $F_{CO,out}$ were defined respectively as:

$F_{CO,\,in} = F_{in} * (Q_{CO,in})$ (2-4)

$F_{CO,\,out} = F_{in} * (Q_{CO,out})$ (2-5)

The conversion of CO, X_{CO} was evaluated using the following equation:

$X_{CO} = (F_{CO,in} - F_{CO,out})/F_{CO,in}$ (2-6)

The carbon monoxide concentrations in the gas flow were detected by TCD. The peak area of CO, which was detected at the outlet of the reactor and marked as S_{CO}, corresponded to the following relationship:

$$S_{CO} = R_{CO} * Q_{CO} \quad (2\text{-}7)$$

where Q_{CO} was the concentration of CO and R_{CO} is the response coefficient of carbon monoxide in TCD. In order to have a reliable measurement, nitrogen, which was inert in the reaction, was chosen as an internal standard. The concentration of N_2 (Q_{N2}) was determined at the same time as that of CO by TCD. The peak area of N_2 (S_{N2}) and response factor of N_2 in TCD (S_{N2}) obey the relationship:

$$S_{N2} = R_{N2} * Q_{N2} \quad (2\text{-}8)$$

At the end or at the beginning of the test, we could measure the peak area of CO and N_2 at ambient temperature, and calculate the ratio of S^{o}_{CO}/S^{o}_{N2}. The initial flow of CO before reaction could be determined by this ratio:

$$F_{CO,\,in} = F_{N2,in} * Q_{CO,in}/Q_{N2,in} \quad (2\text{-}9)$$

When the reaction starts, the flow of carbon monoxide at the reactor outlet drops, while the flow of N_2 remains unchanged ($F^{o}_{N2} = F^{t}_{N2}$). The flow of carbon monoxide at the reactor outlet can be defined by:

$$F_{CO,out} = F_{N2,in} * Q_{CO,out}/Q_{N2,out} \quad (2\text{-}10)$$

$Q_{CO,in}$, $Q_{CO,out}$, $Q_{N2,\,in}$ and $Q_{N2,out}$ can be substituted by relevant peak areas using Eqs. (2-7) and (2-8). The conversion of CO could be then calculated by the following equation:

$$X_{CO}(\%) = \left(1 - \frac{S^{o}_{N_2} \times S_{CO}}{S^{o}_{CO} \times S_{N_2}}\right) \times 100 \quad (2\text{-}11)$$

2.3.3.2 Products distribution

The product distribution was analyzed through a series of peaks obtained by flame ionization detector (FID). The area of each peak (A_i) is proportional with the concentration (Q_i) of the product "i", which obeys the following relationship:

$$A_i = R_i * Q_i \quad (2\text{-}12)$$

Where R_i is the response factor of the product "i" in FID.

The product selectivity (S_i) was reported on carbon basis:

Product selectivity (Sel $_{product}$, C-mol %) = (moles of carbon in the product/total moles of carbon in the products)* 100%;

$$S_i = \frac{i * n_i}{n_{co}^{in} - n_{co}^{out}} \times 100\%$$

$$S_{CO2} = \frac{F_{CO2}^{out}}{F_{CO}^{in} \times X_{CO}} = \frac{R_{CO2} \times A_{CO2}^{out}}{R_{CO} \times A_{CO}^{out}} \times \frac{F_{CO}^{in} \times (1 - X_{CO})}{F_{CO}^{in} \times X_{CO}} = \frac{R_{CO2} \times A_{CO2}^{out}}{R_{CO} \times A_{CO}^{out}} \times \frac{(1 - X_{CO})}{X_{CO}} \times 100\%$$

where $n_{co}^{in}, n_{co}^{out}$ is the mole flow rate of CO in and out of the reactor;

n_i is the mole flow rate of formed product; i: number of carbon atoms in the product.

2.4 References

[1] C. Busetto, G. Del Piero, G. Manara, F. Trifiro, A. Vaccari, Journal of Catalysis, 85 (1984) 260-266.

[2] C. Berger, A. Raichle, R.A. Rakoczy, Y. Traa, J. Weitkamp, Microporous and mesoporous materials, 59 (2003) 1-12.

[3] S. Van Donk, A.H. Janssen, J.H. Bitter, K.P. de Jong, Catalysis Reviews, 45 (2003) 297-319.

[4] T. Reitz, S. Ahmed, M. Krumpelt, R. Kumar, H. Kung, Journal of molecular catalysis A: chemical, 162 (2000) 275-285.

[5] A.S. Al-Dughaither, H. de Lasa, Industrial & Engineering Chemistry Research, 53 (2014) 15303-15316.

[6] G. Crépeau, V. Montouillout, A. Vimont, L. Mariey, T. Cseri, F. Maugé, The Journal of Physical Chemistry B, 110 (2006) 15172-15185.

[7] R. Borade, A. Sayari, A. Adnot, S. Kaliaguine, The Journal of Physical Chemistry, 94 (1990) 5989-5994.

[8] J.A. Lercher, A. Jentys, Studies in surface science and catalysis, 168 (2007) 435-476.

[9] F. Thibault-Starzyk, I. Stan, S. Abelló, A. Bonilla, K. Thomas, C. Fernandez, J.-P. Gilson, J. Pérez-Ramírez, Journal of Catalysis, 264 (2009) 11-14.

[10] C.A. Emeis, Journal of Catalysis, 141 (1993) 347-354.

[11] T. Onfroy, G. Clet, M. Houalla, Microporous and mesoporous materials, 82 (2005) 99-104.

[12] J.W. Evans, M.S. Wainwright, A.J. Bridgewater, D.J. Young, Applied Catalysis, 7 (1983) 75-83.

[13] M.M. Günter, T. Ressler, R.E. Jentoft, B. Bems, Journal of Catalysis, 203 (2001) 133-149.

[14] A.A. Markowicz, R.E. Van Grieken, A. Markowicz, Handbook of X-ray Spectrometry, Dekker, 2002.

[15] P. Kurr, I. Kasatkin, F. Girgsdies, A. Trunschke, R. Schlögl, T. Ressler, Applied Catalysis A: General, 348 (2008) 153-164.

[16] B.S. Clausen, B. Lengeier, B.S. Rasmussen, Journal of Physical Chemistry, 89 (1985) 2319-2324.

[17] J.D. Grunwaldt, A.M. Molenbroek, N.Y. Topsøe, H. Topsøe, B.S. Clausen, Journal of Catalysis, 194 (2000) 452-460.

[18] E.A. Stern, M. Newville, B. Ravel, Y. Yacoby, D. Haskel, Physica B: Condensed Matter, 208–209 (1995) 117-120.

[19] A. Ravel, M. Newville, Journal of synchrotron radiation, 12 (2005) 537-541.

Chapter 3. Optimization of the Cu/ZnO/Al_2O_3/ZSM-5 hybrid catalysts and operating conditions for direct synthesis of Dimethyl Ether from syngas

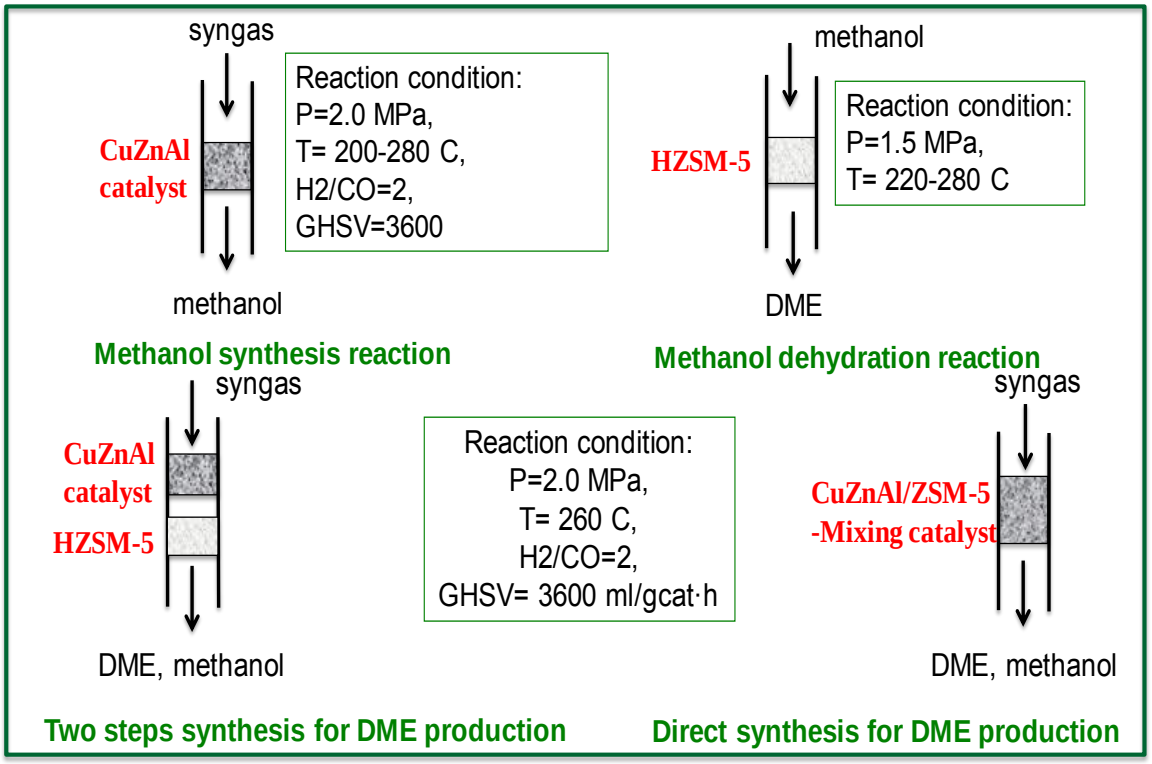

3.1 Introduction

Traditionally, DME is produced from methanol dehydration [1, 2]. However, recently Syngas to DME (STD) processes have been developed for direct DME synthesis over hybrid catalysts containing two functionalities of active sites; metallic sites for methanol formation and acidic sites for methanol dehydration. A highly integrated catalyst system is therefore required that combines the methanol synthesis and methanol dehydration catalysts in a close proximity, for optimum efficiency to get the good activity and DME selectivity [3-5].

Copper based catalyst, mostly $CuO\text{-}ZnO\text{-}Al_2O_3$ (abbreviated as CZA) catalyst, is very active for methanol synthesis, and is used at large scale in petrochemical industry [6, 7]. Considerable amount of research has been done in optimization of the Cu/Zn ratio, catalyst synthesis and processing conditions while preparing CZA catalyst. In CZA catalysts, conversion of syngas to methanol depends on the copper metal surface area. ZnO plays intact role in maintaining active copper metal species by exposing higher number of active sites to reactant molecules; alumina is used to promote the surface area, dispersion and high resistance to the catalyst. As is well known, the CZA catalyst is not only useful for methanol synthesis, but is also active in the WGS reaction [8, 9].

Solid acid catalyst such as γ - Al_2O_3, silica-alumina composites and zeolites such as HZSM-5, HY, HMCM-49, HMCM-22, Ferrierite, silicoaluminophosphates (SAPO) and heteropolyacid are known for methanol dehydration. Among them, HZSM-5 is widely employed due to following advantages: high activity at moderate reaction temperature (thermodynamically favorable), hydrothermal stability and hydrophobic nature (not sensitive to the water formed during dehydration reaction thus preserving the acid sites active for continuous operation) [10]. In addition to the nature and strength of acidity, temperature also plays an important role in product selectivity as by products (e.g. hydrocarbons) are expected at higher temperature. In direct DME synthesis from syngas over hybrid catalyst, the byproduct hydrocarbons (HCs) is a series of reactions by which methanol is first synthesized from syngas, followed by methanol dehydration to DME, and then DME further dehydrated to light olefins at strong acid sites of solid acid catalysts, ultimately, the olefins are converted to HCs over Cu based catalyst with H_2 [11].

The crucial issue for the preparing a high-active hybrid catalyst is optimizing the composition and reaction conditions of two functional components. It has been demonstrated that there are various factors such as temperature, pressure, proximity and ratio of bi-

functional catalyst and acid fraction which influence the conversion of CO, selectivity of DME, and product distribution in the DME synthesis.

In this chapter, direct synthesis of DME from syngas was studied by using the conventional CZA, H-form of zeolite (H-ZSM-5), and hybrid bi-functional catalyst. A physical mixing method, which keeps the active sites free from any detrimental interaction of individual component of bi-functional catalyst, was adapted for the preparation of hybrid bi-functional catalyst. The detailed information of CZA catalyst synthesis is shown in Chapter 2, section 2.1.1. The as prepared catalyst was evaluated in direct DME synthesis to find the optimized reaction conditions. Moreover, the catalytic activity under various reaction conditions was also discussed. The structures of the catalysts were characterized by N_2 adsorption-desorption, X-ray diffraction (XRD), TPR, TPD-NH_3, and correlated to the activity toward DME synthesis. The chemical and physical properties of fresh and deactivated catalysts, such as surface area, Cu crystal size, and acidity by using N_2 adsorption-desorption, and XRD were investigated. The reasons for deactivation of the CZA-ZSM-5(13) hybrid catalyst for DME synthesis are also discussed.

3.2 Results

3.2.1 Chemical and physical properties of the CZA -ZSM-5(13) catalysts

Table 3-1 The physicochemical properties of the CZA and CZA-ZSM-5(13) catalyst

Sample	BET surface area [a] (m^2/g)	H_2 comsumption[b] (mmol H_2/g cat)	Cu surface area[c] (m^2_{Cu}/g_{cat})	Average crystal size d_{CuO} (nm)[d]
CZA-calcined	97.6	6.88	36.2	8.0
CZA-deactivated	64.2	-	21.3	14.8
CZA/ZSM-5(13)	245.6	4.15	23.5	7.6

a, the surface area was determined by N_2 physisorption;
b, H_2 comsumption was calculated by TPR;
c, N_2O decomposition was employed to measure the metallic copper surface area;
d, CuO and Cu crystal size calculated with Scherrer equation at 38.7^o and 43.2^o respectively.

The detailed physicochemical properties of the CZA catalyst and CZA-ZSM-5(13) hybrid catalyst are listed in Table 3-1. The BET surface area of the CZA catalyst was 97.6 m^2/g and the value is consistent with reported data for CZA prepared through co precipitation digestion method [6]. After physically mixed with high surface area HZSM-5, the bi-functional CZA-ZSM-5(13) catalyst showed a total surface area 245.6 m^2/g. The Cu surface

area measured by the titration of Cu surface atoms with N_2O was found to be 38.2 m^2_{Cu}/g_{cat} and 23.5 m^2_{Cu}/g_{cat} for CZA catalyst and CZA-ZSM-5(13) hybrid catalyst, respectively.

It is widely reported that easier reduction of copper species plays an important role in methanol synthesis. Hence, it is rather important to preserve the reduction behavior in hybrid catalysts. Any interaction between CZA and ZSM-5(13) during the preparation might result in harder reducibility of copper species. The reduction behavior of CZA and CZA-ZSM-5(13) was characterized by H_2-TPR. The corresponding reduction profiles are depicted in Figure 3-1.The H_2-TPR profile of CZA showed a main H_2 consumption feature peaking at temperature in the 200 - 350 ^oC range associated to the reduction of CuO species to metallic Cu^0 in one step [1]. A similar reduction behavior is observed in the CZA-ZSM-5(13) hybrid catalyst. This ensures that the active sites of CZA are free from any detrimental interaction during the physical mixing with ZSM-5(13). Further, this can be confirmed by comparing the H_2 consumption on the CZA and CZA/zeolite hydrid catalysts. Table 3-1 clearly shows that the zeolite has no influence on the overall reducibility of the bifunctional catalysts and the physical mixing preparation method preserves the CZA component.

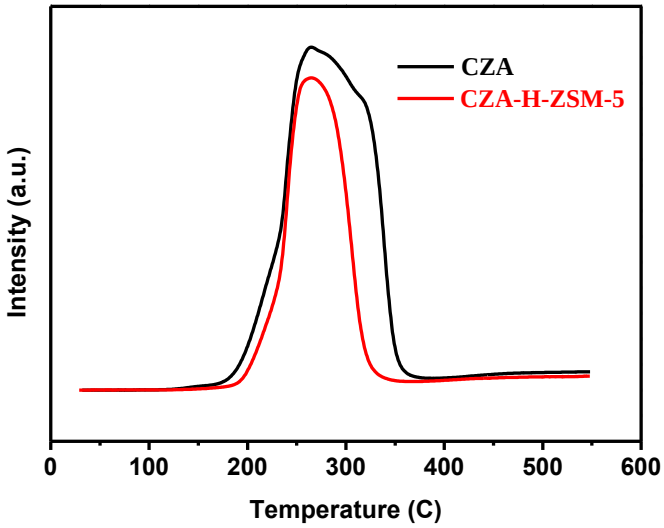

Figure 3-1. TPR profile of the CZA and CZA-ZSM-5(13) catalyst

Fig. 3-2 shows XRD patterns of methanol synthesis catalyst (CZA), dehydration zeolite catalyst (ZSM-5(13)) and bifunctional systems (CZA-ZSM-5(13)). The diffraction patterns of the CZA catalyst show two strong peaks at 2θ = 35.5 ° and 38.7 °, which are the characteristic reflections of CuO [2, 14]. ZnO has not been detected by XRD. This suggests its strong interaction with the existing CuO phase. No reflections due to Al_2O_3 were also observed, suggesting that the Al_2O_3 phase may be in the amorphous state. For the

bifunctional CZA-ZSM-5(13) catalyst, the two distinct peaks at 2θ = 35.6° and 38.6° represent the well-dispersed CuO species in CZA composite of hybrid catalyst. In addition, the typical diffraction peaks in 2θ at 7.5-10^{o} and 21–25^{o} of MFI crystalline phase were also observed in the hybrid catalyst [4]. This suggests that there is no strong interaction between CZA and ZSM-5(13) leading to mixed phases [20]. The CuO crystallite size calculated through Scherrer's equation over CZA and CZA-ZSM-5(13) is found to be similar as shown in Table 3-1. These results are in consistent with the H_2-TPR result proving that the structure of CZA and ZSM-5(13) remain unchanged in the hybrid catalyst prepared through physical mixing method.

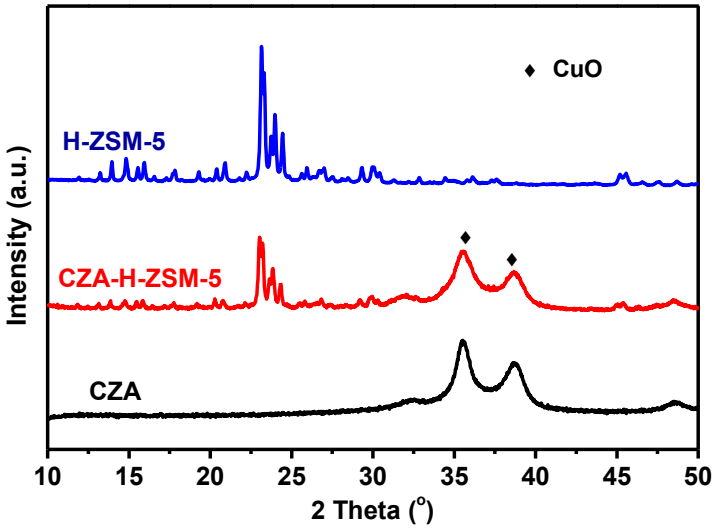

Figure 3-2 XRD patterns of CZA, H-ZSM-5(13), and hybrid catalyst CZA-HZSM-5(13)

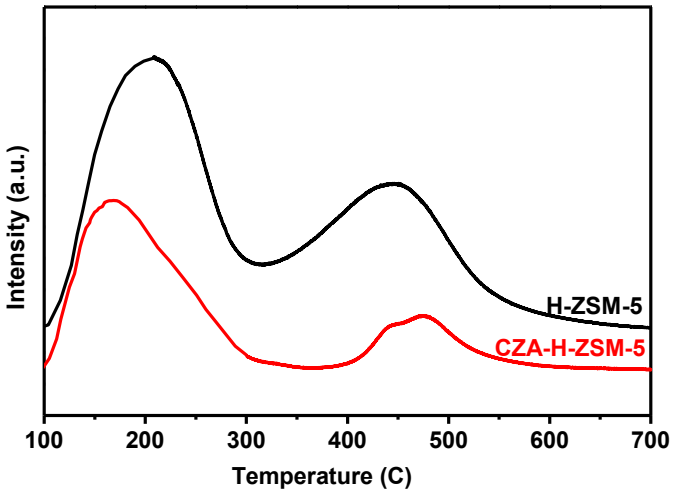

Figure 3-3 NH_3-TPD profiles for HZSM-5(13) and CZA-HZSM-5(13)

The acidic properties of the catalysts were also investigated using temperature programmed desorption (TPD) with NH_3 as a probe molecule. Figure 3-3 shows the NH_3-TPD profiles of ZSM-5(13) and CZA-ZSM-5(13) catalysts. In both samples, two peaks can be observed at around 195 ℃ (T_1) and 430 ℃ (T_2), corresponding to NH_3 desorbing from the weak and strong acid sites, respectively [15, 16]. The quantities (millimoles) of ammonia desorbed at lower and higher temperatures as a result of weak and strong acidity are shown in Table 3-2. The CZA-ZSM-5 sample had a total adsorption capacity of 1.01 mmol $NH_{3/}$ g_{cat}.

Table 3-2. The acidity of the ZSM-5(13) and CZA-ZSM-5(13) catalysts

Catalyst	Peak Ⅰ		Peak Ⅱ		Total acidic sites (mmol NH_3/g)
	T_1 (℃)	Acidic sites (mmol NH_3/g)	T_2 (℃)	Acidic sites (mmol NH_3/g)	
HZSM-5(13)	205.6	0.116	433.8	0.083	0.199
CZA-ZSM-5(13)	178.8	0.0732	471.6	0.0163	0.0895

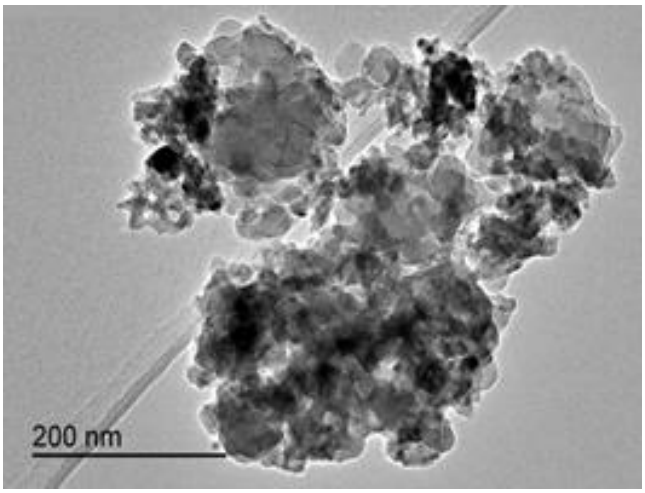

Figure 3-4 TEM micrographs of the CZA-ZSM-5(13) bifunctional catalyst

To ascertain the morphological features, the hybrid CZA-ZSM-5(13) catalyst was studied by TEM analysis. A representative image of CZA-ZSM-5(13) is shown in Figure 3-4. A closer look reveals the spherical particles of CZA comprised over zeolite crystals with square shaped morphology typically known for ZSM-5 crystals. Further, Figure 3-4 confirms the existence of isolated structures of CZA methanol synthesis catalyst and ZSM-5(13) solid acid counterpart without any intimate chemical interaction [4].

In order to examine the copper species evolution during the reduction treatment, X-ray adsorption spectra (Figure 3-5) were measured during the in situ reduction of CZA and CZA-

ZSM-5(13) materials in the presence of H_2 from room temperature to 290 ℃. This information was also used to confirm the attribution of the TPR peaks.

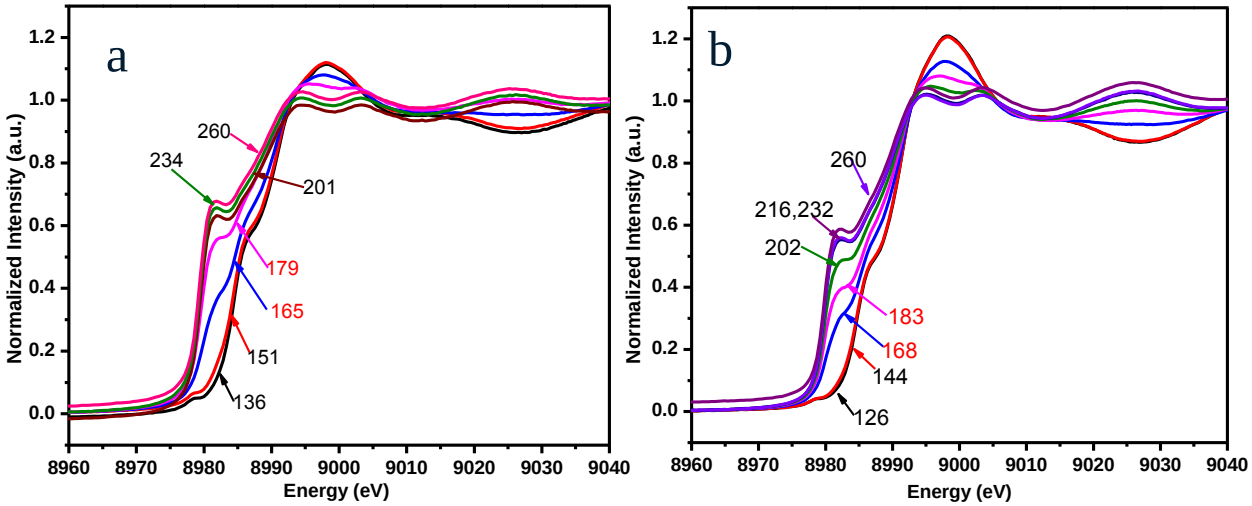

Figure 3-5. Temperature evolution of the Cu K-edge XANES spectra during the in situ reduction of CZA (a) and CZA-ZSM-5(13) (b) in the presence of H_2 from room temperature to 260 ℃

Figure 3-5 shows the stacked background subtracted and normalized XANES spectra measured in situ during the reduction of CZA from room temperature up to 260 ^{o}C. At the low reduction temperature, the Cu^{2+} XANES spectra of CZA catalyst showed a shoulder peak at 8987.6 eV and a wide post-edge peak at 8999.1 eV assigned to the 1s → 4p transition of Cu^{2+} [17]. This feature is characteristic of the presence of CuO in CZA catalyst, wherein Cu^{2+} exists in a distorted octahedral coordination, After the reduction temperature was increased to 210 ℃, a small peak at 8983.0 eV was seen in the Cu K-edge XANES spectra of CZA catalyst, which can be attributed to O_h (octahedral) FCC symmetry of metal Cu in CZA catalyst, as well as two weak lobes in the post-edge region at 8995.6 and 9004.9 eV [18]. This suggests that reduction of the copper oxide into copper metal starts at a temperature close to 165 ^{o}C and is almost completed at 210 ^{o}C as the progressive transformation of the Cu^{2+} XANES spectra into Cu metal has been observed for both CZA and CZA-ZSM-5(13) catalysts.

3.2.2. Catalyst activity testing

3.2.2.1. Methanol synthesis reaction over CZA catalyst

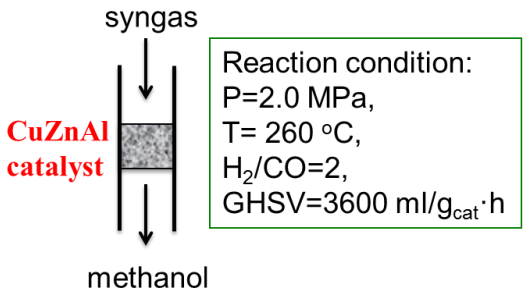

Scheme 3-6 Methanol synthesis reaction over CZA catalyst

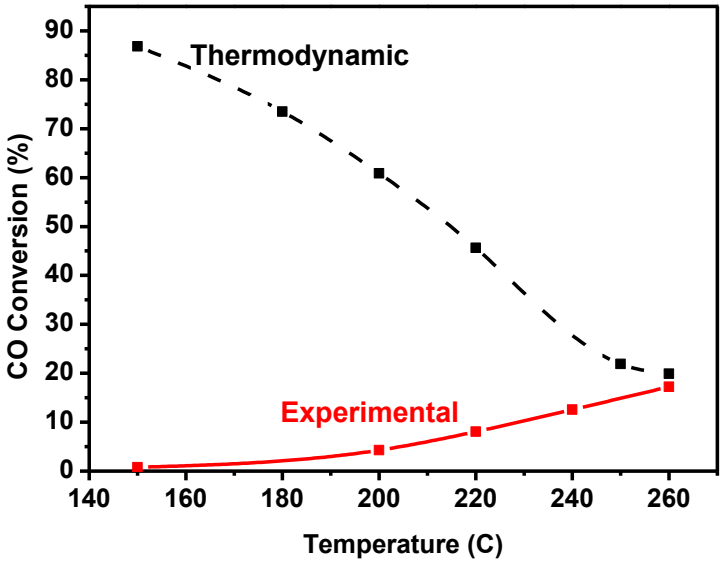

Figure 3-7. Comparison of theoretical equilibrium conversion and experimental CO conversion for CZA at 2.0 MPa. The catalyst was reduced in pure H_2 at 290 ℃, catalyst weight: 250 mg, GHSV= 3600 ml g^{-1} h^{-1}, H_2/CO = 2.

The experimentally observed CO conversion on CZA in the temperature ranges from 150 to 260 ℃ is shown in Figure 3-7. For comparison, theoretical equilibrium conversion at different temperatures has also been given. For accuracy, the activity test was carried out at each point under steady state conditions. As shown in Figure 3-7 the CO conversion increased as a function of temperature as a result of faster kinetics and approached the theoretical equilibrium value at 260 ℃. CO conversion on CZA resulted in methanol as the main reaction product with the [5] byproduct ethanol and CO_2. Figure 3-8 displays the CO conversion as a function of time on stream using CZA catalyst at 260 ℃ during a period of nearly 100 hours. CO conversion decreased from 17.0 to 13.8 % within the first 50 h of the

reaction, but after that time no significant decrease in the activity was observed until 100 h. This deactivation phenomenon could be a typical problem for methanol synthesis catalysts [6, 20]. The predominant path of deactivation is related to the thermal sintering of the metallic copper particles reducing the active surface area of copper responsible for methanol synthesis. This deactivation mechanism was proven by the results of XRD and Cu surface area of CZA catalyst before and after methanol synthesis reaction (Table 3-1 and Figure 3-9).

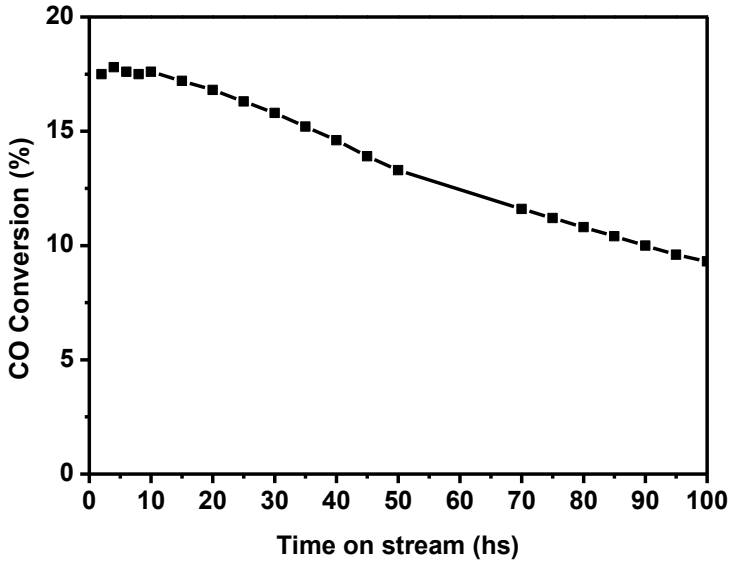

Figure 3-8. Deactivation behavior of CZA catalyst for methanol synthesis. Experimental conditions: T= 260 ℃, P = 2.0 MPa, GHSV= 3600 ml g_{cat}^{-1} h^{-1}, H_2/CO = 2.

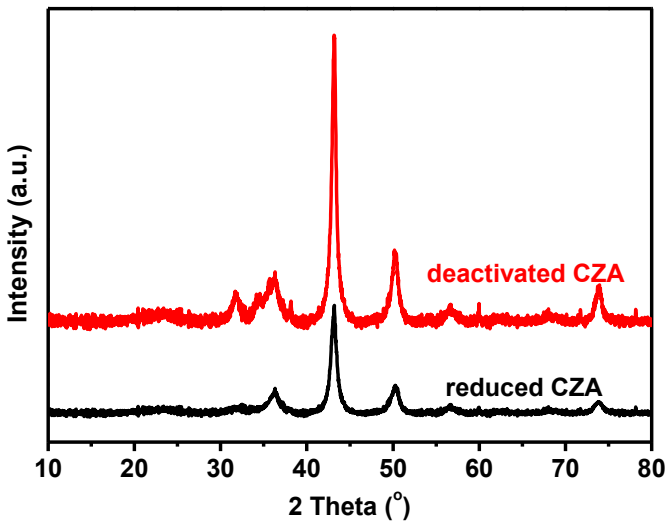

Figure 3-9. XRD patterns of reduced and deactivated CZA catalysts

The XRD patterns of the reduced and deactivated CZA catalysts are shown in Figure 3-9. The XRD peaks of Cu (at 43.2 °,50.4 °, and 74.1 °) and ZnO (at 36.3 ° and 56.7 °) are

observed in the reduced CZA sample, indicating that CuO in methanol synthesis CZA catalyst was reduced completely to Cu. Cu_2O was not detected by XRD. Note that the Cu XRD peaks in the deactivated sample were much narrower and sharper in appearance than those of the reduced counterpart. According to the Scherrer's equation, the crystal sizes of Cu are calculated to be 8.7 nm and 14.8 nm in reduced and deactivated CZA catalysts respectively, indicating that the Cu particles were sintered during the reaction. This was in accordance with Twigg et al.'s [21] study which suggests that copper sintering can be one of the deactivation mechanisms of methanol synthesis catalyst.

3.2.2.2 Methanol dehydration over ZSM-5(13) catalyst

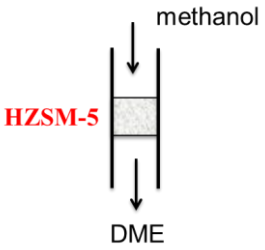

Scheme 3-10 Methanol dehydration reaction over HZSM-5 zeolite

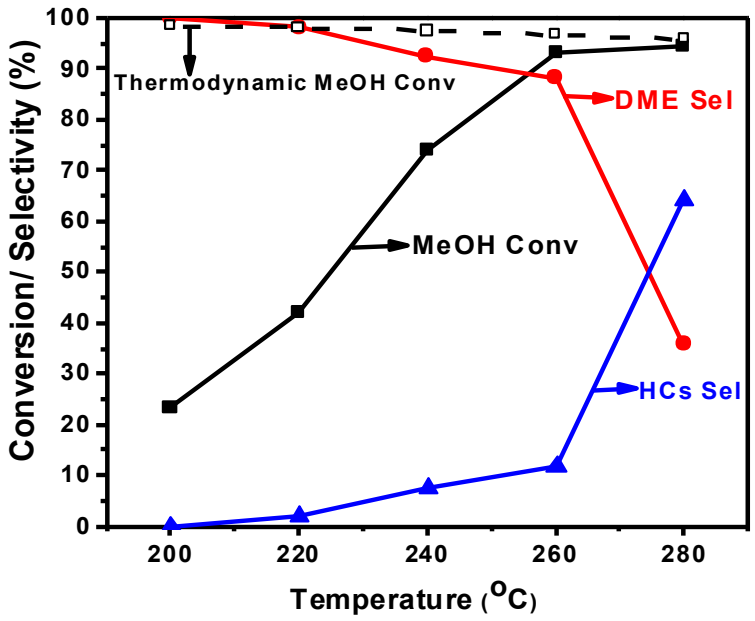

Figure 3-11. The effect of reaction temperature on the conversion of MeOH and the selectivity of DME over HZSM-5 catalyst in methanol dehydration to DME reaction at P = 10 bar, GHSV = 4800 ml g_{cat}^{-1} h^{-1}

The ZSM-5(13) zeolite was also evaluated in dehydration of methanol reaction (scheme 3-10). The conversions of methanol and selectivities to DME over ZSM-5(13) versus reaction temperature are shown in Figure 3-11. As the reaction temperature increased from 200 °C to 280 ℃, the methanol conversion on ZSM-5(13) zeolite increased and achieved nearly 95.0 % However, byproducts such as olefins (mainly $C_{2=}$ - $C_{4=}$) were detected when the reaction temperature was higher than 220 ℃, moreover, the DME selectivity decreased significantly to 35.8 % when the reaction temperature reaches 280 ℃, indicating that the side reaction such as further dehydration of DME to light olefins occurred at high temperature as MTO process due to the strong acid sites of ZSM-5(13) zeolite as evident in the NH_3-TPD results (see Figure 3-3). Considering the methanol conversion and DME selectivity, the optimal temperature of methanol dehydration seems to be 260 ℃, in terms of DME yield.

3.2.2.3. DME synthesis with the dual-catalyst bed reactor containing CZA and ZSM-5(13) catalyst

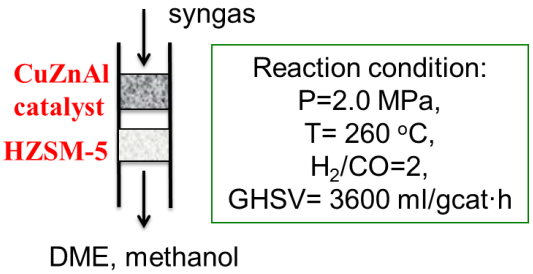

Scheme 3-12 DME synthesis with the dual-catalyst bed reactor

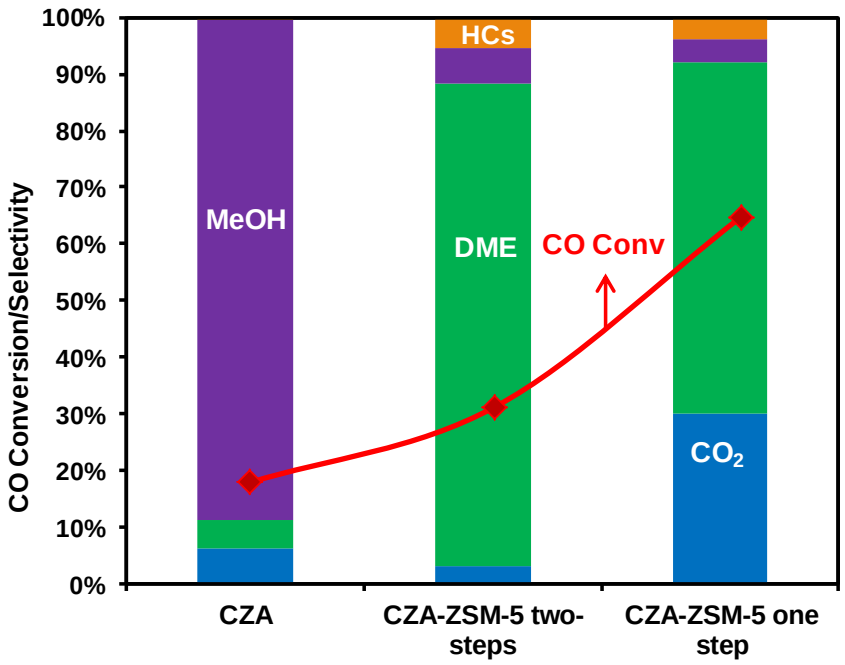

Figure 3-13. CO conversions and product distributions in T = 260 ^{o}C, P = 2.0 MPa, H_2/CO = 2, GHSV= 3600 ml g_{cat}^{-1} h^{-1} based on the total weight of CZA and ZSM-5. The CZA/ZSM-5 weight ratio = 5/3 for both two-step and one-step processes

The CZA and ZSM-5(13) catalysts for methanol synthesis and methanol dehydration were also studied in the dual reactor. The reaction setup is schematically shown in Scheme 3-12. During the reaction, the methanol formed in the first bed on the CZA catalyst was converted into DME on the acid sites of ZSM-5(13) loaded in the second bed. As shown in Figure 3-13, there is an enhancement of CO conversion from 18.6 % to 31.2 % in the dual bed reactor compared to the CZA system for methanol synthesis. When compared to CZA, the methanol selectivity decreased to 6.4 % resulting in DME selectivity of 85.1 %. About 3.2 % CO_2 has been produced. Ultimately, the introduction of ZSM-5(13) in the same reactor bed increased the CO conversion and resulted higher DME selectivity.

3.2.2.4. Direct DME synthesis with hybrid CZA-ZSM-5(13) catalyst

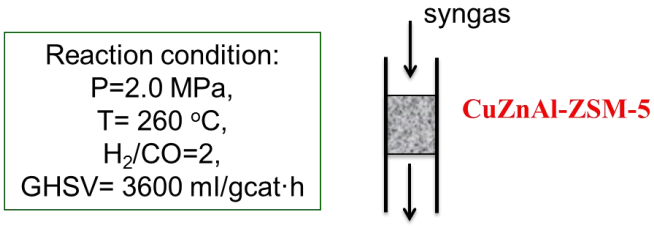

Scheme 3-14. Direct DME synthesis over hybrid catalyst

The CZA-ZSM-5(13) hybrid catalyst prepared by physical mixing method was used for direct DME synthesis from syngas (Scheme 3-14). Further to improve the activity in terms of CO conversion and DME yield more efficient catalyst with optimal composition between CZA and ZSM-5(13) could be necessary. In this hybrid system a balance is required between the mass ratio of methanol synthesis catalyst and solid acid catalyst for achieving maximum CO conversion, enhanced DME selectivity without producing hydrocarbons.

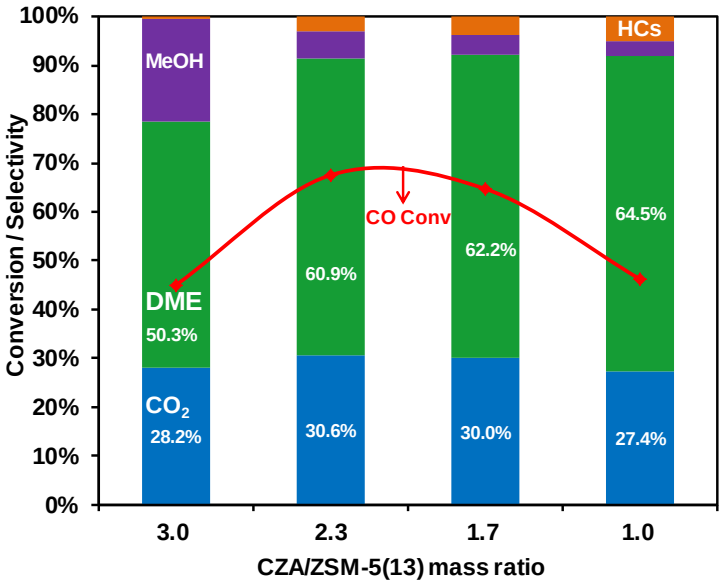

Figure 3-15. The catalytic performance of DME synthesis at the different ratio of Methanol synthesis catalyst (CZA) and methanol dehydration catalyst (ZSM-5(13)) in T = 260 ^{o}C, P = 2.0 MPa, H_2/CO = 2, GHSV= 3600 ml g_{cat}^{-1} h^{-1}.

Herein, the direct DME synthesis process was evaluated over the physically mixed CZA-ZSM-5(13) catalysts with different weight ratios of the CZA to ZSM-5(13). The conversions of CO and the product selectivities over different hybrid catalysts are shown in Figure 3-15. At the very high weight ratio of CZA/ZSM-5 in the hybrid catalyst (CZA/ZSM-5(13) weight ratio = 3), the DME selectivity is lowest. The catalyst exhibits the methanol selectivity of 21.1 % due to insufficient concentration of acid sites. Instead, at the CZA/ZSM-5 (13) ratio equal to 1 (0.5 acid fraction), the amount of zeolite is larger than that required to convert the methanol to DME. Therefore the excess amount of ZSM-5 (13) zeolite has a higher probability to convert the main product DME to hydrocarbons. Moreover, the activity of hybrid catalysts containing ZSM-5(13) firstly increased with the increasing amount of solid acid catalyst, and then it decreased rapidly with increasing acidic amount, suggesting that if the acidity is too low, the amount of methanol formed cannot be dehydrated with sufficient efficiency, the methanol dehydration reaction is the rate-determined step in DME synthesis, the activity of hybrid catalyst increased with the increasing amount of acidity; if the acidity is too high, that means the amount of CZA catalyst is less, therefore, the methanol synthesis reaction is the rate-determined step in DME synthesis, the activity of hybrid catalyst decreased with the further increasing amount of acidity. In short, excessive and insufficient amounts of acid sites were both unfavorable for DME synthesis. Hence, the

optimized ratio (5:3 in the present case) is highly important to get reasonable CO conversion, higher DME selectivity and almost no hydrocarbon byproducts.

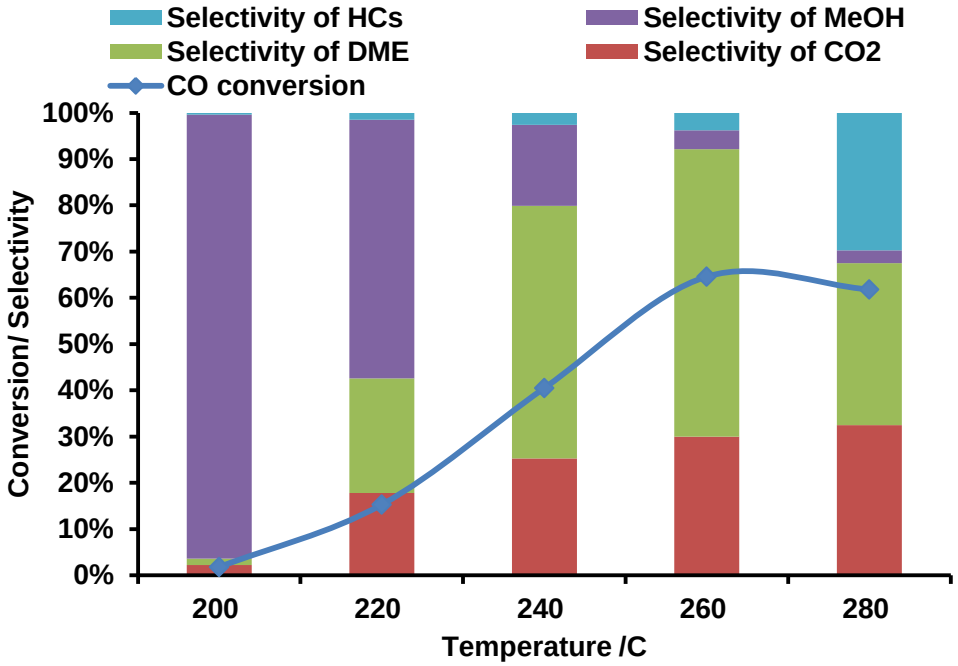

Figure 3-16. Effect of reaction temperature on the direct DME synthesis over CZA-ZSM-5(13) hybrid catalyst; Reaction conditions: T = 200−280 °C, P = 2.0 MPa, GHSV = 3600 mL g_{cat}^{-1} h^{-1}, and H_2 / CO_2 = 2.

Under the optimized weight ratio, the catalyst performance of CZA-ZSM-5(13) hybrid has also been evaluated as a function of temperature (200 – 280 ℃) (Figure 3-16). There was an increase in CO conversion from 1.8 % to 64.6 % as temperature increases from 200 to 260 ℃. Further increase in temperature (280 ℃) leads to the decrease in CO conversion and increase in the selectivity to hydrocarbons. The optimized temperature for direct conversion to DME seems to be 260 ℃ which is consistent with the catalytic results for the individual catalyst components such as methanol synthesis or methanol dehydration.

The DME selectivity also followed the similar trend like CO conversion, reaching a maximum value of 62.2 % at 260 ℃. Apart from this, the selectivity to CO_2 also increased with the reaction temperature as result of higher water gas shift activity as a function of temperature. This highly influences the DME selectivity over hybrid catalyst. The CO_2 selectivity control could be therefore very important while designing the hybrid catalyst for direct DME synthesis.

Moreover, the synergetic effect of hybrid catalyst, a combination of metal and acid function, can be seen from the CO conversion value (64.6 %) when compared to dual bed reactor (31.2 %), where the dehydration of as prepared methanol occurred over solid acid

packed at second stage in the reactor. This particular fact might be correlated to faster dehydration of as formed methanol at the adjacent solid acid counterpart resulting in DME. As a result of this scavenger effect, the hybrid catalyst is more active against the CZA alone where CO conversion is thermodynamically limited. This result infers the superiority of hybrid catalysts for the direct synthesis of DME from syngas.

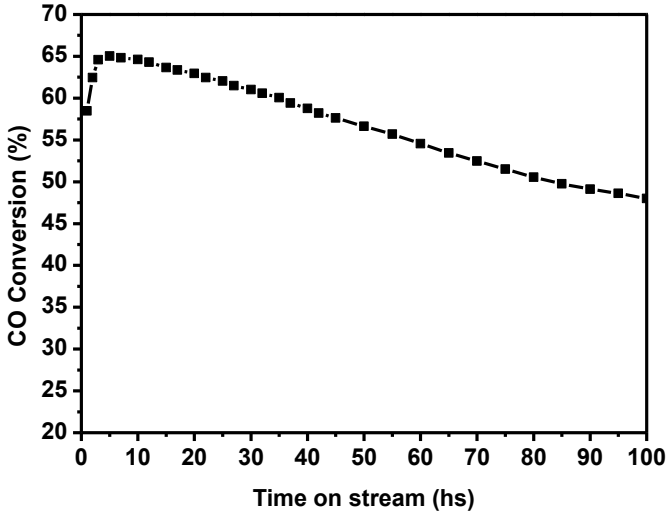

Figure 3-17. CO conversion as a function of time on stream (TOS) in syngas to DME experiment using the bi-functional CZA-ZSM-5 catalyst. Experimental conditions: T= 260 ℃, P = 2.0 MPa, GHSV: 3600 ml g^{-1} h^{-1}, H_2/CO = 2.

The stability of the bi-functional CZA-ZSM-5(13) catalyst with the metal: acid ratio = 5:3 was evaluated over 100 hours of the reaction period. The change in the CO conversion as function of time on stream (TOS) is depicted in Figure 3-17. It is clear that CO conversion decreases from 64.6 % to 52.3 %. This means that the hybrid catalyst deactivated and lost around 19.4 % of its initial activity. The deactivation rate was almost same as that of conventional methanol synthesis catalyst. It can suggest therefore that similar to CZA, the deactivation of hybrid catalyst is probably related to Cu sintering during the reaction. In addition to the copper sintering, other deactivation mechanisms are not excluded. The deactivation of hybrid catalyst is discussed in a greater detail in Chapter 4 of the PhD thesis.

3.3. Conclusion

A traditional Cu-Zn-Al (CZA) and a ZSM-5(13) zeolite have been evaluated in this chapter in methanol synthesis and methanol dehydration respectively. The CZA catalyst showed catalytic performance of methanol synthesis from syngas which was consistent with previous reports. At higher temperature the conversion was limited by the thermodynamics.

When ZSM-5(13) is deployed as a methanol dehydration catalyst, the methanol conversion value between 20.3 to 95.8 % is obtained in the temperature range of 200 - 280 ℃. At higher temperature (280 ℃) significant amounts of hydrocarbon byproduct occurred suggesting that 260 ℃ could be the optimized reaction temperature for very high conversion and reasonably good DME selectivity. Since, the methanol synthesis is a thermodynamically restricted reaction, combination of methanol synthesis with methanol dehydration could lead to high conversions and higher DME yields.

The direct synthesis of DME from syngas was carried out in a single reactor with a dual bed. The results showed an increase in CO conversion to 31.2 % when compared to 18.6 % of methanol synthesis reaction alone. Further a DME selectivity of 85.1 % was also obtained in the same conditions.

In order to improve further the process efficiency through the intimate contact between CZA and ZSM-5(13), a hybrid catalyst prepared by simple physical mixing of individual components was introduced for the direct synthesis of DME from syngas. Variation of catalyst composition showed that the weight ratio between CZA and ZSM-5(13) of 1.7 could be optimal for better CO conversion and DME yield. The results of this study revealed that the overall DME synthesis reaction is principally depends on the fraction of CZA component, while the acid fraction has an important influence on the product distribution, Due to the synergetic interaction, higher CO conversion activity with reasonably good DME selectivity can be obtained over hybrid CZA-ZSM-5 catalysts. The optimized ratio of CZA-ZSM-5(13) allows selective synthesis of DME without formation of undesirable hydrocarbons. However, direct synthesis of DME from syngas results also in CO_2 formation, which reduces carbon efficiently of the process. In addition, the time on stream study showed a gradual deactivation. It could be due to the copper sintering and other deactivation phenomena.

The following challenges have been identified for direct DME synthesis from syngas over hybrid copper-zeolite catalysts:

- undesirable CO_2 formation;
- catalyst deactivation
- insufficient activity.

These challenges are addressed in chapters 4, 5 and 6 of the thesis. .

3.4. References

[1] T.A. Semelsberger, R.L. Borup, H.L. Greene, Journal of Power Sources, 156 (2006) 497-511.

[2] J.B. Hansen, B. Voss, F. Joensen, I.D. Siguroardottir, Large scale manufacture of dimethyl ether-A new alternative diesel fuel from natural gas, in, SAE Technical Paper, 1995.

[3] G. Yang, N. Tsubaki, J. Shamoto, Y. Yoneyama, Y. Zhang, Journal of the American Chemical Society, 132 (2010) 8129-8136.

[4] G. Bonura, M. Cordaro, C. Cannilla, A. Mezzapica, L. Spadaro, F. Arena, F. Frusteri, Catalysis Today, 228 (2014) 51-57.

[5] A. Garc á-Trenco, A. Vidal-Moya, A. Mart ínez, Catalysis Today, 179 (2012) 43-51.

[6] K. Waugh, Catalysis Today, 15 (1992) 51-75.

[7] M. Behrens, F. Studt, I. Kasatkin, S. K ühl, M. H ävecker, F. Abild-Pedersen, S. Zander, F. Girgsdies, P. Kurr, B.-L. Kniep, Science, 336 (2012) 893-897.

[8] F. Hayer, H. Bakhtiary-Davijany, R. Myrstad, A. Holmen, P. Pfeifer, H.J. Venvik, Chemical Engineering Journal, 167 (2011) 610-615.

[9] J.-H. Fei, M.-X. Yang, Z.-Y. Hou, X.-M. Zheng, Energy & fuels, 18 (2004) 1584-1587.

[10] J. Abu-Dahrieh, D. Rooney, A. Goguet, Y. Saih, Chemical Engineering Journal, 203 (2012) 201-211.

[11] W. Wang, Y. Jiang, M. Hunger, Catalysis Today, 113 (2006) 102-114.

[12] L. Wang, Y. Qi, Y. Wei, D. Fang, S. Meng, Z. Liu, Catal Lett, 106 (2006) 61-66.

[13] P. Kurr, I. Kasatkin, F. Girgsdies, A. Trunschke, R. Schl ögl, T. Ressler, Applied Catalysis A: General, 348 (2008) 153-164.

[14] J.M. Beiramar, A. Griboval - Constant, A.Y. Khodakov, ChemCatChem, 6 (2014) 1788-1793.

[15] A.S. Al-Dughaither, H. de Lasa, Industrial & Engineering Chemistry Research, 53 (2014) 15303-15316.

[16] P. Padmaja, P.K. Pillai, K.G.K. Warrier, M. Padmanabhan, Journal of Porous Materials, 11 (2004) 147-155.

[17] S. Velu, K. Suzuki, C.S. Gopinath, H. Yoshida, T. Hattori, Physical Chemistry Chemical Physics, 4 (2002) 1990-1999.

[18] N.B. Castagnola, A.J. Kropf, C.L. Marshall, Applied Catalysis A: General, 290 (2005) 110-122.

[19] J.S. Lee, K.H. Lee, S.Y. Lee, Y.G. Kim, Journal of Catalysis, 144 (1993) 414-424.

[20] M. Kurtz, H. Wilmer, T. Genger, O. Hinrichsen, M. Muhler, Catal Lett, 86 (2003) 77-80.

[21] M.V. Twigg, M.S. Spencer, Applied Catalysis A: General, 212 (2001) 161-174.

[22] R. Borade, A. Sayari, A. Adnot, S. Kaliaguine, Journal of Physical Chemistry, 94 (1990) 5989-5994.

[23] P.A. Jacobs, R. Von Ballmoos, The Journal of Physical Chemistry, 86 (1982) 3050-3052.

[24] V. Zholobenko, L. Kustov, V.Y. Borovkov, V. Kazansky, Zeolites, 8 (1988) 175-178.

[25] Y. Matsunaga, H. Yamazaki, T. Yokoi, T. Tatsumi, J.N. Kondo, The Journal of Physical Chemistry C, 117 (2013) 14043-14050.

Chapter 4. The role of external acid sites of ZSM-5 in deactivation of hybrid CuZnAl/ZSM-5 catalyst for direct dimethyl ether synthesis from syngas

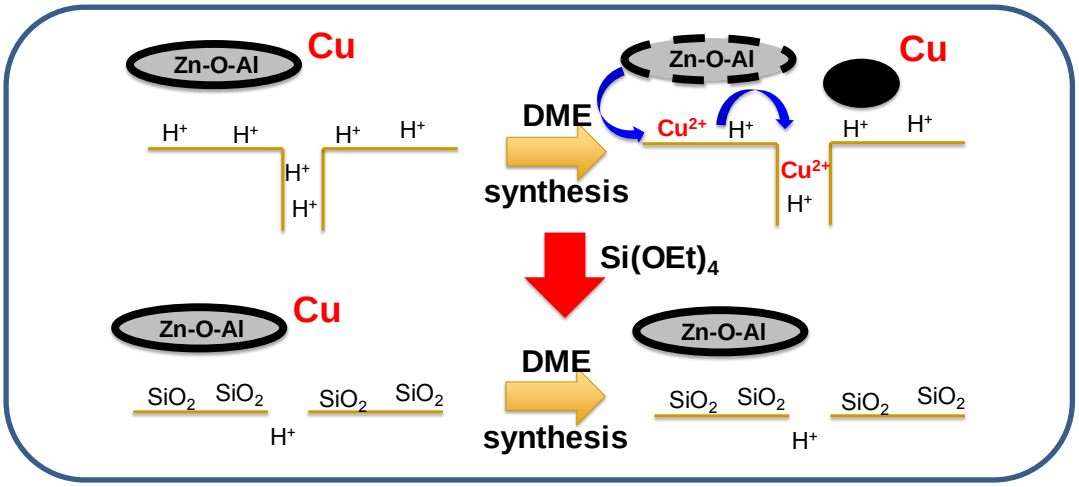

This chapter has been published as:

V. Ordomsky, M. Cai, V. Sushkevich, S. Moldovan, O. Ersen, C. Lancelot, V. Valtchev, A. Khodakov, Applied Catalysis A: General, 486 (2014) 266-275

Abstract

Direct synthesis of dimethyl ether (DME) from syngas was investigated on a series of hybrid CZA/ZSM-5(x), where x stands for ratio of Si/Al, catalysts prepared by kneading. It was found that the initial performance of the catalysts was a function of both zeolite crystallite sizes and Si/Al ratio. The activity of the hybrid catalysts gradually decreased with time on stream because of simultaneous copper sintering, copper oxidation and ion exchange with zeolite hydroxyl groups. Copper sintering led to the decrease in the number of metal active sites, while ion exchange of Cu^{2+} ions with the hydroxyl groups of the zeolite resulted in lower concentration of acid sites for methanol dehydration. Copper sintering and ion exchange could be slowed down by selective neutralisation of the acid sites on the zeolite outer surface by silylation. Both catalyst stability and dimethyl ether productivity were significantly improved.

4.1 Introduction

In order to obtain a good synergy between CO hydrogenation and dehydration of methanol, methanol synthesis and methanol dehydration active phases should be in the close proximity to each other. However, conventional catalyst preparation methods which provide the highest degree of mixing between active sites in the composites like impregnation and co-precipitation could be not very efficient in this case. This drawback is a consequence of the interaction of metallic copper with acid sites previously observed in CuO-ZnO/γ-Al_2O_3 [1-3] and CuZnAl/SiO_2-Al_2O_3 [4] composites. That was the reason why the most efficient catalysts for DME synthesis reported so far, were prepared using physical mixing of the individual compounds. Recently Tsubaki et al [5, 6] have developed an original technique which can weaken the interaction between methanol synthesis catalyst and zeolite and thus, improve the reaction selectivity to DME. It has been shown that core-shell catalyst with Cr/ZnO core and zeolite shell improves DME selectivity by suppressing side reaction such as undesirable hydrocarbon synthesis; C_2-C_4 alkanes are mostly produced.

However, even in the case of the physical mixing or encapsulation method, the interactions of the metals with acid sites could lead to partial deactivation. Several possible reasons of the DME synthesis catalyst deactivation have been reported in the literature: coke deposition [7, 8], Cu sintering [9] or copper and zinc ion exchange with protons of zeolite [10, 11]. García-Trenco [10] et al. showed the presence of isolated Cu^{2+} cations occupying exchange positions in the HZSM-5 zeolite by EPR spectroscopy. The decrease in Brönsted acidity resulted in suppression of the catalyst activity due to the reduced zeolite activity in methanol dehydration. The same authors studied the influence of zeolite morphology in hybrid CuZnAl/zeolite catalysts in DME synthesis [12]. It was found that the deactivation increased with increasing the external surface area and surface Al concentration of the zeolite co-catalyst. These results confirm that the interactions between metals and acid sites are detrimental for the process since they cause the deactivation of the catalyst during DME synthesis. They also indicate important role of zeolite outer surface area in the deactivation of DME synthesis catalysts. Despite of noticeable deactivation of composite CuZnAl/ZSM-5 catalysts in DME synthesis, very few works have addressed so far possible strategies to enhance the catalyst stability. A stable catalyst is indispensable however for the design of efficient processes for direct DME synthesis.

In this chapter, we have investigated influence of Si/Al ratio, zeolite crystallite size and acid sites on the zeolite outer surface on the structure, catalytic performance and stability of

composite CZA/ZSM-5(x) catalysts for DME synthesis. A new method is proposed to improve the stability of DME synthesis catalysts.

Three different ZSM-5 zeolites after converting into H-form (see section 2.12) with different crystallite sizes and Si/Al ratios were used in this work; ZSM-5(13), ZSM-5(25) from Zeolyst and ZSM-5(45) from Sud-Chemie. CZA catalyst was prepared as mentioned in section 2.1.1. Selective neutralization of the acid sites on the zeolite outer surface by silylation was carried out as shown below.

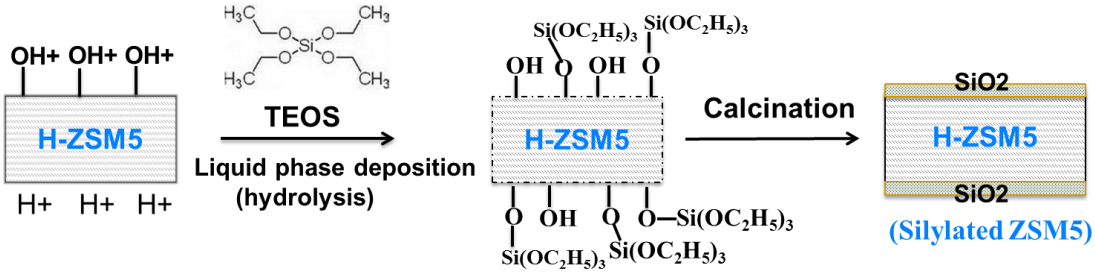

Scheme 4-1: Scheme of silylation reaction between TEOS and the surface hydroxyl groups of ZSM-5(x)

The surface modified, silylated samples were prepared by the chemical liquid deposition using TEOS as a silica source. 5 g of dried zeolite in H-form was added to the solution of 1 g of TEOS in 50 cm^3 of n-hexane and refluxed for 24 h at 50 ℃. The modified sample was dried at 100 ℃ for 12 h and calcined at 550 ℃ (heating rate: 2 ℃/min) for 5 h in air. The calcined silylated zeolites are denoted as SiO_2/ZSM-5-I(13) and SiO_2/ZSM-5-II(45).

4.2 Results

4.2.1 Chemical and physical properties of zeolite

The parent zeolite samples had different chemical compositions and also different size and morphology of zeolite crystallites. ZSM-5-I(13) zeolite has uniform particle size distribution in the range 5-7 μm (Figure 4-1). The zeolite particles consisted of agglomerates of intergrown zeolite crystallites. Again the zeolite crystallites built the agglomerates of sample ZSM-5-II(45), however in this case the individual crystallites with the size ranging between 40 and 100 nm were clearly observed (Figure 4-1).

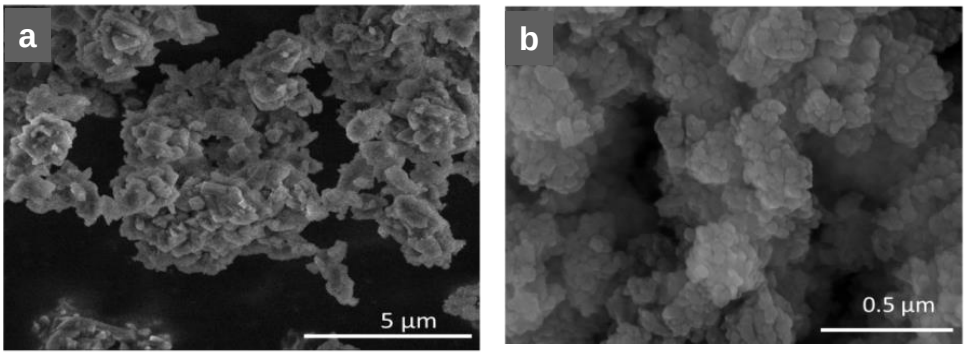

Figure 4-1. SEM images of ZSM-5-I(13) (a), and ZSM-5-II(45) (b)

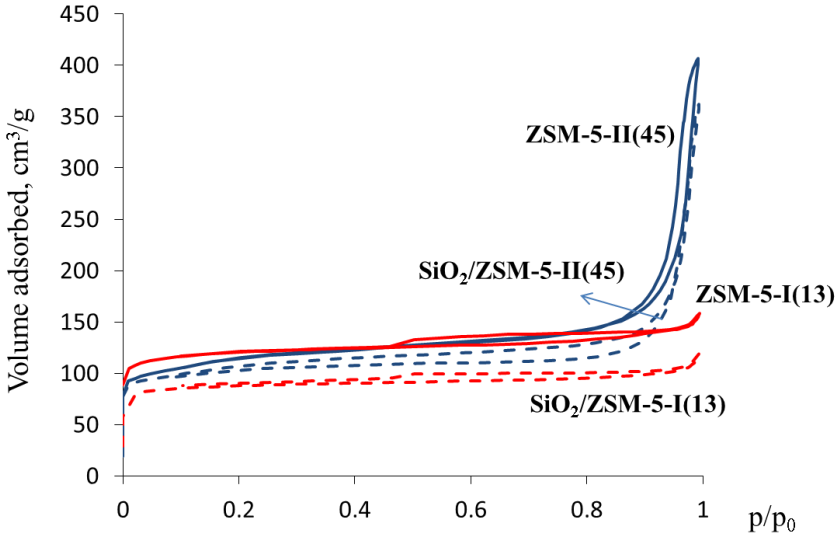

Figure 4-2. Nitrogen adsorption/desorption isotherms over parent and silylated zeolites

Different crystallite sizes of ZSM-5-I(13) and ZSM-5-II(45) result in different low temperature nitrogen adsorption data (Figure 4-2). The adsorption equilibrium isotherm for ZSM-5-I(13) is of type I in the Brunauer classification and characteristic of microporous solids. The isotherm of ZSM-5-II(45) exhibits an additional step at $p/p_0 \approx 0.8$. The adsorption step in the range of p/p_0 = 0.8 - 1.0 can be explained by filling the intercrystalline pores between nanocrystallites [13].

The ZSM-5-I(13) and ZSM-5-II(45) samples were silylated by TEOS. The kinetic diameter of TEOS (8.9 Å) is much larger than the pore mouth of MFI-type zeolite (5.4-5.6 Å). Thus, only hydroxyl groups on the outer surface could react with hydrolyzed silicon species and form Si-O-Si or Si-O-Al bonds. The analysis of the Al content shows only slight changes in the Si/Al ratio after silylation procedure (Table 4-1). Previously, silylation with TEOS was used to reduce the concentration of acid sites on the external surface of zeolites [14]. Besides blocking surface activity of zeolite, TEOS and silica species deposited on the external surface

might block the zeolite pores and impose diffusion limitations [15]. Low temperature nitrogen adsorption (Table 4-1, Figure 4-2) shows only slight decrease in the total surface area or micropore volume of zeolite ZSM-5-II(45). Differently to ZSM-5-II(45), the silylated ZSM-5-I(13) sample demonstrates a significant decrease in the surface area (from 432 to 350 m^2/g) and volume (from 0.17 to 0.14 cm^3/g). Larger crystallite size and higher acidity of ZSM-5-I(13) result in the higher probability of the pore blockage and decrease in the surface area and volume during silylation in comparison with ZSM-5-II(45).

Table 4-1. Zeolite characterization

Catalyst	Crystallite size	Si/Al ratio	Al content (mmol/g)	S_{BET} (m2/g)	V_{mic} (cm3/g)	V_{tot}(<350nm) (cm3/g)	$TPD_{(NH3)}$ (µmol/g)
ZSM-5-I(13)	5–7 µm	13	1.28	432	0.17	0.23	993
SiO_2/ZSM5(13)	–	14	1.18	350	0.14	0.22	931
ZSM-5(45)	~0.5 µm	45	0.37	383	0.16	0.63	360
SiO_2/ZSM5(45)	–	48	0.34	354	0.15	0.56	303

The acidity of materials was studied by NH_3-TPD (Figure 4-3, Table 4-1). All zeolites exhibit a low-temperature (100-300 ˚C) and a high-temperature (400-600 ˚C) ammonia desorption peaks. The high temperature peak is usually assigned to ammonia desorption from bridging hydroxyl groups of zeolites (Si-OH-Al) [35]. The identification of the low temperature peak is still controversial. This peak is usually assigned to desorption of physically adsorbed ammonia or desorption of ammonia from silanol groups or extra framework aluminum species [16]. The total amount of acid sites in ZSM-5-I(13) zeolite is almost three times more significant than in ZSM-5-II(45) zeolite. The acidity of ZSM-5 zeolite is usually associated with aluminum content. Thus, higher concentration of acidic sites in the ZSM-5-I(13) zeolite corresponds to higher aluminum content in this zeolite (Table 4-1). NH_3-TPD shows that silica deposition over ZSM-5-I(13) and ZSM-5-II(45) leads respectively to 6 and 16% decrease in the amount of acid sites in comparison with the parent zeolites, while the strength of acid sites is not affected (Figure 4-3, Table 4-1). The larger decrease in the amount of acid sites in the ZSM-5-II (45) sample is obviously due to the higher outer surface area of zeolite nanocrystals. A relatively small drop in the concentration of acid sites after silylation confirms preferential adsorption of TEOS on the zeolite outer surface. The ZSM-5 structure is constituted by two intersecting channel systems. Partial blockage of the pores does not affect the total zeolite acidity measured by NH_3-TPD

because of relatively small size of NH_3 molecules and their possible migration thought the ZSM-5 channel system.

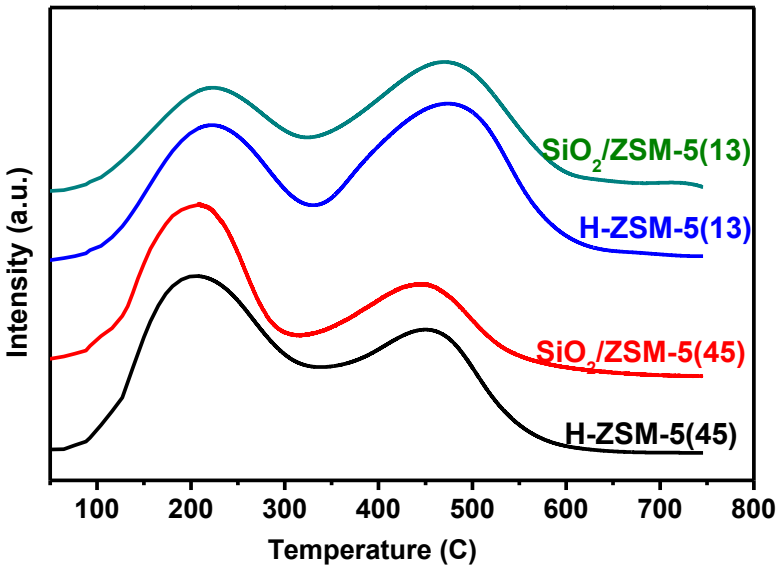

Figure 4-3. TPD-NH_3 profiles for zeolites before (HZSM-5-I(13), HZSM-5-II(45)) and after silylation (SiO_2/ZSM-5-I(13), SiO_2/ZSM-5-I(45))

4.2.2. Influence of Si/Al ratio and zeolite crystallite size on the catalytic performance of CZA-ZSM-5 catalysts

The catalytic activities and selectivities in DME synthesis of the CZA-zeolite mixture are shown in Figures 4-4, 4-5 and 4-6. The carbon monoxide conversions and selectivities are strongly affected by the concentration of acid sites and zeolite crystallite sizes. Note that ZSM-5-I(25) and ZSM-5-I(13) have rather similar morphology and relatively large crystallite sizes (5-7 μm). The strength of acid sites determined by TPD of NH_3 for all zeolites is similar (Figure 4-3). This suggests that the catalysts principally differ in the concentration of acid sites and in the size of the crystals.

Let us first evaluate the phenomena due to the different concentration of Brönsted acid sites. The ZSM-5-I(25) zeolite has a concentration of Brönsted acid sites twice lower than ZSM-5-I(13), while the crystallite size is the same for both the zeolites. Interestingly, the activity of the CZA-ZSM-5-I(25) catalyst is much lower compared to the ZSM-5-I(13) counterpart (Figure 4-4). Carbon monoxide conversion is about 35% on CZA-ZSM-5(25) in comparison with 65% over CZA-ZSM-5-I(13). In addition, differently to CZA-ZSM-5-I(13), CZA-ZSM-5-I(25) exhibits much higher methanol selectivity (Figure 4-5). Higher methanol selectivity on CZA-ZSM-5-I(25) indicates relatively slow kinetics of methanol dehydration which can be due to lower concentration of Brönsted acid sites in this catalyst. The same

dependence of the activity of the hybrid catalyst in DME synthesis on Si/Al ratio in zeolites has been observed earlier [17]. Lower carbon monoxide conversion observed on CZA-ZSM-5-I(25) could be also due to thermodynamic constrains. Indeed, methanol is one of major products on this catalyst and the theoretical equilibrium conversion of CO to methanol is only 20-30 % at these conditions [17].

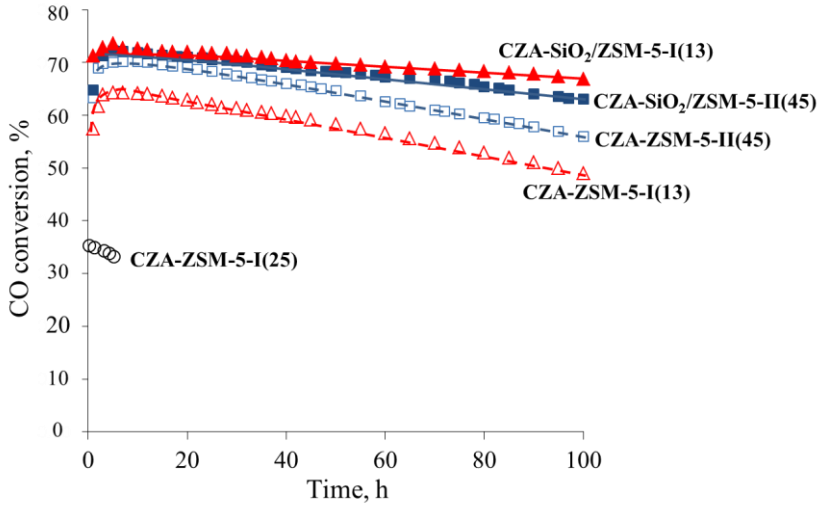

Figure 4-4. CO conversion in time during DME synthesis over hybrid catalysts CZA-zeolite with zeolites before (ZSM-5-I(13), ZSM-5-I(25), ZSM-5-II(45)) and after silylation (SiO_2/ZSM-5-I(13), SiO_2/ZSM-5-I(45)) (T=260 ˚C, 3600 $cm^3_{gas}g_{cat}^{-1}h^{-1}$, H_2/CO=2, 20 bar).

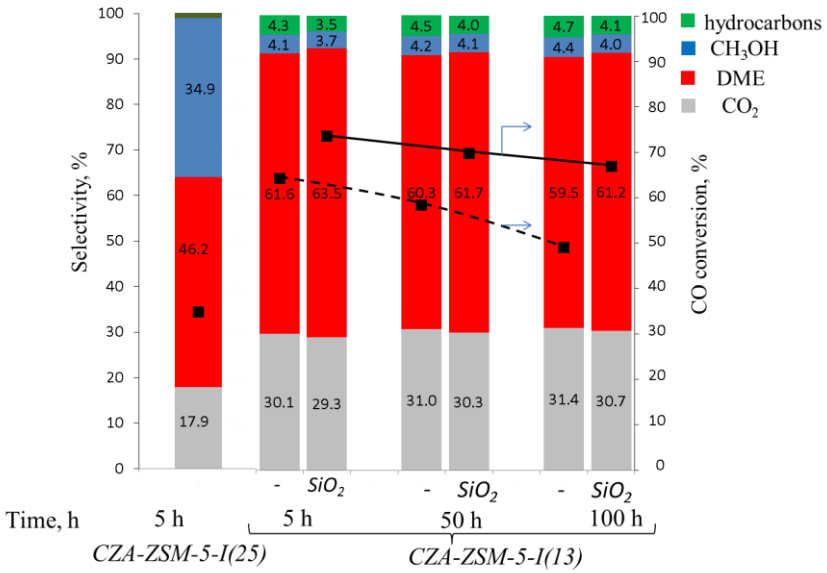

Figure 4-5. Selectivity to main products during DME synthesis over CZA hybrid catalyst with ZSM-5-I(25) (TOS 5 h) and with ZSM-5-I(13) before and after silylation (TOS: 5, 50 and 100 h) (T= 260 ˚C, GHSV= 3600 $cm^3_{gas}g_{cat}^{-1}h^{-1}$, H_2/CO=2, 20 bar).

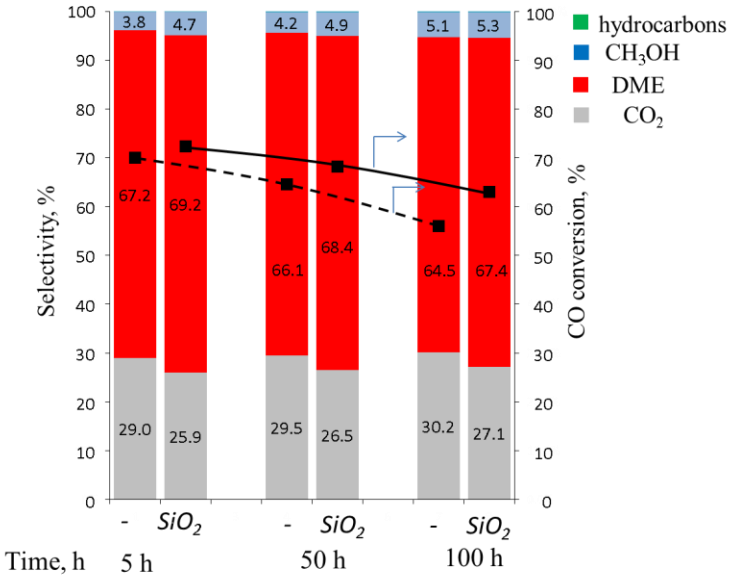

Figure 4-6. Selectivity to main products during DME synthesis over CZA hybrid catalyst with ZSM-5-II(45) before and after silylation (TOS: 5, 50 and 100 h) (T=260 ˚C, GHSV= 3600 $cm^3_{gas}g_{cat}^{-1}h^{-1}$, H_2/CO=2, 20 bar).

Higher concentration of acid sites in zeolite could be favorable for methanol dehydration. Under the same reaction conditions, CZA-ZSM-5-I(13) with a higher fraction of acid sites exhibits a much higher DME selectivity (S_{DME}= 61 %) at the conversion of 65 %. The methanol selectivity was only 4% on CZA-ZSM-5-I(13).

In addition to the Brönsted acid sites, a zeolite crystallite diameter also affects the performance of CZA-ZSM-5 catalysts. Figure 4-4 shows that carbon monoxide conversion on the CZA-ZSM-5-II(45) composite catalyst is comparable to that on CZA-ZSM-5-I(13), although, the number of acid sites in CZA-ZSM-5-II(45) is several times lower than CZA-ZSM-5-I(13). This fact is most probably due to the different crystallite size of these two samples (Figure 4-1). Indeed, the ZSM-5-I(13) zeolite represents intergrown agglomerates of zeolite crystals with size of around 5-7 μm in comparison with the nanocrystalls of ZSM-5-II(45) with size of 40-100 nm. Smaller crystallite sizes of ZSM-5-II(45) should result in higher accessibility of Brönsted sites. This could lead to more efficient methanol dehydration in comparison with ZSM-5-I(13). The higher activity and DME yield during methanol dehydration with decrease in the size of ZSM-5 crystals has been explained earlier by smaller mass transport resistance [18].

The ZSM-5-II(45) based catalyst exhibits DME selectivity of 67 % compared to the DME selectivity of 61 % observed over CZA-ZSM-5-I(13) at carbon monoxide conversion

of 60-70 % (Figures 4-5 and 4-6). The ratio of DME to CO_2 selectivities is almost equal to 2:1 over the catalyst containing ZSM-5-I(13). This indicates almost full consumption of water produced in methanol dehydration in WGS reaction. Zeolite could possible play a role in WGS reaction; the CO_2 selectivity over CZA-ZSM-5-II(45) is significantly lower than on other zeolites. This observation might be attributed to higher concentration of acid sites in ZSM-5-I(13) which should result in the higher water capacity (holdup) in the catalyst. Higher water concentration would result in deeper WGS reaction over this system. The more hydrophobic ZSM-5-II(45) should lead to the lower water adsorption and lower probability of the WGS reaction. In addition CZA-ZSM-5-I(13) produces some amounts of hydrocarbons. The formation of light hydrocarbons over CZA-ZSM-5-I(13) might be explained by higher concentration of acid sites and thus by higher probability of methanol and DME conversion into olefins in comparison with CZA-ZSM-5-II(45). The presence of saturated hydrocarbons (ethane, propane, butane) is probably due to subsequent hydrogenation of olefins into alkanes over CZA [19]. Methane formation is most probably a result of CO and CO_2 hydrogenation over CZA catalyst. Indeed, some amounts of methane are usually observed in syngas conversion on copper catalysts [20]. Hydrocarbon production over CZA-ZSM-5 catalyst could be possibly reduced by selective neutralization of strong zeolite acid sites. Previously it was shown that modification of ZSM-5 by Sb_2O_3 or MgO increased the selectivity to DME from 55 to 65-69 % [19, 21] In addition, higher DME selectivity can be also favored by smaller zeolite crystallite sizes. Smaller ZSM-5-II(45) crystallite size reduces methanol and DME residence time inside the zeolite matrix and thus the probability of secondary reactions (e.g. hydrocarbon formation).

4.2.3. Influence of silylation of zeolite external surface on the catalyst structure and stability

4.2.3.1. Catalytic properties of catalysts with silylated zeolites

One of the major problems of direct DME synthesis from syngas is catalyst deactivation. All studied CZA-ZSM-5 composite catalysts showed a gradual decrease in carbon monoxide conversion with time on stream (Figure 4-4). The CO conversion decreased for the CZA-ZSM-5-I(13) catalyst from 64 to 49% and for CZA-ZSM-5-II(45) from 70 to 56 % respectively during the first 100 h of the reaction. The results are consistent with previous reports about the stability of CZA-ZSM-5 catalysts prepared by kneading [11].

The stability of CZA-ZSM-5-I(13) and CZA-ZSM-5-II(45) catalysts was improved in this work using silylation with TEOS. Figure 4-4 shows that the conversion on both the

silylated zeolites was much more stable than on the parent catalysts. For CZA-ZSM-5-I(13) catalyst silylation also led to the increase in initial carbon monoxide conversion from 63 to 74%. Higher DME selectivity was also observed on silylated catalysts. For CZA-ZSM-5-I(13), silylation leads to the increase in DME selectivity from 61 to 63% after 5 h of the reaction, while for CZA-ZSM-5-II(45) the DME selectivity rises after silylation from 67 to 69%. At the same time, the selectivity to CO_2 decreases on both catalysts. Lower CO_2 selectivity after silylation can be attributed to lower WGS activity over more hydrophobic CZA-ZSM-5-II(45) and might be explained again by a decrease in the concentration of adsorbed water after the interface between CZA catalyst and zeolite after silylation. In order to identify the reasons of deactivation and to evaluate the influence on silylation on the catalyst stability, the parent and silylated hybrid CZA-zeolite catalysts before and after the catalytic experiments have been extensively studied by TEM and FTIR spectroscopy.

4.2.3.2 Physicochemical properties of catalysts before and after deactivation

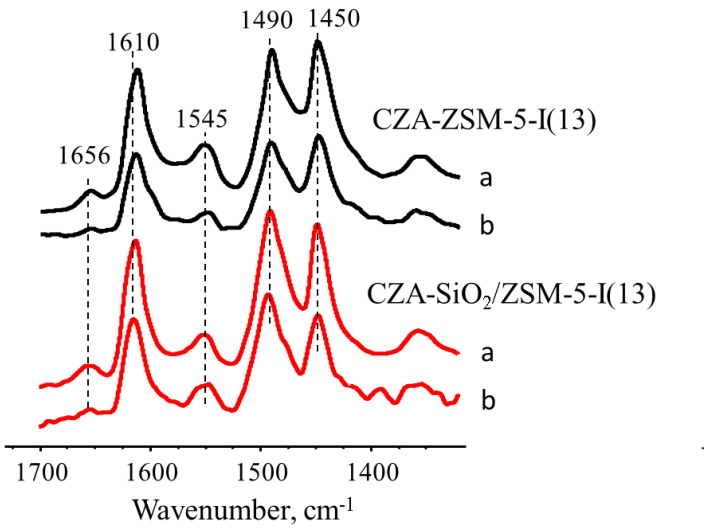

Figure 4-7. IR spectra of Py adsorption over the CZA-ZSM-5-I(13) hybrid non silylated catalyst before (a) and after the reaction (b) and over silylated catalyst before (a) and after the reaction (b). The catalysts were (re)-reduced prior to Py adsorption.

Zeolite acidity in the fast deactivating hybrid CZA-ZSM-5-I(13) catalyst has been investigated by Py adsorption. Figure 4-7 shows the results of Py adsorption over CZA-ZSM-5-I(13) before and after the catalytic tests. In the range of 1400-1700 cm^{-1}, the chemically adsorbed pyridine exhibited a usual set of bands: two bands at 1545 and 1656 cm^{-1} assigned to pyridinium ion (PyH^+), two bands at 1450 and 1610 cm^{-1} related to coordinatively adsorbed pyridine on Lewis sites. The band at 1490 cm^{-1} was attributed to Py species

adsorbed on Lewis and Brönsted sites [22]. The intensity of the band corresponding to pyridinium ion (PyH^+) significantly decreases after the catalytic experiment. This corresponds to the decrease in the number of Brönsted acid sites. The Lewis acidity remains almost unchanged for both catalysts before and after the reaction. In addition to the zeolite Lewis sites, the Lewis acidity in the spent catalysts seems to be also related to cationic copper species which concentration may increase during the reaction.

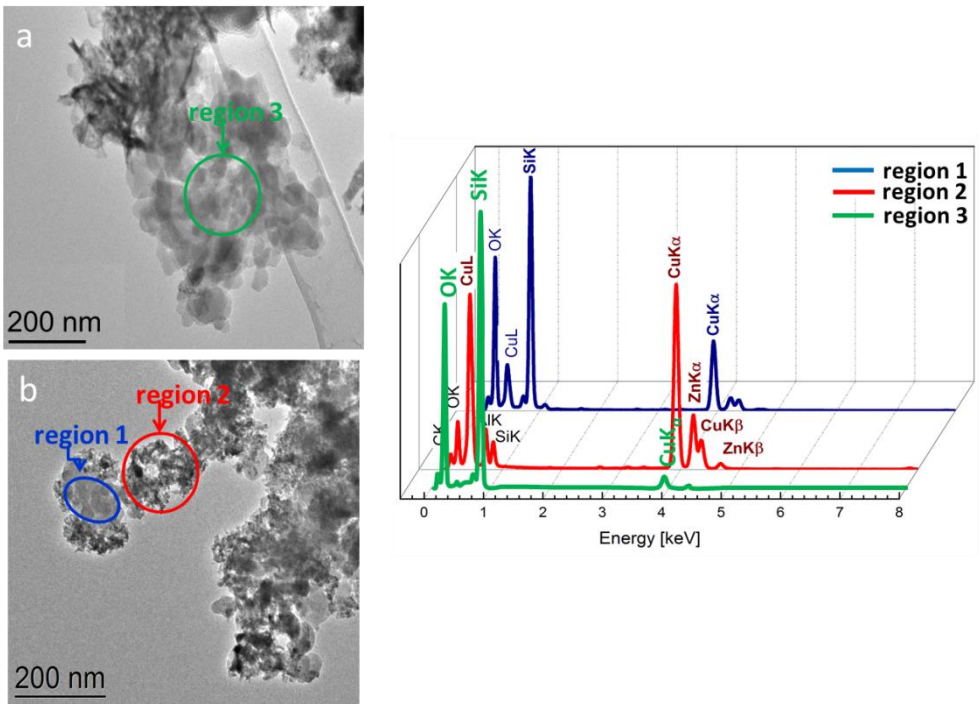

Figure 4-8 TEM micrograph and corresponding EDX spectra of a representative region within the CZA-ZSM-5-I(13) catalyst before (a) and after reaction (b). The encircled areas represent a ZSM-5 Si-rich region (blue and green) and Co and Zn – rich area (red) as identified by the EDX analysis.

In order to find the reasons responsible for the drop in the number of Brönsted acid sites after the reaction, the local elemental composition of hybrid CZA-ZSM-5-I(13) catalyst before and after catalytic experiment was analyzed by TEM–EDX and STEM-HAADF (Figure 4-8). Owing to the contrasts in the TEM mode, we were able to distinguish between the zeolite and metal-rich regions. The chemical composition of these regions was further investigated using EDX. Silicon was predominant in the zeolite area of the catalysts before and after reaction as shown by Figure 4-8 (blue and green encircled region and spectra), whereas the other regions, which show different contrasts, appear to be dominated by Cu, Zn and at smaller expense Al. The mean size of the zeolite crystals is of several tens of nm, whereas the CZA grains appear as platelets (ZnO) or needle-like shaped (alumina) with mean

sizes of about 20 nm. Catalyst spacemen were deposited on a carbon membrane supported by a Cu grid. Consequently, traces of Cu (region 1) could be detected in regions that appear to be pure zeolite. Note however, that the signal of Cu from the catalyst before reaction (region 3) was significantly lower in comparison with the signal from the region 1 indicating the presence of Cu within the zeolite crystal or in the close proximity to zeolite crystal after the reaction. Taking into account the decrease in the number of Brönsted acid sites in zeolite, this observation might be explained by migration of copper during the reaction followed by ion exchange of copper ions with zeolite hydroxyl groups. Similar phenomenon was observed earlier by the group of Martinez [10] at higher temperatures with identification of Cu^{2+} by EPR. The authors suggested that interaction between protons and Cu is one of the main reasons of the catalyst deactivation [10, 12].

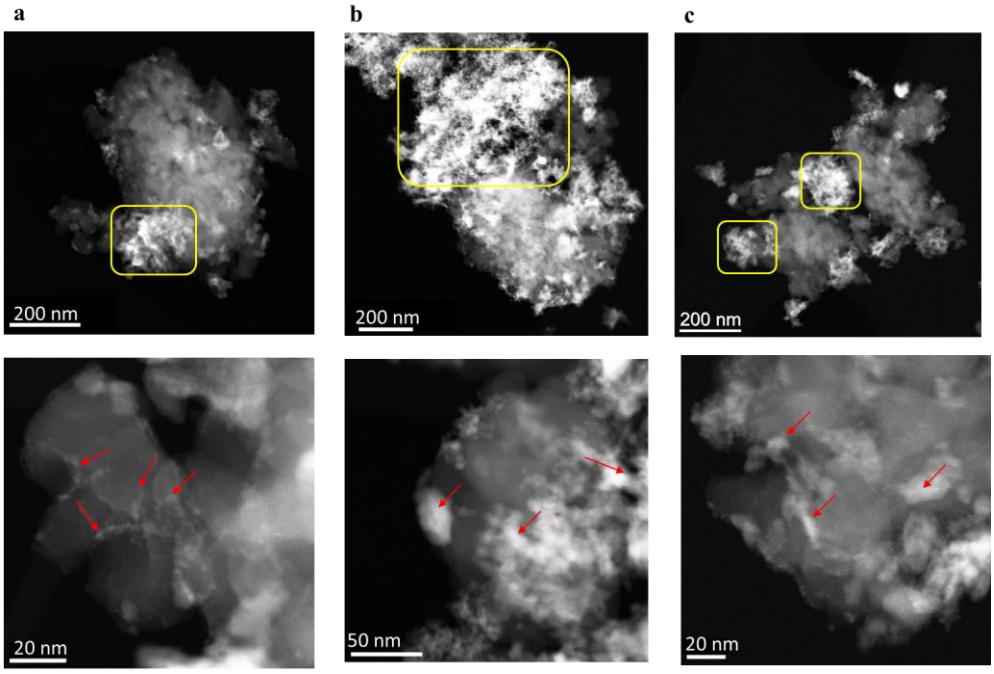

Figure 4-9 STEM-HAADF micrographs of the CZA-ZSM-5-I(13) hybrid catalysts before the reaction (a), after the reaction (b) and CZA-SiO2/ZSM-5-I(13) after the reaction (c). The rectangular areas mark the metal-rich regions, whereas the red arrows point to metallic atomic clusters and/or nanoparticles.

The metal distribution within the CZA-ZSM-5 catalysts was studied by direct analysis of contrasts from the STEM-HAADF micrographs. Because of higher sensitivity to the Z atomic number, this mode is particularly suitable for the assessment of the distribution of metallic nanoparticles. The metal distribution in CZA-ZSM-5-I(13) zeolite composite with and without the TEOS treatment has been analyzed before and after reaction (Figure 4-9).

After catalyst activation in hydrogen (Figure 4-9a), Cu is located exclusively on the CZA grains, either as NPs with a mean size of 5 nm or as a thin metallic layer. The thickness of the Cu metallic layer varies from several nm to 15 nm, as depicted by the Figure 4-9a. After the reaction, the morphology of the catalyst changes drastically in terms of metal distribution. Larger metal NPs with mean sizes superior to 10-15 nm are detected not only on the CZA grains but on the zeolite as well (Figure 4-9b). The thin metal layer completely disappeared from the grains, most probably being assimilated by the larger neighboring particles during the reaction. This phenomenon can be interpreted by assuming metal sintering on the surface of the CZA and subsequent copper diffusion to the zeolite. Such phenomenon can be responsible for copper migration followed by oxidation, subsequent exchange of Cu^{2+} ions with zeolite hydroxyl groups. The outline of the catalyst deactivation processes is shown in Figure 4-10.

The spent silylated CZA-SiO_2/ZSM-5-I(13) sample shows major differences in location of copper NPs, relative to the non-silylated catalyst (Figure 4-9). The STEM-HAADF analysis shows a clear separation of CZA and zeolite phases in spent CZA-SiO_2/ZSM-5-I(13) catalyst. Differently to the spent CZA-ZSM-5-I(13) catalyst prepared without TEOS pretreatment, copper species were not detected in CZA-SiO_2/ZSM-5-I(13) inside the zeolite.

Thus, TEM-EDX and STEM-HAADF have provided valuable information on copper localization in the silylated CZA-zeolite prior and after the reaction. Silylation of zeolite surface by TEOS results in less significant Cu sintering and ion exchange with zeolite protons. Consequently, the silylated catalyst shows better stability (Figure 4-1). Our results suggest that neutralization of hydroxyl group at the external surface reduces copper sintering and ion exchange with protons of zeolites (Figure 4-10) which are usually observed on non-silylated catalysts.

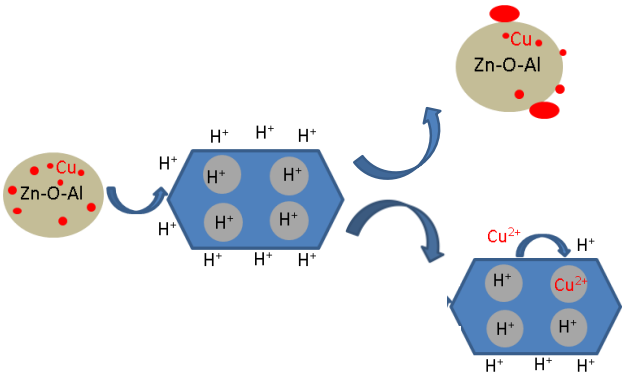

Figure 4-10 Schematic presentation of copper migration leading simultaneously to ion exchange with hydroxyl groups of the ZSM-5 zeolite and copper sintering.

Note that Cu sintering in Cu-ZSM-5 catalyst during NO decomposition was observed previously. Fierro et al [23] found that migration of Cu inside of zeolite pores was facilitated by the presence of water vapor. Water promotes formation of positively charged mobile copper clusters. Copper sintering seems to proceed according to particle migration and coalescence mechanism. Similar mechanism of nanoparticle sintering facilitated by the presence of water was previously observed for supported nickel and cobalt catalysts [24, 25]. In addition to water, hydroxyl groups on the zeolite outer surface can obviously contribute to higher copper mobility in hybrid catalysts. Water seems to play a major role in copper sintering. To identify the effect of water on copper sintering, we conducted a specific experiment. In this experiment, water was added to the catalyst in a flow of hydrogen in the absence of carbon monoxide (Figure 4-11). The amount of added water roughly corresponded to water amounts produced under typical reaction conditions (DME synthesis). Figure 4-11 shows that the conversion of CO decreases rapidly from 60 to 10% after 24 h of catalyst exposure to water and hydrogen at the reaction temperature. This suggests that indeed water significantly facilitates the migration of Cu.

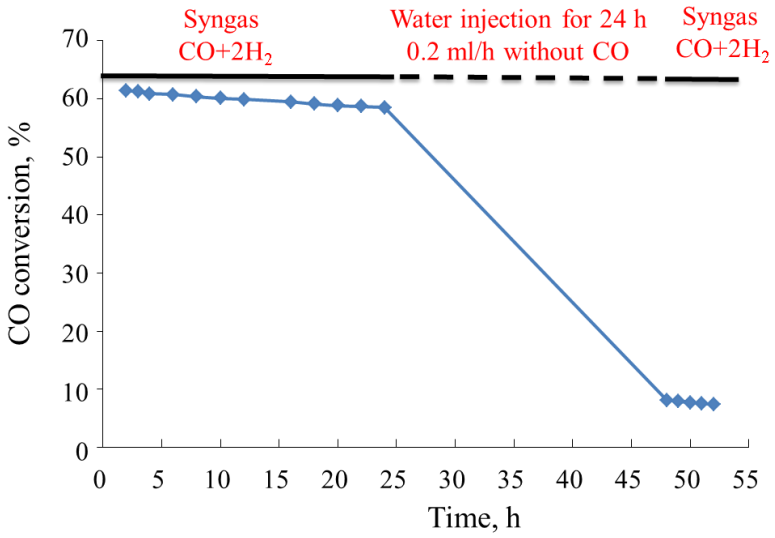

Figure 4-11. CO conversion in time during DME synthesis (T=260 ˚C, GHSV = 3600 $cm^3 gas g_{cat}^{-1} h^{-1}$, H_2/CO=2, 20 bar) over hybrid catalysts CZA-ZSM-5-I(13) before and after addition of 0.2 cm^3/h of H_2O during 24 h in hydrogen flow (T=260 ˚C, GHSV = 1200 $cm^3 H_2 g_{cat}^{-1} h^{-1}$, 20 bar).

The changes in the oxidation state during the reaction were also investigated by FTIR spectroscopy using low temperature CO adsorption. Figure 4-12 displays IR spectra of CO adsorption as a function of coverage over parent CZA-ZSM-5-I(13). At the very low

coverage the most intense band is found at 2115 cm^{-1}. Further addition of CO leads to the appearance of the band at 2170 cm^{-1} which shifts to 2164 cm^{-1} with the increase in the amount of adsorbed CO. Finally another band emerges at 2136 cm^{-1}. The lower frequency band at 2115 cm^{-1} corresponds to the strongest adsorption of CO. In agreement with previous reports [26-28], the band at 2115 cm^{-1} could be related to the reduced copper species (Cu^0 or Cu^+). It is well known that copper carbonyls are not very stable. Copper carbonyl stability could be enhanced when CO adsorbs on well dispersed nanoparticles at low temperature. The band at 2164 cm^{-1} might be assigned to CO adsorption over Brönsted acid sites [29]. The same band might also have CO adsorbed either to extra framework cations (Zn^{2+}, Cu^{2+}). The band at 2136 cm^{-1} is usually assigned to physically adsorbed CO. It appears only at relatively higher carbon monoxide pressures.

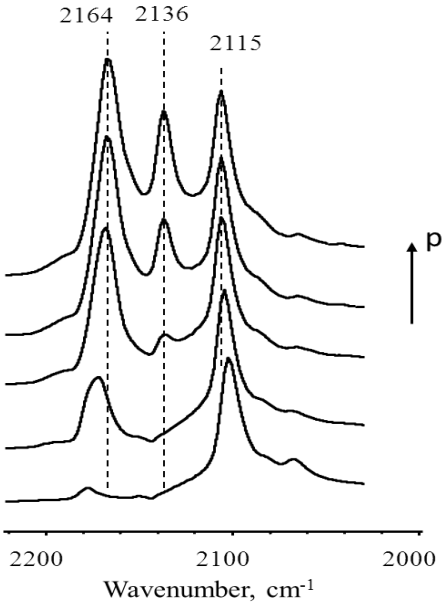

Figure 4-12. FTIR spectra of CZA-ZSM-5-I(13) hybrid catalyst after adsorption of CO at low temperature (-173 ˚C) at gradually increasing pressures. The catalyst was reduced prior to CO adsorption.

Figure 4-13 shows IR spectra of adsorbed CO on the pure CZA and hybrid catalysts prepared using the parent and silylated ZSM-5-I(13) zeolites before and after the reaction. The spectrum of CO adsorbed over pure CZA shows bands of CO at 2164 and 2115 cm^{-1}. Mixing of CZA with parent and silylated ZSM-5-I(13) zeolites results in modification of the band shape and intensity. The intensity of the band at 2164 cm^{-1} increases for the non-modified zeolite system and almost does not change in the case of silylated ZSM-5. Taking into account that Brönsted acidity decreases during reaction over CZA-ZSM-5-I(13), the

increase in the intensity of the band at 2164 cm^{-1} might be possibly explained by high adsorption of CO over forming cationic Cu^{2+} sites. In the case of silylated sample, the band of CO over metallic Cu is still broad and shifts to higher wavenumbers similarly to parent CZA. It is indicative of the presence of Cu sites with slightly different electronic properties or chemical environment [30]. The position of this band is more affected by the reaction in non silylated ZSM-5-I(13) catalyst. Mixing with parent zeolite results in significant narrowing of the band and a low frequency shift of the band at 2164 cm^{-1}. This fact might be explained by interaction of zeolite with positively charged copper clusters in CZA which may form in the catalyst during the pretreatments. It is interesting to note that the non-silylated catalyst shows a significant decrease in the intensity of the band at 2115 cm^{-1} after the reaction. Low intensity of the band at 2115 cm^{-1} can be assigned to the low concentration of available copper sites in the spent CZA-ZSM-5-I(13) catalyst probably because of copper sintering, oxidation and ion exchange. At the same time, the intensity of the band at 2115 cm^{-1} attributed to copper metal sites in the silylated catalysts is affected to a much lesser extent by the exposure to the reaction conditions. Neutralization of the acid sites on zeolite outer surface seems to prevent copper migration with its ion exchange and sintering in SiO_2/ZSM-5-I(13). Our results correlate with the results of the group of Martinez [12] who observed the effect of the external surface area and surface Al concentration of the zeolite co-catalyst on the catalyst deactivation.

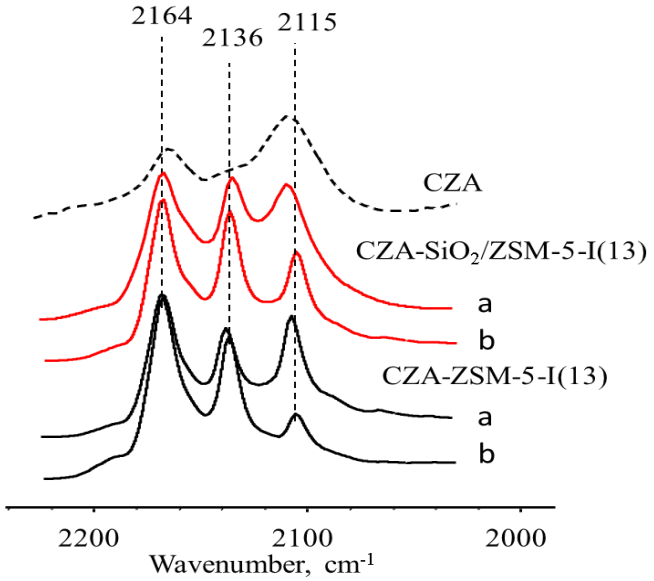

Figure 4-13. IR bands resulting from CO adsorption at -173 ˚C on the CZA catalyst, CZA-ZSM-5-I(13) hybrid catalyst before (a) and after the reaction (b) and on the CZA-SiO_2/ZSM-

5-I(13) hybrid catalyst before (a) and after the reaction (b). The catalysts were reduced prior to CO adsorption.

Thus, the pronounced increase in the catalyst stability during DME synthesis after silylation might be explained by suppression of Cu migration and ion exchange on the outer surface of zeolite due to neutralization of the surface acid sites by TEOS. The possible alternative explanation of the catalyst deactivation could be coke formation during reaction. The coke may form by polymerization of olefins or condensation of reactive oxygenates during reaction [7, 8]. In order to verify this assumption, TPO of the spent catalysts has been conducted with detection of forming CO_2 (Figure 4-14). The results indicate similar character of the adsorbed coke species for all samples. The amount of forming CO_2 is very low (7-8 $\cdot 10^{-6}$ mmol/g) and comparable for silylated and non silylated ZSM-5-I(13) and ZSM-5-II(45) zeolites. These results suggest that silylation does not influence to any noticeable extent coke deposition. The experiment with addition of water (Figure 4-11) also supports this assumption.

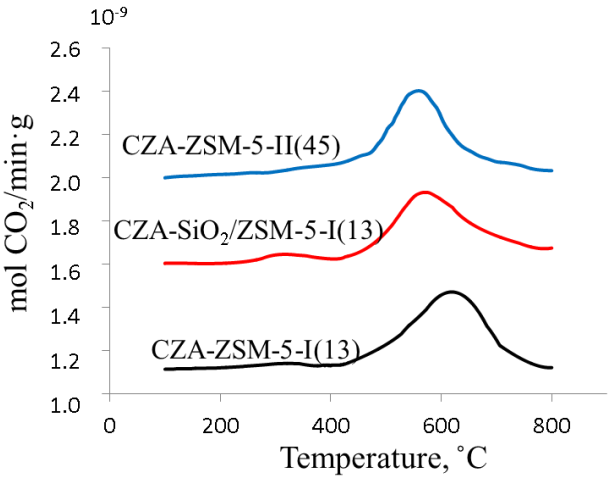

Figure 4-14. TPO of the CZA-ZSM-5-I (13), CZA-ZSM-5-II (45) and CZA-SiO_2/ZSM-5-I (13) hybrid catalysts after the reaction with detection of CO_2.

Note that silylation can improve not only the catalyst stability but also the catalyst initial activity. One might anticipate that copper on the surface of CZA reacts with the protons of non-silylated ZSM-5-I(13) already during pretreatment of the catalyst in the reactor. It reduces amount of active Cu species for methanol synthesis. Significant interaction between ZSM-5 and CZA with ion exchange of Cu during hybrid catalyst preparation has been observed earlier [10, 12]. In the silylated catalyst, the reaction between copper and Brönsted acid sites during activation could be hindered by SiO_2 protective layer on the zeolite

outer surface. Thus, the silylated catalyst can show higher reaction rate compared to non-silylated counterpart immediately after the exposure to the reaction medium.

The selectivity slightly evolves with reaction time over both the parent and silylated catalysts. The selectivity to DME decreases by 2-3 % over parent catalysts with simultaneous very slight increase in the selectivity to CO_2 and methanol (Figure 4-2, 3). A slight increase in methanol selectivity is related to the continuous decrease in the concentration of Brönsted acid sites during the reaction and thus slower methanol dehydration rate. The acid sites in pores of the parent non-silylated zeolites are neutralized by migrating Cu^{2+} ions. At the same time, these catalysts can show a higher activity in WGS reaction which can be due to easier water dissociation over Cu^{2+} ions [31]. At the same time, silylation of zeolite outer surface hinders copper migration into zeolite pores. Thus, the concentration of zeolite acid sites is reduced to a lesser extent in the silylated samples during the reaction. Silylation leads to the increase in the selectivity to DME by 2 % over both catalytic systems. This corresponds to the highest selectivity to DME (69 %) observed on SiO_2/ZSM-5-(45) catalyst [21]. The increase in DME selectivity after silylation is accompanied by a significant decrease in the selectivity to CO_2 and hydrocarbons. Previously it was shown that DME selectivity could be improved by the promotion of copper-zeolite catalysts by metal oxides (ZrO_2, MgO, Sb_2O_3). Indeed, addition of metal oxides reduces zeolite acidity and hydrocarbon production. However promotion with metal oxides does not improve the catalyst stability [10, 19, 21]. Indeed, metal oxides are usually distributed almost uniformly inside the zeolite lattice. Silylation with TEOS results in selective neutralization of the acid sites on the zeolite surface and produces a much more significant effect on the catalyst stability than the promotion with metal oxides.

4.3. Conclusion

The catalytic performance of hybrid Cu–ZnO–Al_2O_3/ZSM-5 prepared by kneading in direct DME synthesis from syngas depends on the zeolite crystallite size and Si/Al ratio. Higher concentration of the zeolite Brönsted acid sites and smaller zeolite crystallite sizes favour higher DME productivity.

The decrease in the catalytic performance of hybrid catalysts with time on stream is due to the combination of several phenomena: copper sintering, copper oxidation, migration and ion exchange with hydroxyl groups in zeolite pores.

The catalyst stability can be enhanced by selective neutralization of acid sites on zeolite outer surface with TEOS. Selective neutralization of Brönsted acid sites on the outer zeolite surface slows down copper sintering and migration and results in the better catalyst stability and slightly higher selectivity to DME. The effect of silylation on the catalytic performance and stability was more pronounced for the zeolite with abundant Brönsted acidity and small outer surface area.

4.4. References

[1] J.L. Li, X.G. Zhang, T. Inui, Applied Catalysis A: General, 147 (1996) 23-33.

[2] Q. Ge, Y. Huang, F. Qiu, S. Li, Applied Catalysis A: General, 167 (1998) 23-30.

[3] G.R. Moradi, S. Nosrati, F. Yaripor, Catalysis Communications, 8 (2007) 598-606.

[4] S.P. Naik, H. Du, H. Wan, V. Bui, J.D. Miller, W.W. Zmierczak, Industrial and Engineering Chemistry Research, 47 (2008) 9791-9794.

[5] K. Pinkaew, G. Yang, T. Vitidsant, Y. Jin, C. Zeng, Y. Yoneyama, N. Tsubaki, Fuel, 111 (2013) 727-732.

[6] G. Yang, M. Thongkam, T. Vitidsant, Y. Yoneyama, Y. Tan, N. Tsubaki, Catalysis Today, 171 (2011) 229-235.

[7] J. Abu-Dahrieh, D. Rooney, A. Goguet, Y. Saih, Chemical Engineering Journal, 203 (2012) 201-211.

[8] I. Sierra, J. Ereña, A.T. Aguayo, J.M. Arandes, M. Olazar, J. Bilbao, Applied Catalysis B: Environmental, 106 (2011) 167-173.

[9] J.W. Jung, Y.J. Lee, S.H. Um, P.J. Yoo, D.H. Lee, K.-W. Jun, J.W. Bae, Applied Catalysis B: Environmental, 126 (2012) 1-8.

[10] A. García-Trenco, A. Vidal-Moya, A. Martínez, Catalysis Today, 179 (2012) 43-51.

[11] T. Takeguchi, K.-i. Yanagisawa, T. Inui, M. Inoue, Applied Catalysis A: General, 192 (2000) 201-209.

[12] A. García-Trenco, S. Valencia, A. Martínez, Applied Catalysis A: General, 468 (2013) 102-111.

[13] A. Simon-Masseron, J.P. Marques, J.M. Lopes, F.R. Ribeiro, I. Gener, M. Guisnet, Applied Catalysis A: General, 316 (2007) 75-82.

[14] S. Zheng, H.R. Heydenrych, A. Jentys, J.A. Lercher, Journal of Physical Chemistry B, 106 (2002) 9552-9558.

[15] R.W. Weber, K.P. Möller, C.T. O'Connor, Microporous and Mesoporous Materials, 35–36 (2000) 533-543.

[16] C.V. Hidalgo, H. Itoh, T. Hattori, M. Niwa, Y. Murakami, Journal of Catalysis, 85 (1984) 362-369.

[17] J.-H. Kim, M.J. Park, S.J. Kim, O.-S. Joo, K.-D. Jung, Applied Catalysis A: General, 264 (2004) 37-41.

[18] A.A. Rownaghi, F. Rezaei, M. Stante, J. Hedlund, Applied Catalysis B: Environmental, 119–120 (2012) 56-61.

[19] D. Mao, W. Yang, J. Xia, B. Zhang, Q. Song, Q. Chen, Journal of Catalysis, 230 (2005) 140-149.

[20] J. Wang, P.A. Chernavskii, A.Y. Khodakov, Y. Wang, Journal of Catalysis, 286 (2012) 51-61.

[21] D. Mao, J. Xia, B. Zhang, G. Lu, Energy Conversion and Management, 51 (2010) 1134-1139.

[22] M. Guisnet, P. Ayrault, C. Coutanceau, M.F. Alvarez, J. Datka, Journal of the Chemical Society - Faraday Transactions, 93 (1997) 1661-1665.

[23] G. Fierro, G. Ferraris, G. Moretti, Applied Catalysis B: Environmental, 91 (2009) 499-506.

[24] J. Sehested, Journal of Catalysis, 217 (2003) 417-426.

[25] M. Sadeqzadeh, J. Hong, P. Fongarland, D. Curulla-Ferré, F. Luck, J. Bousquet, D. Schweich, A.Y. Khodakov, Industrial and Engineering Chemistry Research, 51 (2012) 11955-11964.

[26] A.E. Baber, X. Yang, H.Y. Kim, K. Mudiyanselage, M. Soldemo, J. Weissenrieder, S.D. Senanayake, A. Al-Mahboob, J.T. Sadowski, J. Evans, J.A. Rodriguez, P. Liu, F.M. Hoffmann, J.G. Chen, D.J. Stacchiola, Angewandte Chemie - International Edition, 53 (2014) 5336-5340.

[27] V. Sanchez-Escribano, L. Arrighi, P. Riani, R. Marazza, G. Busca, Langmuir, 22 (2006) 9214-9219.

[28] G. Busca, U. Costantino, F. Marmottini, T. Montanari, P. Patrono, F. Pinzari, G. Ramis, Applied Catalysis A: General, 310 (2006) 70-78.

[29] S. Bordiga, E. Escalona Platero, C. Otero Areán, C. Lamberti, A. Zecchina, Journal of Catalysis, 137 (1992) 179-185.

[30] A. Kitla, O.V. Safonova, K. Föttinger, Catalysis Letters, 143 (2013) 517-530.

[31] G.G. Olympiou, C.M. Kalamaras, C.D. Zeinalipour-Yazdi, A.M. Efstathiou, Catalysis Today, 127 (2007) 304-318.

Chapter 5. Direct Dimethyl Ether Synthesis from Syngas on Copper-Zeolite Hybrid Catalysts with a Wide Range of Zeolite Particle Sizes

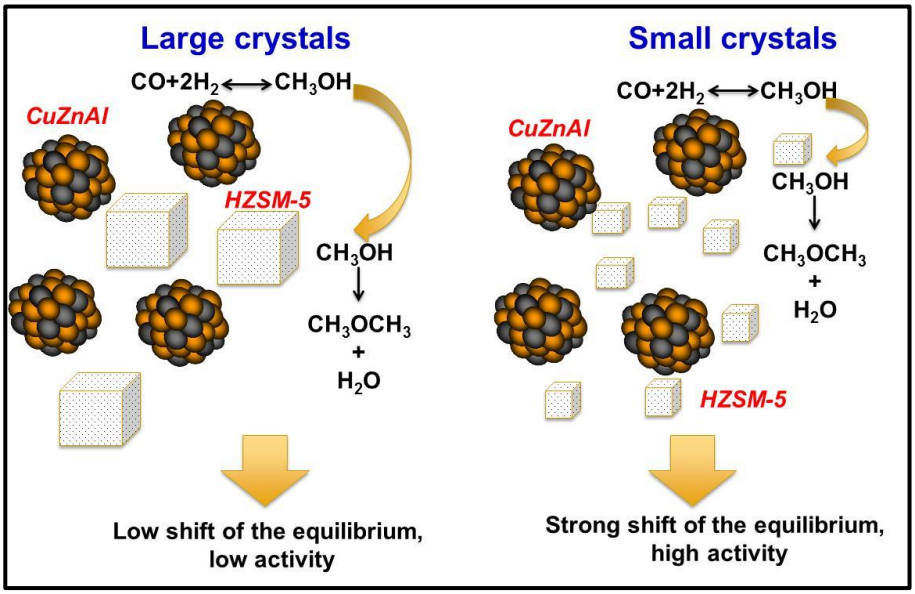

Abstract

This paper reports on the direct dimethyl synthesis from syngas on a bifunctional copper-zeolite catalyst. Both laboratory synthetized and commercial zeolites were used in this work. The catalyst performance is evaluated under pressure in a continuous fixed bed milli-reactor. The relationships between zeolite particle sizes, acidity and catalytic performance of the bifunctional catalysts in dimethyl synthesis have been studied. The catalysts and catalyst precursors were characterized using a wide range of characterization techniques: nitrogen adsorption-desorption measurements, X-ray diffraction (XRD), ^{27}Al NMR, scanning electron microscopy (SEM), and Fourier transform infrared spectroscopy with adsorbed molecular probes.

It is found that the reaction rate in direct DME synthesis is strongly affected by the sizes of zeolite particles. The bifunctional catalysts containing small individual nanosized zeolite crystallites (60-100 nm) were much more active in dimethyl synthesis that the counterparts containing micron-sized zeolite crystal agglomerates. The phenomenon is interpreted in terms of enhanced diffusion of the reaction intermediates from the copper catalyst to the acid sites in the small zeolite nanocrystals. The catalyst deactivation was related to the acid sites on the external surface of zeolites. It is established that the catalyst deactivation is less significant with the catalysts containing ZSM-5 zeolites with lower concentration of acid sites on the zeolite external surface. A new methodology to enhance the catalytic performance and stability of copper-zeolite hybrid catalysts for direct DME synthesis is proposed.

5.1 Introduction

Direct DME synthesis requires highly efficient bifunctional catalytic systems which would combine a carbon monoxide hydrogenation function for methanol synthesis and an acidic function for methanol dehydration. The crucial issue in catalyst design could be therefore, optimization of the catalyst composition and interaction between these functions [1]. Both well-dispersed copper particles with a high reducibility and large amounts of weak acidic sites are required for preparation of the bifunctional catalysts with satisfactory catalytic performance [2].

The Cu-ZnO-Al_2O_3 (CZA) catalyst for methanol synthesis has been successfully developed several decades ago. Recently, much of the efforts have been dedicated to the design of methanol dehydration active phase in the bifunctional catalysts for direct DME synthesis from syngas. The methanol dehydration occurs on an acid catalyst. Alumina has been first used [3-6] as an acid catalyst for methanol dehydration. The alumina-based catalysts, however, either pure or doped, are relatively sensitive towards deactivation by competitive adsorption of steam and also by coke formation. The zeolite based catalysts have several advantages for methanol dehydration to DME relevant to more conventional alumina such as tunable acidity and better stability in the presence of steam [7, 8]. The ZSM-5 zeolite has mostly been used as the acid component in bifunctional DME synthesis catalysts [9]. Other zeolites and microporous materials such as Ferrierite [10], MCM-22, ITQ-2, IM-5, and TNU-9, polymeric Naflon resins [11], several microporous silicoaluminophosphates (such as SAPO-5, -11, -18 and 34) [12] and phosphorus modified γ-Al_2O_3 [13] have also been investigated. The catalytic performance of the zeolites for methanol dehydration was correlated to the concentration of Brönsted acid sites. In addition to zeolite acidity, other zeolite characteristics such as morphology and porous structure could be also important for the design of efficient catalysts. Composite catalysts for direct DME synthesis from syngas were prepared by Martinez using different zeolites (ZSM-5, FER, IM-5, TNU-9, MCM-22, ITQ-2) [14]. The authors attributed difference in the catalyst stability to different zeolite morphology. The ZSM-5 zeolite was found to be more efficient in direct DME synthesis than Mordenite zeolite [15]. This was attributed to three dimensional pore system of ZSM-5 zeolite which facilitates diffusion of reagents and reaction products.

In addition, the influence of zeolite particle sizes on the catalytic performance is often considered in relation with zeolite shape selectivity [16-18]. The shape selectivity can be obtained by using the zeolite with channel dimensions approaching the sizes of the reacting

molecules. This results in large differences in the diffusivity of linear and non-linear isomers. A significant number of reports [19-23] have been dedicated to the evaluation of the zeolite crystallite size and molecular shape selectivity in hydrocracking reactions. No information is available however, about the effect of zeolite crystallite sizes on the catalytic performance of copper-zeolite catalysts in DME synthesis.

It is still not clear whether large or small zeolite crystallites could be optimal for this reaction. Jentoft et al [21] found that the activity, selectivity and stability of the K-LTL zeolite-supported platinum catalysts in n-hexane reforming could be correlated with the ratio of the external surface area to the intracrystalline pore volume. Bonetto et al [22] tested the beta zeolite with different crystal sizes in gas-oil cracking. The zeolite with the optimum crystallite size of 0.40 μm showed the best performance in terms of stability, activity and selectivity. The beta zeolite with a wide range of crystallite sizes was also tested as catalyst for degradation of high density polyethylene [23]. Zeolite nanocrystallites with very large external surface area showed the best performance in this reaction. In the conversion of methyl cyclohexane, the USY zeolites with the crystallite sizes in the range between 0.4 and 0.9 μm mostly affected the product distribution rather than the conversion. The selectivity variations were associated with hydrogen transfer, ring-opening/cracking and transalkylation

The effect of zeolite crystallite sizes was also studied for methanol conversion reaction. Smaller H-UZM-12 zeolites [24] were found less active and stable in this reaction, probably because of fast build-up of bulky coke molecules on the external surface of zeolite crystallites. Coke deposition inhibited the methanol diffusion to intrazeolitic acid sites, rendering them ultimately inaccessible for catalysis. The SAPO-34 and ZSM-5 crystallites of 200–500 nm showed [25] the best conversions and lifetimes because of their large external surfaces and short diffusion lengths. The zeolites with the smallest crystallites (<150 nm) deactivated more rapidly due to pore blocking by heavy coke deposits. Note however, that the effect of zeolite crystallite sizes could be even more complex for bifunctional catalysts, where in addition to chemical reaction, the transport of reagents and intermediates between different active phases should be taken into consideration. Very often in addition to individual crystallites, zeolites also contain agglomerates. In the composite catalysts prepared by mechanical mixing the presence of these agglomerates may significantly affect transport of reacting molecules and have strong influence on the catalytic performance.

The goal of the present work is to elucidate the influence of zeolite particle sizes and acidity on the performance and stability of the copper-zeolite hybrid bifunctional catalysts for

direct DME synthesis from syngas and to suggest new methodology for the improvements of the catalyst activity, selectivity and stability. A series of hybrid catalysts were prepared using ZSM-5 zeolites with different crystallite or aggregate sizes. The catalysts and catalyst precursors were characterized using a combination of characterization techniques. The catalyst performance in direct DME synthesis was investigated in a fixed bed reactor. The experiments were conducted beyond 100 h in order to evaluate the influence of the catalyst structure on the deactivation rate under the reaction conditions.

5.2 Synthesis of nano-sized ZSM-5

The chemicals used to prepare the nano-sized ZSM-5 crystallites were sodium aluminate (w (Al_2O_3) = 54 %, w (Na_2O) = 41 %), tetra-n-propylammonium hydroxide (TPAOH, Alfa Aesar, 20 wt.% water solution), tetraethyl orthosilicate (TEOS, Aldrich, 98%) and distilled water produced in our laboratory. Appropriate amounts of sodium aluminate, TPAOH and water were mixed and stirred with magnetic stirrer until the system gets clear. Thereafter, TEOS was added to the solution and hydrolyzed at 80 ℃ for 24 h. The final molar oxide composition of the reaction mixture was $1.23Na_2O$: 9.74TPAOH: $1.0Al_2O_3$: $43.2SiO_2$: $806H_2O$. Aliquots of clear solution was divided in four autoclaves and heated at 100, 120, 150 and 170 ℃. The synthesis duration at 120, 150 and 170 ℃ was 5 days. The synthesis at 100 ℃ was performed for 7 days. Recovered solid phases of the samples were washed with distilled water until the pH of the supernatant was 7, dried at 80 ℃ and calcined at 550 ℃ for 5 h (heating rate 1.75 ℃/min).

After the first calcination, the zeolite was exchanged three times with a 2 M ammonium nitrate solution (NH_4NO_3), under reflux at 80 ℃ for 6 h. A ratio volume of solution/mass of catalyst of 100 mL g^{-1} was used. After exchange, the zeolite was filtered and washed with deionized water and dried overnight at 100 ℃. The zeolite in the NH_4^+ form was then calcined under dry air flow (80 cm^3 min^{-1} g^{-1}) at 550 ℃ for 6h with the ramp of 2 ℃/min to obtain its H- form.

The ZSM-5 samples are labeled according to average particle size which was calculated from the SEM images. For example, the sample labeled ZSM-5@65 is a ZSM-5 with an average individual crystallite size of 65 nm. The individual zeolite size of the laboratory synthetized samples increases with the crystallization temperature: ZSM-5@65 (100 ℃), ZSM-5@80 (120 ℃), ZSM-5@95 (150 ℃) and ZSM-5@110 (170 ℃). Commercial ZSM-5 zeolites, after converting to H-form with larger crystallite agglomerates (500 nm, 500-1000

nm and 2000-5000 nm) ZSM-5@500; Si/Al =45 from Sud-Chemie (MFI90), ZSM-5@800; Zeolyst; CBV 5524G; Si/Al=25 and ZSM-5@5000; Zeolyst; CBV 2314; Si/Al=13 were also used in this work for comparison.

5.3 Results

5.3.1. Zeolite morphology and texture

The XRD patterns of the ZSM-5 samples are shown in Figure 5-1. The patterns are almost identical, as all the diffraction peaks obtained can be indexed to MFI-type structure [26]. The high peak intensities and absence of the baseline drift in diffraction patterns of both as-synthesized and commercial ZSM-5 zeolites indicate good crystallinity.

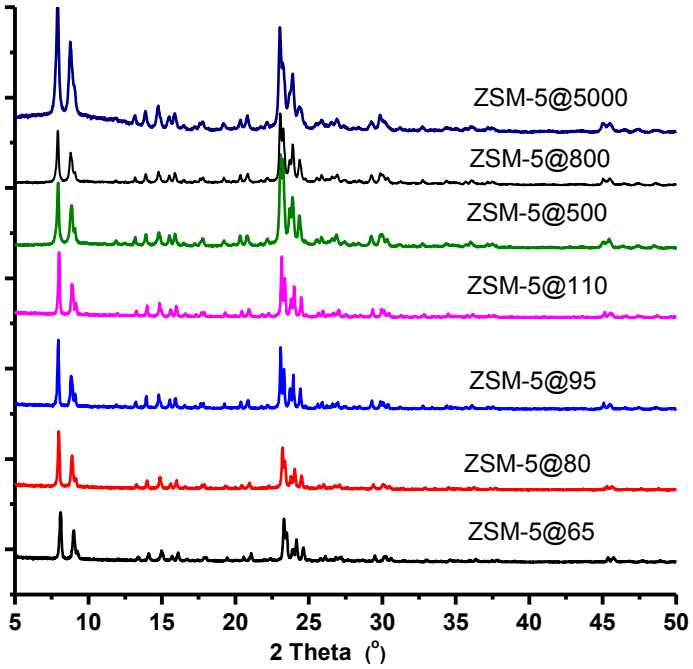

Figure 5-1. XRD patterns of ZSM-5 zeolites.

Scanning electron microscopy (SEM) is an efficient tool for investigation of zeolite morphology. Representative SEM micrographs of zeolite samples are displayed in Figure 5-2. The zeolites synthetized in this work (ZSM-5@65, ZSM-5@80, ZSM-5@95 and ZSM-5@110) exhibit crystallites in the nano-scale range with size below 200 nm. The crystallite size increases as the crystallization temperature increases from 100 to 170 ℃, as complex aggregates built of smaller nanoparticles are obtained at 100 and 120 ℃, whereas single crystallites dominate the product synthesized at 150 ℃ and 170 ℃. Differently to the samples synthetized in this work, the commercial ZSM-5@500, ZSM-5@800 and ZSM-

5@5000 zeolites contain larger crystallite aggregates which involve a larger number of individual zeolite nanocrystals. The average sizes of zeolite particles calculated from SEM images are given in Table 1. The average particle size of ZSM-5 samples varies from 65 nm in ZSM-5@65 sample to 5000 nm in ZSM-5@5000

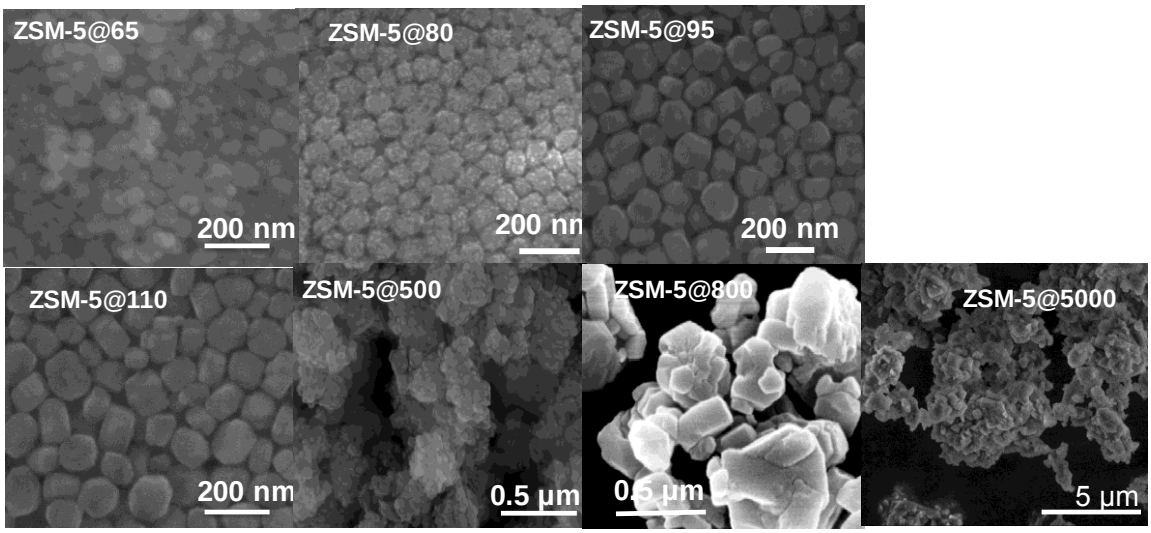

Figure 5-2. SEM images of ZSM-5 zeolites.

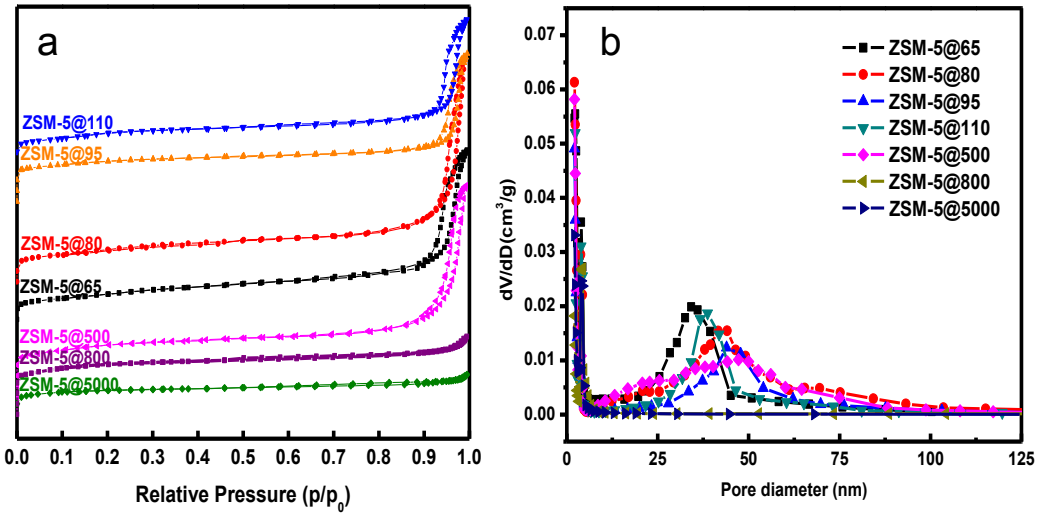

Figure 5-3. Nitrogen adsorption-desorption isotherms (a) and BJH mesopore size distribution curves (b).

The isotherms of nitrogen adsorption-desorption on the zeolites are shown in Figure 5-3a. The BET surface area of the zeolites varies between 305 and 400 m^2/g. As expected, the external surface area varies with the sizes of the zeolite individual crystallites. The isotherms of all the zeolites exhibit an uptake at low partial pressure indicative of the presence of micropores. The ZSM-5@800 and ZSM-5@5000 samples displayed a Type-I isotherm, fast uptake at low relative pressure followed by plateau at without hysteresis, which

is usually observed for microporous materials with relatively low external surface areas. Other zeolites exhibit a combination of Type I and IV isotherms which besides the uptake at low relative pressure exhibit a hysteresis loop at high relatively pressure ($P/P_o > 0.8$). The presence of hysteresis at high relative pressures indicates the presence of meso- and macropores. The H1 type hysteresis is usually attributed to filling and emptying of cylinder mesopores of rather constant cross section [27]. The BJH mesopore size distribution curves are shown in Figure 5-3b. The evaluation of average mesopore sizes using BJH method gives the values between 25 and 50 nm in the zeolite samples. It is worth mentioning that the mesopore diameter increases with the increase in the zeolite crystallite sizes from ZSM-5@60 to ZSM-5@110.

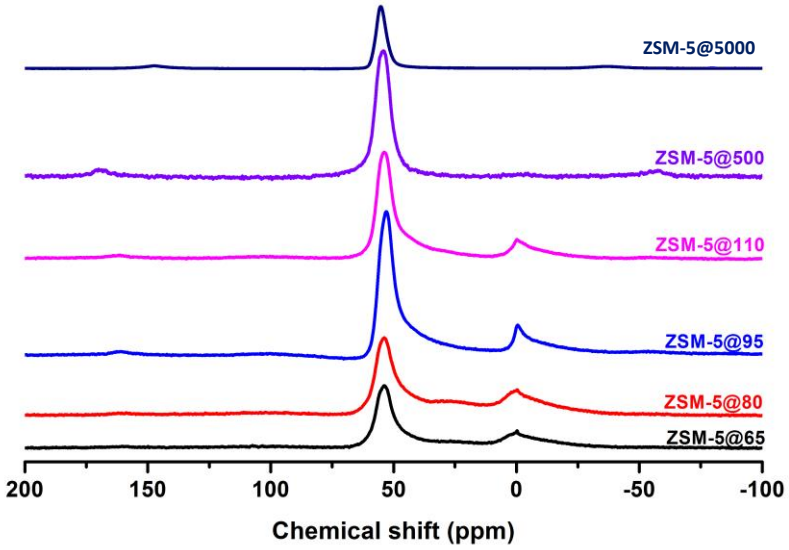

Figure 5-4. Normalised ^{27}Al MAS NMR spectra of various ZSM-5 zeolites.

^{27}Al MAS solid state NMR spectra (Figure 5-4) were collected for selected samples in order to determine the effect of particle size on the environment around the aluminum atoms in the framework. The spectra display a strong chemical shift at 50 ppm, which corresponds to tetrahedrally coordinated aluminum present in the ZSM-5 zeolite [28]. Additionally, a weak peak was observed at 0 ppm indicating the presence of a small amount of extra framework octahedrally coordinated aluminum in the samples. The intensity of the signal at 50 ppm is weaker on ZSM-5@65 and ZSM-5@80, indicating their lower framework Al content. Additionally, a broad signal of low intensity in the range of 25-35 ppm, attributed to the pentacoordinated aluminum [$Al(O)_5$], was found only in the sample ZSM-5@65 and ZSM-5@80, ascribed to less ordered T_d framework Al atoms present in not perfectly crystalline zeolites. ^{27}Al NMR results indicate, however, lower zeolite crystallinity for very small zeolite nanocrystallites in ZSM-5@65 and ZSM-5@80 zeolites. Lower zeolite

crystallinity might lead to lower concentration of Brönsted acid sites in smaller nanocrystallites compared to the samples with large crystallites. Only tetrahedrally coordinated Al^{3+} ions are found in the commercial ZSM-5@500 and ZSM-5@5000 samples.

5.3.2. Zeolite acidity

To study the influence of morphology on the concentration and acidic properties of ZSM-5 hydroxyl groups, we have investigated their FTIR spectra. The FTIR spectra of zeolites in the region of OH stretching vibration are shown in Figure 5-5. They show the presence of an intense peak at 3740 cm^{-1}, which can be attributed to silanol hydroxyl groups on the external zeolite surface or silanol groups related to the defect sites [29]. A peak at 3620 cm^{-1} is also observed which can assigned to the bridged Si-OH-Al groups which correspond to the zeolite Brönsted acid sites [30]. The intensity of the FTIR band at 3620 cm^{-1} assigned to the bridged hydroxyl groups increases with the increase in zeolite crystallite sizes from ZSM-5@65 to ZSM-5@110.

Interestingly, the area of the band at 3740 cm^{-1} decreases as the crystallite size of the samples increases with the order of ZSM-5@65 > ZSM-5@80 > ZSM-5@95 > ZSM-5@110. This confirms that ZSM-5@65 and ZSM-5@80 samples have larger external surface area and defect sites on the external surface owing to the very small crystallites. The results are consistent with the N_2 adsorption and ^{27}Al NMR data which showed somewhat lower crystallinity of these samples. The peaks at 3670-3665 cm^{-1} were also detectable in ZSM-5@95, ZSM-5@110 and ZSM-5@5000. These peaks might be due to the vibration of hydroxyl groups, having intermediate acidity between those of γ-$A1_2O_3$ and zeolite. They are associated with extraframework aluminum species [31].

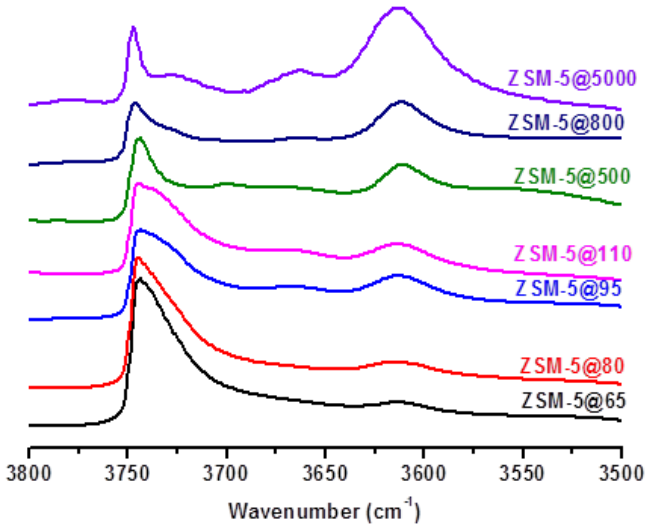

Figure 5-5. FTIR spectra of zeolites in the region of OH stretching vibrations.

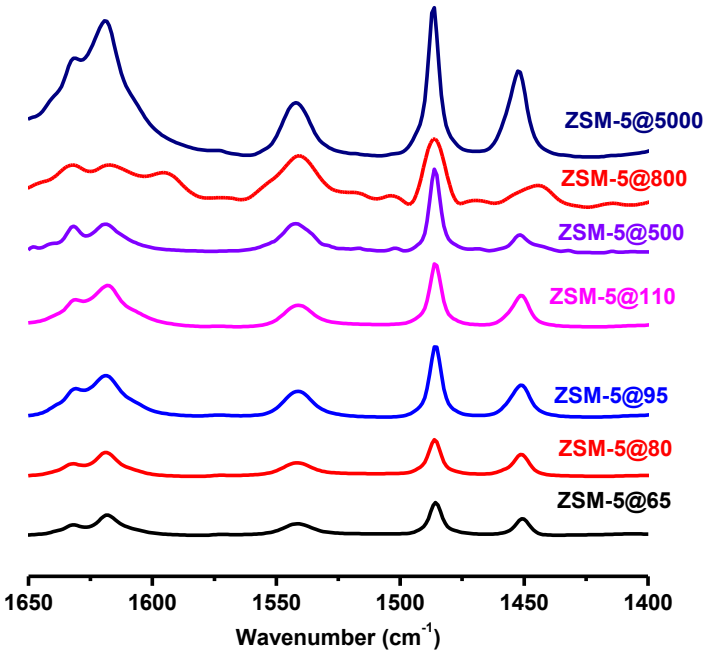

Figure 5-6. FTIR spectra of zeolites with adsorbed pyridine.

The FTIR spectra of adsorbed pyridine (Py, pK_b=3.5) were used for characterization of both Brönsted and Lewis acidic sites in the zeolites [32]. The IR spectra of the zeolites with pyridine adsorbed at 150 ℃ are shown in Figure 5-6. The intense IR bands at 1540, 1490 and 1450 cm^{-1} are observed. The bands at 1540 cm^{-1} is attributed to Py adsorbed on Brönsted acid hydroxyl group of the zeolites (PyH^+ species), while the band at 1450 cm^{-1} corresponds to Py adsorption on the zeolite Lewis acid sites. The results obtained using pyridine adsorption is consistent with the characterization of hydroxyl group in the zeolites using FTIR spectroscopy (Figure 5-5). The peak at 1490 cm^{-1} is due to pyridine adsorbed on both Brönsted and Lewis acid sites. It can be observed that the intensity of the bands corresponding to Brönsted and Lewis acid sites increases in the order: ZSM-5@5000 > ZSM-5@800>ZSM-5@500 > ZSM-5@110 ≈ ZSM-5@95> ZSM-5@80 > ZSM-5@65. The amounts of Py adsorbed on Brönsted (BAS) and Lewis acid sites in the zeolites calculated from the FTIR data are shown in Table 5-1. The spectra of adsorbed pyridine indicate higher concentration of Brönsted and Lewis acid sites in the zeolite samples containing larger crystallite agglomerates. Indeed, the intensity of IR bands at 1540 and 1450 cm^{-1} is significantly higher in ZSM-5@800 zeolite compared to ZSM-5@80. Note that both samples have the same Si/Al ratio. Hence, one might suggest that nanocrystals contain more Lewis sides than the Brönsted sides. This is often related with specific conditions of synthesis of nanosized crystals.

5.3.3. Acidity of the external surface of zeolite crystallites

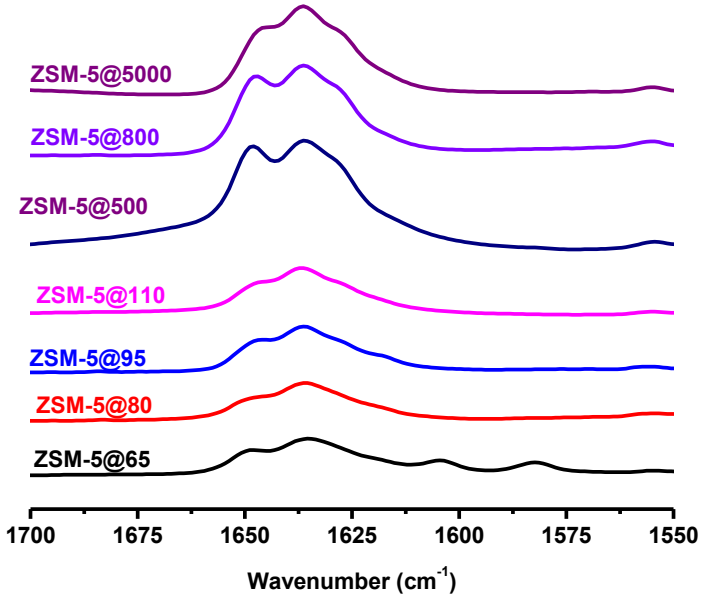

Figure 5-7. FTIR spectra of zeolites with adsorbed lutidine.

The zeolite acidity on the external surface of zeolites was characterized by lutidine (2,6-dimethylpyridine, pK_b = 8.7) adsorption. The diameter of lutidine (6.7 Å) is larger than the channel diameter of ZSM-5 zeolites. This molecule is often used for evaluation of the acid sites located on the external surface and in the meso- and macropores of zeolites [33]. The FTIR spectra of adsorbed lutidine are shown in Figure 5-7. The spectra show the FTIR bands at 1610 and 1640 cm^{-1} which can be assigned to the lutidine molecules adsorbed on the Brönsted sites located on the outer surface of the zeolites. The amounts of adsorbed lutidine were calculated using the extinction molar coefficients of protonated lutidine [34]. The amounts of adsorbed lutidine are shown in Table 5-1. The concentration of protonated lutidine is also different for the zeolite with different crystallite sizes. ZSM-5@5000 has the higher concentration of external surface acid sites, followed by the order: ZSM-5@5000 > ZSM-5@800>ZSM-5@500>>ZSM-5@95≈ZSM-5@110≈ZSM-5@80 ≈ ZSM-5@65.

Table 5-1. Characterization of ZSM-5 zeolites

Zeolite	Si/Al ratio	Part. size, nm	S_{BET} m^2/g	S_{ext} m^2/g	S_{micro} m^2/g	V_{total} cm^3/g	V_{micro} cm^3/g	Py ads, μmol/gcat		Lu ads. BS* $\mu mol/g_{cat}$
								BS*	LS*	
ZSM-5@65	36	65	382	206	176	0.586	0.093	48	53	39
ZSM-5@80	24	80	395	201	194	0.627	0.104	52	69	41
ZSM-5@95	31	95	352	182	170	0.544	0.095	108	116	38
ZSM-5@110	27	110	369	180	189	0.493	0.092	92	97	42
ZSM-5@500	45	500	383	197	186	0.529	0.091	109	164	93
ZSM-5@800	25	500-1000	381	139	242	0.258	0.118	149	196	101
ZSM-5@5000	13	~5000	305	61	241	0.188	0.116	217	291	111

BS: Brönsted acid sites;

LS: Lewis acid sites.

Lu ads BS: External Brönsted acid sites.

5.3.4 Characterization of the CZA methanol synthesis catalyst

The CZA catalyst was prepared using conventional coprecipitation. The characterization information of this catalyst has been already presented in chapter 3. The XRD patterns of the CZA catalyst are presented in Figure 3-1. Only CuO and ZnO diffraction peaks are detected. No diffraction peaks of Al_2O_3 phase were present even at aluminum content of 10 %. This suggests that aluminum oxide is probably present in the amorphous form. The XRD peaks at 32.5 °; 35.5 °; 38.7 °; 48.7 °; 58.3 °; 61.5 °; 67.9 ° were assigned to the CuO tenorite phase, while the peaks in 2θ = 31.8°; 36.3°; 47.7°; 62.9° were attributed to the ZnO zincite phase. After the reduction the copper particles in the CZA catalysts were measured by TEM. The copper nanoparticles with mean size of 5 nm or embedding the plate like Zn and Al oxide grains were detected. The thickness of the Cu metallic layer varied from a few to 15 nm.

The H_2-TPR profile (see chapter 3, Figure 3-2) of the CZA catalyst exhibits a broad reduction peak at 270 ℃. The peak integration suggests that in the temperature range from room temperature to 400 ℃, hydrogen consumption corresponds to the reduction of CuO into metallic copper. The TPR profile of the CZA is also consistent with previous reports [35].

5.3.5. Catalytic performance in DME synthesis

The catalytic performance data of mechanical mixtures of CZA and zeolite with different crystallite sizes at 260 ℃ and 20 bar are given in Figure 5-8 and Table 5-2. Dimethyl ether, methanol, carbon dioxide, hydrocarbons and water were the major products of carbon monoxide hydrogenation. Figure 5-8 displays CO conversion measured on different catalysts at GHSV=3600 cm^3/g_{cat} h as a function of reaction time. Carbon monoxide conversion slowly decreases with time on stream which can be attributed to the catalyst deactivation. Previous reports [36] suggest that the deactivation of CZA/ZSM-5 catalysts can be due to several phenomena: copper sintering, copper oxidation and migration to the cationic positions of zeolite, coke deposition). The deactivation phenomena are discussed in a great detail in chapter 4.

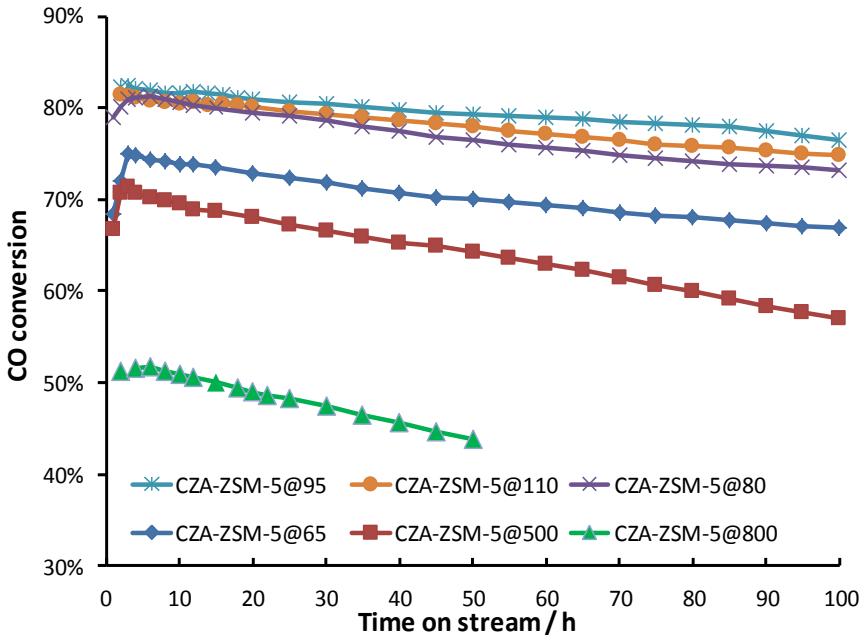

Figure 5-8. Carbon monoxide conversion on the hybrid CZA-ZSM-5 catalysts as function of time on stream (T=260 °C, P=20 bar, H_2/CO=2, GHSV=3600 cm^3/g_{cat} h)

Interestingly, carbon monoxide conversion rate is principally affected by the zeolite particle sizes. Higher reaction rate is observed on the catalysts containing smaller individual zeolite crystallites, while the reaction rate was much lower on the catalysts containing larger zeolite crystallite agglomerates (CZA-ZSM-5@500, CZA-ZSM-5@800 and CZA-ZSM-5@5000). At GHSV=3600 cm^3/g_{cat} h (Table 5-2), the CO conversion showed the following order of activity for the hybrid catalysts: CZA-ZSM-5@95 > CZA-ZSM-5@110 > CZA-ZSM-5@80 > CZA-ZSM-5@65 > CZA-ZSM-5@500 > CZA-ZSM-5@5000>CZA-ZSM-5@800. The CO conversion profiles over hybrid catalysts CZA-ZSM-5 widely varied with

the particle size of ZSM-5: nano-sized ZSM-5@95, ZSM-5@110, and ZSM-5@80 maintained CO conversion of 83.2 %, while the ZSM-5@500, ZSM-5@800 and ZSM-5@500 zeolites exhibited lower CO conversion. The catalytic results obtained at carbon monoxide conversion between 60 and 80 % indicate much slower deactivation of hybrid catalyst constituted by smaller individual zeolite crystallites. The following order relative to the deactivation rate was observed for the studied catalysts: CZA-ZSM-5@5000 > CZA-ZSM-5@500 > CZA-ZSM-5@65 > CZA-ZSM-5@80 > CZA-ZSM-5@110 > CZA-ZSM-5@95.

Table 5-2. The catalytic performance of hybrid catalysts at different GHSV

Catalyst	Integral reaction rate, 10^{-6} $mol_{CO}/s\ g_{cat}$	Conversion, %	S_{CH3OH}, %	S_{DME}, %	S_{CO2}, %	S_{HC}, %
GHSV=3600 cm^3/g_{cat} h						
CZA/ZSM-5@65	9.82	75.0	4.5	69.8	25.3	0.40
CZA/ZSM-5@80	10.6	81.1	1.6	72.3	25.9	0.20
CZA/ZSM-5@95	10.7	82.2	1.6	71.4	26.6	0.40
CZA/ZSM-5@110	10.7	81.4	0.9	72.5	26.3	0.30
CZA/ZSM-5@500	9.3	71.3	5.4	67.7	27.3	0.10
CZA/ZSM-5@800	6.7	51.2	22.3	56.7	19.1	1.9
CZA/ZSM-5@5000	8.5	64.6	4.0	62.2	30.0	3.80
GHSV=7200 cm^3/g_{cat} h						
CZA/ZSM-5@80	15.8	56.8	0.9	73.3	25.5	0.3
CZA/ZSM-5@95	19.3	69.5	1.1	73.4	25.1	0.4
CZA/ZSM-5@110	16.4	59.1	0.8	73.4	25.5	0.3
CZA/ZSM-5@500	13.1	47.1	6.1	68.6	25.1	0.2
CZA/ZSM-5@800	9.8	35.3	18.2	48.7	32.2	1.0
CZA/ZSM-5@5000	9.4	34.0	4.8	66.4	26.7	2.1
GHSV=14400 cm^3/g_{cat} h						
CZA/ZSM-5@80	18.9	34	1.5	73.0	25.3	0.20
CZA/ZSM-5@95	26.0	46.8	1.0	73.9	24.8	0.30
CZA/ZSM-5@110	20.5	37	1.1	73.2	25.3	0.40
CZA/ZSM-5@500	14.4	26	1.5	71.3	27	0.20
CZA/ZSM-5@5000	10.5	19	5.4	70.8	20.5	3.30

To evaluate in a more comprehensive manner the influence of the carbon monoxide conversion on the reaction selectivity, the catalytic tests with the hybrid CZA/ZSM-5 catalysts were conducted at different gas spaces velocities. The results are shown in Table 5-2. As expected, higher gas space velocity leads to lower carbon monoxide conversion which was accompanied by noticeable modifications in the selectivity patterns. DME synthesis is a consecutive reaction which involves carbon monoxide hydrogenation to methanol followed by methanol dehydration. The selectivity of carbon monoxide hydrogenation could be dependent on the conversion level. Methanol is a primary product of carbon monoxide hydrogenation. As expected, the selectivity to methanol is higher at lower carbon monoxide conversion. At higher conversions, however, only very small amounts of methanol are produced. Note that even at the same conversion level, higher methanol selectivity (at the expense of DME selectivity) was observed on the catalysts with larger zeolite agglomerates (CZA-ZSM-5@500, CZA-ZSM-5@800 and CZA-ZSM-5@5000). Carbon dioxide selectivity however is not influenced by carbon monoxide conversion. Higher selectivity to carbon dioxide at different conversions can be due to very high rate of water gas shift reaction under the reaction conditions. Carbon dioxide formation is also favored by thermodynamics. Hydrocarbons are only present in trace amounts; their selectivity is not much affected by carbon monoxide conversion.

5.4 Discussion

5.4.1. Zeolite particle sizes and performance of bifunctional CZA-ZSM-5 catalysts for DME synthesis

The present work reveals a strong impact of zeolite particle size on the catalytic performance of CZA-ZSM-5 catalyst in direct DME synthesis from syngas. DME synthesis involves bifunctional catalysts. Carbon monoxide hydrogenation to methanol occurs on copper catalysts, while methanol dehydration involves the ZSM-5 zeolite. Methanol synthesis over the copper catalysts at 260 ℃ is a reversible reaction. At the reaction temperatures employed in this work, the yield of methanol from H_2/CO in over a methanol synthesis catalyst would be principally dependent on the thermodynamic equilibrium rather on the reaction kinetics. Addition of methanol dehydration function to the methanol synthesis catalysts shifts the thermodynamic equilibrium and favors DME formation. Methanol dehydration involves the zeolite acid sites [37]. In binfunctional copper zeolite catalysts the DME yield could be a function of the rates of both methanol synthesis and methanol

dehydration. The concentration and distribution of zeolite acid sites is therefore important for DME productivity.

The results obtained in the present work show that in addition to the zeolite acidity, the zeolite crystallite size and crystallite aggregation can also strongly affect the rate of direct DME synthesis. The rate of carbon monoxide conversion versus reciprocal zeolite particle sizes is shown in Figure 5-9. Higher DME production rates were observed on the catalysts containing smaller zeolite crystallites, while the reaction rate was much lower in the catalysts with larger zeolite aggregates. Surprisingly, that zeolite size has even a more significant effect of the reaction rate than the concentration of Brönsted acid sites. Indeed, the overall concentration of Brönsted acid sites measured by Py adsorption was higher in ZSM-5@500 (d_{aggl} = 500 nm) than in the ZSM-5@65, ZSM-5@80, ZSM-5@95 and ZSM-5@110 which contain smaller particles. ZSM-5@500 is built up of smaller but heavily intergrown crystallites. This limits the access to crystallite surface. Despite of lower concentration of zeolite acid sites, much higher carbon monoxide DME production rate was observed on the catalysts containing smaller highly accessible zeolite particles.

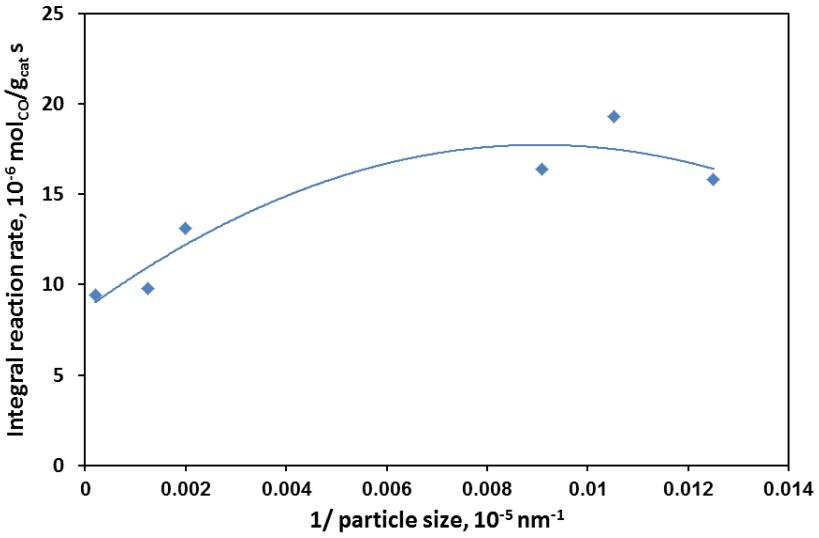

Figure 5-9. Carbon monoxide conversion as a function of reciprocal zeolite particle size in hybrid CZA-ZSM-5 catalysts (T=260 °C, GHSV=7200 cm^3/g_{cat} h, P=20 bar, H_2/CO=2).

The concept of multi-functional catalysis was developed by Weiss [38]. It was suggested that in bi-functional catalysis, the kinetic steps of the consequent reactions are coupled to each other through the processes of diffusion of these intermediates from one type of sites to another. The two types of active sites in bifunctional catalysts should be as closer as possible for higher catalytic activity and selectivity [39]. Depending on the diffusion rate

of the reaction intermediates, the observed influence of the zeolite particle size on the rate of DME synthesis can be due to at least two different phenomena. First, it can be assumed that in bifunctional CZA-ZSM-5 catalysts methanol dehydration preferentially occurs on the zeolite external surface or in the mesopores. Because of diffusion limitations under the reaction conditions, the acid sites located inside the zeolite crystallite would be less accessible for the reacting molecules. However, our recent work [36] has ruled out this hypothesis. In this work the zeolite external surface was sylilated with TEOS in order to reduce its acidity. The catalytic data obtained with sylilatated zeolites did not shown any significant decrease in the reaction rate. This suggests that the acidity of zeolite external surface or mesopores is not a determining factor for higher carbon monoxide hydrogenation rate.

The second hypothesis which can explain the positive effect of smaller zeolite crystallites on the catalytic performance can be assigned to the enhanced transport of methanol produced on the CZA catalyst to the ZSM-5 crystallites for dehydration. In this case, smaller zeolite particles (crystallites or agglomerates) reduce methanol transport limitations and diffusion path inside the zeolites. The dehydration in this case occurs both inside the zeolite crystallite and on the external surface. The reaction rate is probably strongly affected by the methanol transport from the methanol synthesis catalyst to the zeolite external surface which serves as an interface between hydrogenation and acidic component in the bi-functional catalysts. Smaller crystallite sizes or mesopores lead to shortening the diffusion path lengths and improve transport of the reaction intermediates [40]. The presence of larger zeolite agglomerates in ZSM-5@500, ZSM-5@800 and ZSM-5@5000 make the contact between the methanol synthesis catalyst and zeolite more difficult. Figure 5-10 shows TEM image of CZA-ZSM-5@500 catalysts. It can be seen that the contact between CZA and ZSM-5 components is strongly affected by the size and roughness of the zeolite particles. A poor contact between methanol synthesis catalysts and zeolite agglomerates in the catalyst prepared by mechanical mixing leads to significant transport limitations for methanol and thus to lower overall reaction rate.

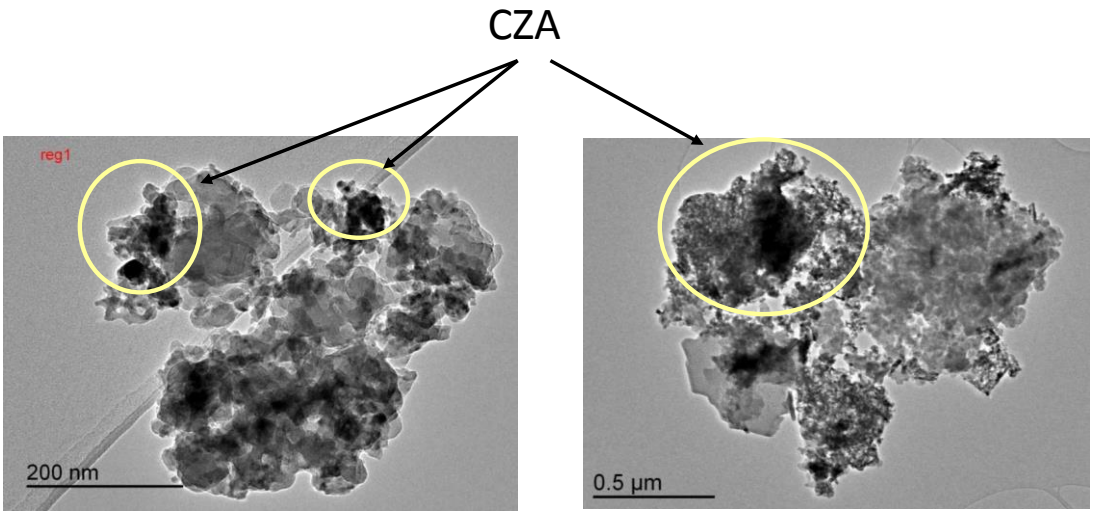

Figure 5-10. Localization of copper methanol synthesis component in CZA-ZSM-5@500 containing larger intergrown zeolite agglomerates

The influence of transport phenomena on the reaction rate and selectivity was previously observed for hydroisomerisation reactions occurring on Pt/zeolite catalysts. Guisnet et al. [41] showed that the rate and selectivity of n-C_{16} hydroisomerization is determined by the degree of intimacy between metallic and acidic functions. Recently Kim et al. [42] investigated the effect of zeolite crystal thickness and Pt location on the performance of bi-functional Pt/ZSM-5 catalysts for hydroisomerisation and observed similar phenomena. The hypothesis about enhanced transport of the reaction intermediates in the catalysts containing smaller zeolite crystallites is also consistent with the selectivity data measured for the catalysts containing zeolite with variable crystallite sizes. Higher methanol selectivity systematically was observed on CZA-ZSM5@500, CZA-ZSM-5@800 and CZA-ZSM-5@5000 at different conversion levels. This indicates much slower methanol dehydration on the catalysts containing larger zeolite particles which probably arises due to the mass transfer limitations. Our results suggest that in addition to the size for individual zeolite crystallites, the presence of zeolite agglomerate may also significantly affect the rate of catalysts reactions in bifunctional catalysts. Indeed, the rate of diffusion can be limited not by individual zeolite crystallite sizes but by the diameter of zeolite intergrown agglomerates.

5.4.2. Catalyst stability

The bifunctional CZA-ZSM-5 catalysts for direct DME synthesis prepared using zeolites with a wide range of crystallite sizes showed different stability. Nano-sized ZSM-5@95, ZSM-5@110, and ZSM-5@80 did not show appreciable deactivation for up to 100 h,

while the ZSM-5@5000 and ZSM-5@500 zeolites are noticeably deactivated. The fact that the deactivation phenomenon took place in a sample containing small crystallites (ZSM-5@500), which are heavily agglomerated and thus built larger particles, show that the accessibility to zeolite crystals is of paramount importance. Catalyst deactivation was more significant at higher carbon monoxide conversion (60-80 %). First we evaluated the role of total zeolite Brönsted acidity in the catalyst deactivation. No reasonable correlation between the deactivation rate and total concentration of Brönsted acid sites measured using Py adsorption was observed.

The deactivation CZA-ZSM-5 catalysts can be due to several phenomena: copper sintering [43] copper oxidation, carbon deposition, etc… The detailed mechanisms of deactivation of hybrid copper-zeolite catalysts have been disclosed in previous reports. Those reports emphasize the role of external zeolite surface in catalyst deactivation. Garcia-Trenco et al [44] attributed deactivation of hydride CZA-ZSM-5 catalyst to the aluminum extra-framework species located at the surface of contact between the CZA and zeolite particles. It was suggested that these species could migrate to the CZA catalyst during DME synthesis through a water-assisted mechanism, modifying the interaction between Cu and ZnO_x. On the basis of ex-situ characterization conducted in our recent report [36], deactivation of CZA-ZSM-5 catalyst was attributed to copper sintering, oxidation and ion exchange, which are enhanced in the presence of higher concentration of Brönsted acid sites on the external surface of zeolite. The deactivation was slowed down by neutralization of the acid sites on the zeolite outer surface with tetraethyl orthosilicate (TEOS).

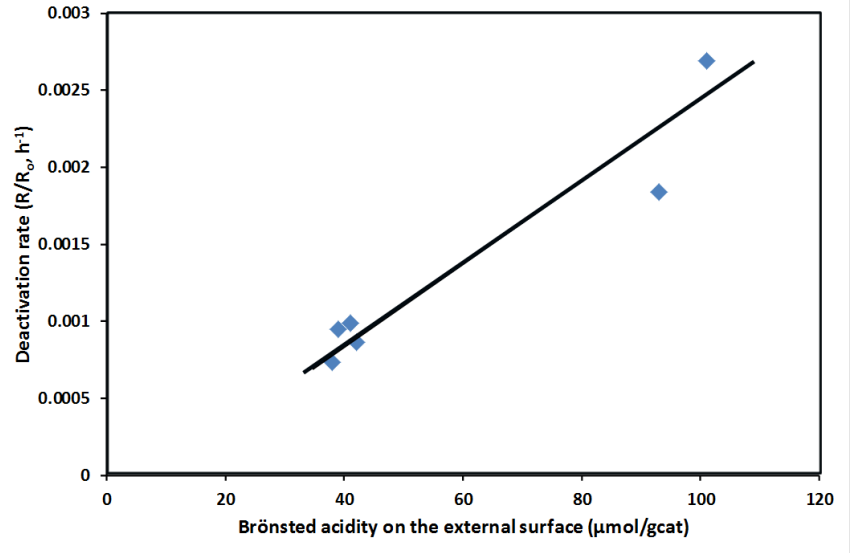

Figure 5-11. Rate of deactivation of CZA-ZSM-5 catalysts as a function of the concentration of Brönsted acid sites on the zeolite external surface measured by lutidine adsorption.

In order to further clarify the effects of the external surface acidity on the deactivation of hybrid catalysts with variable zeolite crystallites, the deactivation rates of different catalysts were compared as a function of the concentration of Brönsted acid sites on external zeolite surface area. The surface sites on the external surface of zeolite were measured by lutidine adsorption. Figure 5-11 shows the rate for catalyst deactivation measured at carbon monoxide conversion of 60-80 % versus the concentration of Brönsted acid sites on the external surface of zeolites estimated from the lutidine adsorption. A more rapid deactivation occurs on the catalysts with higher concentration of acid sites on the external surface. Very high concentration of Brönsted sites on the external surface of ZSM-5@5000 leads to a higher deactivation rate. At the same time, ZSM-5@95 which has a lowest surface acidity on the external surface showed better stability. In agreement with previous report [36], higher surface acid sites of zeolite could lead to intensification of the Cu migration, which results in copper sintering during DME synthesis. A decrease in the number of acid sites on the zeolite external surface can lead therefore to better catalyst stability.

5.5 Conclusion

The obtained results point out a correlation between the performance of bifunctional hybrid CZA-ZSM-5 catalysts for direct DME synthesis and zeolite particle sizes. The catalyst containing smaller individual zeolite crystallites showed higher carbon monoxide conversion rates and higher DME productivities. The observed effects were attributed to the methanol transport phenomena in bifinctional hybrid catalysts from the copper catalyst to the zeolite acid sites. The methanol transport is enhanced in the catalysts containing smaller zeolite crystallites, while the presence of crystallite intergrown agglomerates introduces diffusion limitations. The influence of zeolite particles sizes on the catalytic performance seems even more significant than the effect of total concentration of zeolite Brönsted acid sites.

The catalysts showed noticeable deactivation with time on stream. The deactivation rate was correlated with the concentration of Brönsted acid sites on the external surface of zeolite crystallites. Lower concentration of Brönsted sites on the zeolite external surface leads to a less rapid deactivation and better stability of copper-zeolite hybrid catalysts.

The results obtained in this chapter indicate a new methodology for catalyst design for direct DME synthesis from syngas. Smaller zeolite ZSM-5 crystallite size and lower concentration of Brönsted acid sites on the zeolite external surface seem to be beneficial for

the design of active, selective and stable hybrid CZA-ZSM-5 catalysts for direct DME synthesis from syngas.

5.6 References

[1] J.W. Jeong, C.-I. Ahn, D.H. Lee, S.H. Um, J.W. Bae, Catalysis letters, 143 (2013) 666-672.

[2] J.W. Jung, Y.J. Lee, S.H. Um, P.J. Yoo, D.H. Lee, K.-W. Jun, J.W. Bae, Applied Catalysis B: Environmental, 126 (2012) 1-8.

[3] J.-L. Li, X.-G. Zhang, T. Inui, Applied Catalysis A: General, 147 (1996) 23-33.

[4] T. Takeguchi, K.-i. Yanagisawa, T. Inui, M. Inoue, Applied Catalysis A: General, 192 (2000) 201-209.

[5] D. Mao, W. Yang, J. Xia, B. Zhang, G. Lu, Journal of Molecular Catalysis A: Chemical, 250 (2006) 138-144.

[6] I. Sierra, J. Ereña, A.T. Aguayo, J.M. Arandes, J. Bilbao, Applied Catalysis B: Environmental, 94 (2010) 108-116.

[7] V. Vishwanathan, K.-W. Jun, J.-W. Kim, H.-S. Roh, Applied Catalysis A: General, 276 (2004) 251-255.

[8] J. Fei, Z. Hou, B. Zhu, H. Lou, X. Zheng, Applied Catalysis A: General, 304 (2006) 49-54.

[9] J.-H. Kim, M.J. Park, S.J. Kim, O.-S. Joo, K.-D. Jung, Applied Catalysis A: General, 264 (2004) 37-41.

[10] J.W. Bae, S.-H. Kang, Y.-J. Lee, K.-W. Jun, Applied Catalysis B: Environmental, 90 (2009) 426-435.

[11] A. Ciftci, N.A. Sezgi, T. Dogu, Industrial & Engineering Chemistry Research, 49 (2010) 6753-6762.

[12] K.S. Yoo, J.-H. Kim, M.-J. Park, S.-J. Kim, O.-S. Joo, K.-D. Jung, Applied Catalysis A: General, 330 (2007) 57-62.

[13] F. Yaripour, F. Baghaei, I. Schmidt, J. Perregaard, Catalysis Communications, 6 (2005) 542-549.

[14] A. García-Trenco, S. Valencia, A. Martínez, Applied Catalysis A: General, 468 (2013) 102-111.

[15] M. Stiefel, R. Ahmad, U. Arnold, M. Döring, Fuel Processing Technology, 92 (2011) 1466-1474.

[16] P. Weisz, V. Frilette, The Journal of Physical Chemistry, 64 (1960) 382-382.

[17] T.F. Degnan, Journal of Catalysis, 216 (2003) 32-46.

[18] B. Smit, T.L. Maesen, Nature, 451 (2008) 671-678.

[19] E. Verheyen, C. Jo, M. Kurttepeli, G. Vanbutsele, E. Gobechiya, T.I. Korányi, S. Bals, G. Van Tendeloo, R. Ryoo, C.E. Kirschhock, Journal of Catalysis, 300 (2013) 70-80.

[20] B. Vandegehuchte, J. Thybaut, A. Martinez, M. Arribas, G. Marin, Applied Catalysis A: General, 441 (2012) 10-20.

[21] R. Jentoft, M. Tsapatsis, M. Davis, B. Gates, Journal of Catalysis, 179 (1998) 565-580.

[22] L. Bonetto, M. Camblor, A. Corma, J. Perez-Pariente, Applied Catalysis A: General, 82 (1992) 37-50.

[23] Y.J. Lee, J.-H. Kim, S.H. Kim, S.B. Hong, G. Seo, Applied Catalysis B: Environmental, 83 (2008) 160-167.

[24] J.H. Lee, M.B. Park, J.K. Lee, H.-K. Min, M.K. Song, S.B. Hong, Journal of the American Chemical Society, 132 (2010) 12971-12982.

[25] H.-G. Jang, H.-K. Min, J.K. Lee, S.B. Hong, G. Seo, Applied Catalysis A: General, 437 (2012) 120-130.

[26] M. Firoozi, M. Baghalha, M. Asadi, Catalysis Communications, 10 (2009) 1582-1585.

[27] D. Everett, JA Barker, ibid, (1958) 125.

[28] G. Majano, A. Darwiche, S. Mintova, V. Valtchev, Industrial & engineering chemistry research, 48 (2009) 7084-7091.

[29] J.A. Lercher, A. Jentys, Studies in surface science and catalysis, 168 (2007) 435-476.

[30] A. Zecchina, S. Bordiga, G. Spoto, D. Scarano, G. Petrini, G. Leofanti, M. Padovan, C.O. Areán, Journal of the Chemical Society, Faraday Transactions, 88 (1992) 2959-2969.

[31] I. Kiricsi, C. Flego, G. Pazzuconi, W.J. Parker, R. Millini, C. Perego, G. Bellussi, The Journal of Physical Chemistry, 98 (1994) 4627-4634.

[32] G. Crépeau, V. Montouillout, A. Vimont, L. Mariey, T. Cseri, F. Maugé, The Journal of Physical Chemistry B, 110 (2006) 15172-15185.

[33] F. Thibault-Starzyk, I. Stan, S. Abelló, A. Bonilla, K. Thomas, C. Fernandez, J.-P. Gilson, J. Pérez-Ramírez, Journal of Catalysis, 264 (2009) 11-14.

[34] T. Onfroy, G. Clet, M. Houalla, Microporous and Mesoporous Materials, 82 (2005) 99-104.

[35] J.M. Beiramar, A. Griboval‐Constant, A.Y. Khodakov, ChemCatChem, 6 (2014) 1788-1793.

[36] V. Ordomsky, M. Cai, V. Sushkevich, S. Moldovan, O. Ersen, C. Lancelot, V. Valtchev, A. Khodakov, Applied Catalysis A: General, 486 (2014) 266-275.

[37] M. Migliori, A. Aloise, G. Giordano, Catalysis Today, 227 (2014) 138-143.

[38] P.B. Weisz, Advances in catalysis, 13 (1962) 137.

[39] J. Cejka, Introduction to zeolite science and practice, Elsevier, 2007.

[40] M. Choi, K. Na, J. Kim, Y. Sakamoto, O. Terasaki, R. Ryoo, Nature, 461 (2009) 246-249.

[41] N. Batalha, L. Pinard, C. Bouchy, E. Guillon, M. Guisnet, Journal of Catalysis, 307 (2013) 122-131.

[42] J. Kim, W. Kim, Y. Seo, J.-C. Kim, R. Ryoo, Journal of Catalysis, 301 (2013) 187-197.

[43] F.S. Barbosa, V.S. Ruiz, J.L. Monteiro, R.R. de Avillez, L.E. Borges, L.G. Appel, Catalysis letters, 126 (2008) 173-178.

[44] A. García-Trenco, A. Martínez, Catalysis Today, 227 (2014) 144-153.

Chapter 6. Effect of Sn additives on the CuZnAl-HZSM-5 hybrid catalysts for the direct DME synthesis from syngas

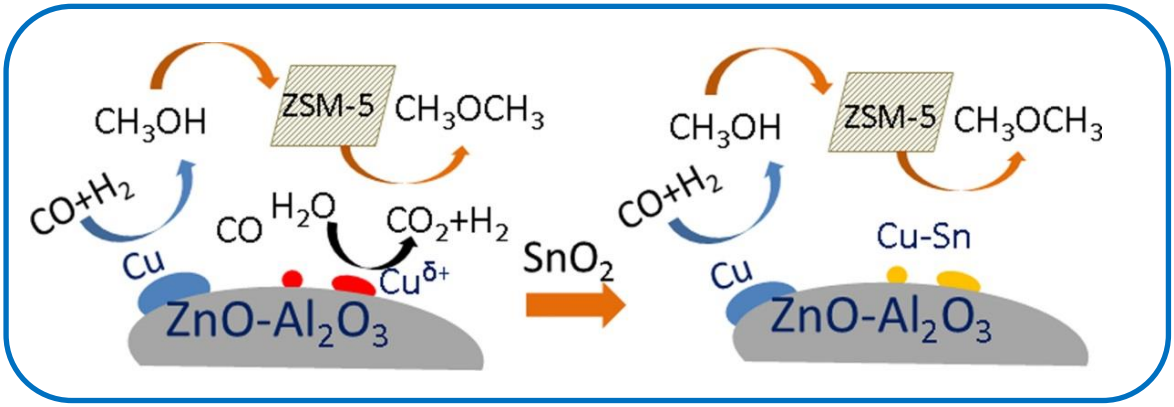

This chapter has been published as:

Cai M, V Subramanian, V.V. Sushkevich, V.V Ordomsky, A.Y. Khodakov, Effect of Sn additives on the CuZnAl-HZSM-5 hybrid catalysts for the direct DME synthesis from syngas, Applied Catalysis A: General, 2015, 502: 370-379

Abstract

Tin-promoted bifunctional Cu-Zn-Al/HZSM-5 catalysts were prepared in order to increase the selectivity of carbon monoxide hydrogenation to dimethyl ether (DME). The catalysts were characterized by H_2-TPR, XRD, XPS and IR. The characterization revealed that the electronic properties and surface distribution of Cu in the catalysts were significantly changed by tin addition leading to the decrease in the fraction of positively charged Cu sites. Addition of tin suppressed the water gas shift reaction and decreases the selectivity to undesirable CO_2. As a result, the selectivity to valuable DME and methanol noticeably increased for the mildly promoted catalysts. Further increase in Sn loading led to the decrease in the rate of carbon monoxide conversion.

6.1 Introduction

In the direct synthesis of DME, the copper based catalysts exhibit high activity in both methanol synthesis and water gas shift reactions, which could result in the ample amount of CO_2. Most of previous works have addressed either optimization of overall activity of bifunctional catalysts for direct DME synthesis or lowering hydrocarbon production, while very few reports have focused on reducing carbon dioxide selectivity. Thus, Sun et al. [1] studied the effect of addition of different amounts of ZrO_2 in $CuO/ZnO/ZrO_2$/HZSM-5 instead of commonly used alumina. The authors explained the increase in the activity and selectivity of the catalyst to DME by Cu^+ species stabilized by ZrO_2 in the presence of metallic Cu. Moreover, a study reported by Li et al. [2] gave similar results about addition of La_2O_3 promoter with better catalytic performance compared with Cu-ZrO_2/γ-Al_2O_3 catalyst in CO conversion and enhanced DME selectivity due to the higher dispersion of copper species. Manganese has been also found as effective promoter of the catalyst activity in DME synthesis [3] and [4]. The authors have explained the effect by formation of Cu-Mn spinel oxide with higher dispersion of metallic copper in the reduced catalyst and higher rate in WGSR. Thus, these works have been more focused on the development of active catalyst usually by increase of the copper surface area.

Note that CO_2 is a major product in this reaction; its production can drastically undermine the carbon efficiency of the whole process. One of the ways to reduce the CO_2 selectivity in direct DME synthesis could be catalyst promotion. It can be expected that the efficient promoter would reduce the rate of WGSR, while the rate of DME synthesis could be only slightly affected.

Tin has been used as a promoter for a number of metal catalysts where it principally affects their hydrogenation activity. There have been numerous studies during the last decade devoted to noble metal hydrogenation catalysts (Pd, Pt, Ru) modified by tin [5-7]. Particularly, the alloys of tin with platinum have been shown to significantly enhance the selectivity of the hydrogenation to the α-β-unsaturated aldehydes. The reason of this catalytic effect is not well understood and different hypotheses exist: Sn might induce electronic effects on Pt, changing its adsorption properties or act a site-blocking agent changing the adsorption site of the molecules. To the best of our knowledge, the effect of tin on Cu hydrogenation catalysts has not been yet addressed in the literature.

The goal of the present work is to reduce the carbon dioxide selectivity in direct DME synthesis from syngas by promotion of CZA–HZSM-5(45) hybrid catalysts with tin. We suggest that there could be different active species for methanol synthesis and WGSR. Indeed, it has been shown earlier that activity in WGSR correlates with the amount of Cu^{+} sites with low redox potential between Cu^{+} and Cu^{2+} during WGSR [8]. At the same time, the activity in methanol synthesis correlates usually with surface area of metallic copper in the catalyst [9]. Thus, it might be possible to selectively deactivate the most active positively charged copper sites by electron donation from tin with increase in the selectivity to methanol and DME. A combination of characterization techniques (in-situ XRD, TPR, XPS, in-situ XANES and FTIR) were used to characterize the properties of the promoted catalysts. The catalytic performances in direct DME synthesis and water gas shift reaction were evaluated in a fixed reactor.

6.2 Results and discussion

6.2.1 Catalyst characterization

The ZSM-5(45) zeolite used for the preparation of hybrid catalysts has uniform particle size distribution in the range 5–7 μm (Figure. 6-1a). The zeolite particles consist of agglomerates of intergrown zeolite crystallites. The acidity of materials was studied by TPD-NH_3 (Figure. 6-1b). ZSM-5(45) exhibits the ammonia desorption at two temperatures: a low-temperature peak at 100-300 °C and a high-temperature peak at 400–600 °C corresponding respectively to the weaker and stronger acid sites. The total amount of acid sites determined by TPD of NH_3 is 993 μmol/g. The aluminum content in the sample determined by ICP analysis is higher (1280 μmol/g) due to the fact that a part of aluminum could be in extraframework positions with significantly weaker adsorption of ammonia.

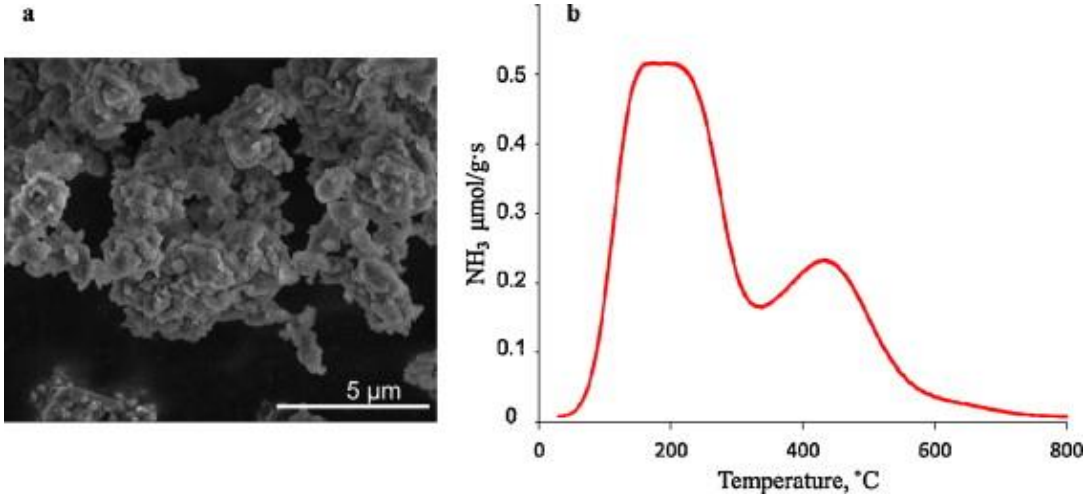

Figure. 6-1 SEM micrograph of ZSM-5 (a) and TPD-NH_3 profile for zeolite ZSM-5(45) (b).

The XRD patterns of calcined CZA catalysts with and without Sn are depicted in Figure. 6-2. The observed diffraction lines are assigned to CuO and ZnO. The absence of any peaks relevant to Al_2O_3 can be correlated to the amorphous nature of the alumina. Also, no extra peaks corresponding to tin oxide were seen in the XRD patterns. This can be due to low tin content (<1 wt.%) and its high dispersion in matrix CuO–ZnO. Interestingly, tin promotion does not affect the width of CuO and ZnO peaks. Thus, the size of copper and zinc oxide nanoparticles does not change after the tin promotion.

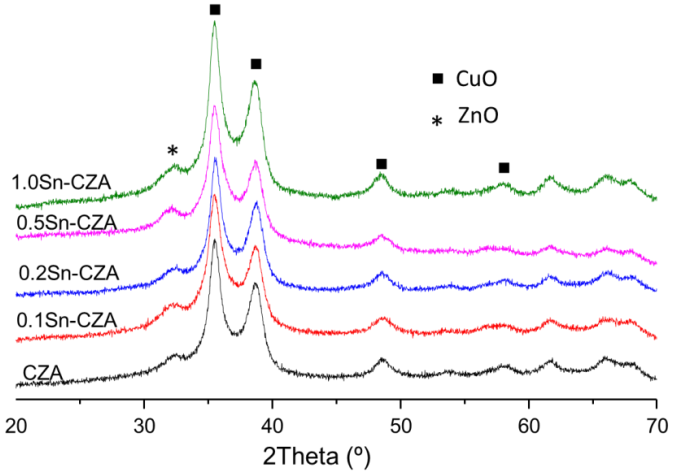

Figure. 6-2. XRD patterns of the parent and Sn promoted CuO-ZnO-Al_2O_3 catalysts.

Table 6-1. Characterization of CZA and Sn modified Sn-CZA catalysts.

Sample	TPR results		XPS analysis Cu 2p 3/2		Cu surface are and dispersion	
	T (°C)	H_2 consumption (mmol H_2/g_{cat})	Position (eV)	Area	S_{BET} (m^2/g_{cat})	D (%)
CZA	264	6.9	932.8	5572.3	36.2	12.2
0.1Sn–CZA	265	5	932.5	5149.5	31.2	14.5
0.5Sn–CZA	273	4.7	932.5	5004.4	24.5	12
1.0Sn–CZA	280	4.3	932.4	4817.2	18.9	10.2

To evaluate the reduction behavior, all the catalysts were analyzed by TPR. The reduction temperature lies between 264 and 280 °C (Table 6-1, Figure. 6-3). The parent catalyst, without the Sn promotion, showed a lowest reduction temperature of 264 °C. An increase in Sn content from 0.1 to 1.0 wt.%, results in higher reduction temperature. The same effect of the promotion with tin was earlier observed in Pt catalysts [10]. The effect has been explained by a reduction of both metals (Pt and Sn) with subsequent alloy formation. Reduction of the parent CZA sample results in the hydrogen consumption (Table 6-1) similar

to the content of CuO in the sample (7.3 mmol/g_{cat}). This indicates almost total reduction of Cu. Promotion by tin leads to lower hydrogen consumption (Table 6-1, Figure. 6-3). This suggests interaction of tin with copper with probable incorporation of tin species into copper oxide and/or possible deposition on the surface of copper oxide with decrease in the catalyst reducibility. Presence of tin in this case might suppress adsorption and migration of hydrogen on the surface with decrease of the rate of copper reduction. N_2O decomposition (Table 6-1) shows that the surface area of Cu decreases from 36 to 19 m^2/g with the increase in the tin content. The effect can be due to the formation of Cu–Sn mixed species but without significant segregation of copper with decrease of the amount of active Cu atoms.

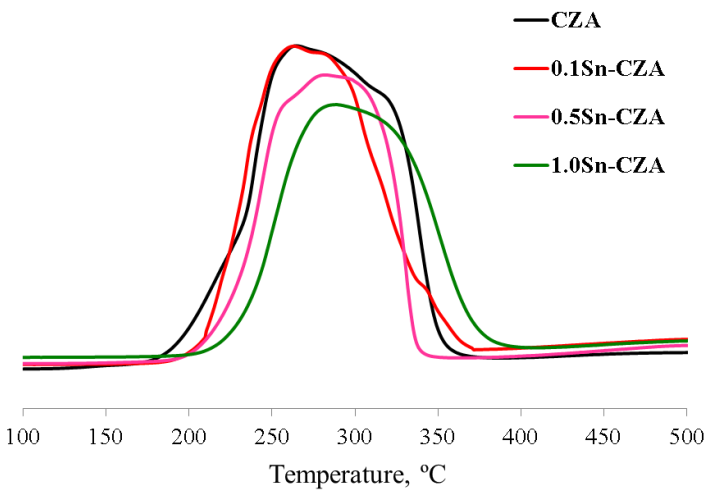

Figure. 6-3. TPR patterns of the parent and Sn promoted CuO-ZnO-Al_2O_3 catalysts.

To elucidate the change in the surface composition after Sn doping, XPS analysis was performed on the CZA and tin containing catalysts pretreated under both oxidizing and reducing atmospheres. As shown in the Figure. 6-4a, the Cu 2p3/2 binding energy was observed at 933.0 eV and the presence of Cu^{2+} shake up satellite peaks at 942 eV and 962 eV confirms the existence of mainly Cu^{2+} state in the catalysts after oxidation [11]. The XPS spectra of the oxidized catalysts were almost identical. The Cu 2p XPS spectra of xSn–CZA catalysts reduced in H_2 at 290 °C are shown in Figure. 6-4b. The disappearance of satellite peaks and simultaneous shift of the principal Cu 2p3/2 peak towards lower binding energies upon H_2-reduction are indicative of copper reduction to Cu^+ or Cu^0[12] and [13]. XPS indicates almost complete copper reduction. Somewhat lower hydrogen consumption in TPR experiments can be due to autoreduction of non-reduced part of copper oxide into metallic copper at higher temperatures over tin promoted catalysts. The Cu 2p3/2 BE values and widths of Cu^+ and Cu^0 species are almost identical. These species are difficult to distinguish from the XPS spectra [14]. However, it is interesting to note that the maximum of the peak is

slightly shifting for tin treated catalysts in the direction of lower BE (Figure. 6-4, Table 6-1). Earlier the shift of the XPS peak to the lower BE has been observed over reduced noble metal catalysts promoted by tin [15] and was explained by charge transfer from Sn to the noble metal due to the formation of alloy with tin. The area of Cu 2p3/2 peak decreases with increase in the tin content (Table 6-1). This could be due to the analysis of only surface species by XPS where content of Cu should be lower due to the presence of tin.

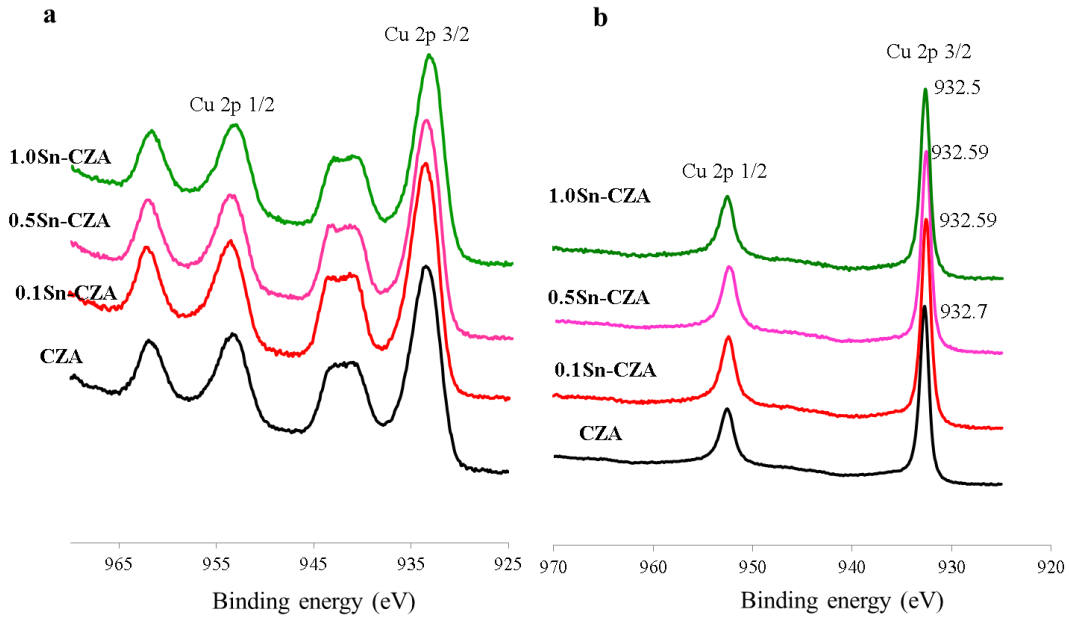

Figure. 6-4. XPS spectra (Cu 2p region) of the parent and Sn promoted CuO-ZnO-Al_2O_3 catalysts before (a) and after reduction (b).

For better clarity, the Sn 3d5/2 XPS spectra have been analyzed before and after reduction of the catalysts. The spectra recorded over fresh catalyst (Figure. 6-5) show a peak about 486.5 eV which might be assigned to the oxidized tin (Sn IV or Sn II) [16]. A new peak appears at 485 eV after reduction which might be assigned to metallic tin. Thus, the XPS results suggest that tin is partially reduced to metallic state. However, the relative amount of metallic tin seems to be significantly smaller in comparison with residual tin oxide species and does not depend on the amount of tin in the sample (Figure. 6-5). The XPS results have been supported by in situ XRD and XANES data of the parent CZA and promoted 1Sn-CZA catalysts.

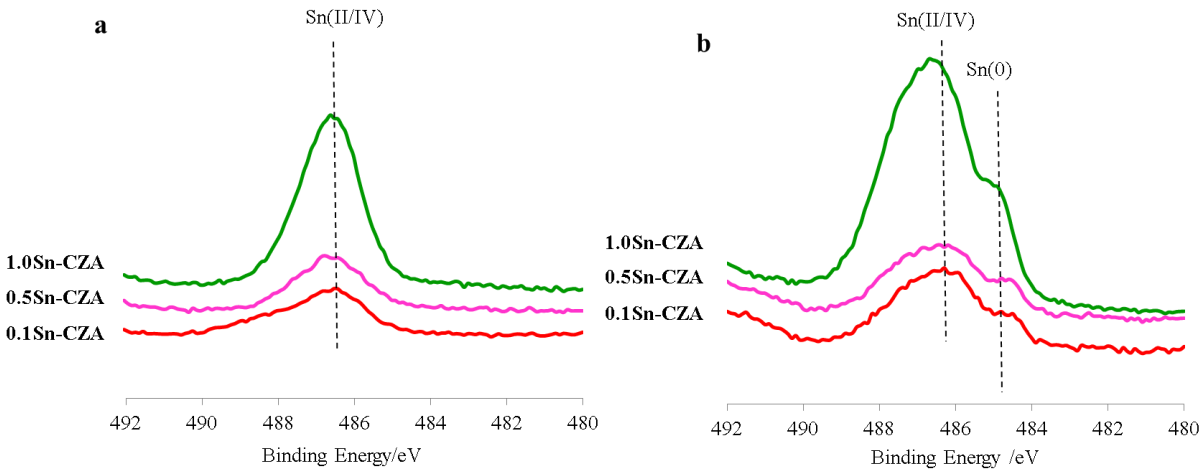

Figure. 6-5. XPS spectra (Sn 3d5/2 region) of the Sn promoted CuO-ZnO-Al_2O_3 catalysts before (a) and after reduction (b).

The in-situ XRD patterns of calcined and reduced catalysts are shown in Figure. 6-6. The XRD patterns of the calcined catalyst are indicative of the presence of CuO and ZnO oxides over both catalysts without effect of tin on XRD patterns. The size of CuO crystallites calculated using the Scherrer equation was about 8 nm for both samples. The in-situ XRD suggests that CuO reduction into Cu is complete at 290 °C with formation of similar Cu crystallites over both catalysts with sizes about 12 nm.

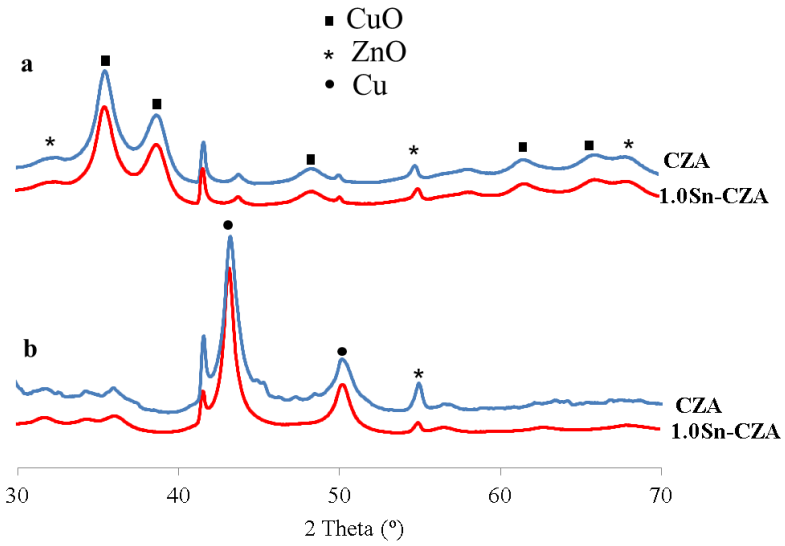

Figure. 6-6. In situ XRD patterns of CZA or 1.0Sn-CZA measured at before (a) and after (b) reduction in hydrogen.

Figure. 6-7 shows the in-situ Cu K-edge XANES spectra of the non-promoted and tin-promoted samples in comparison with reference materials before and after reduction. CuO sample shows the pre-edge absorption at 8984 eV ascribed to a dipole forbidden transition

from 1s to 3d orbital in Cu^{2+} [17]. The oxidized CZA and 1.0Sn-CZA catalysts exhibit XANES spectra similar to that of CuO. However, the pre-edge adsorption over CZA catalysts becomes less obvious in comparison with the reference CuO catalyst. This fact might be explained by smaller sizes of CuO crystallites in CZA catalysts with incorporation of Cu^{2+} into the $ZnO\text{-}Al_2O_3$ framework with different coordination environment and electronic states in comparison with CuO leading to distortion of octahedral coordination [18]. Indeed, TEM analysis of CZA catalyst indicates the high dispersion of Cu in $ZnO\text{-}Al_2O_3$ matrix [19].

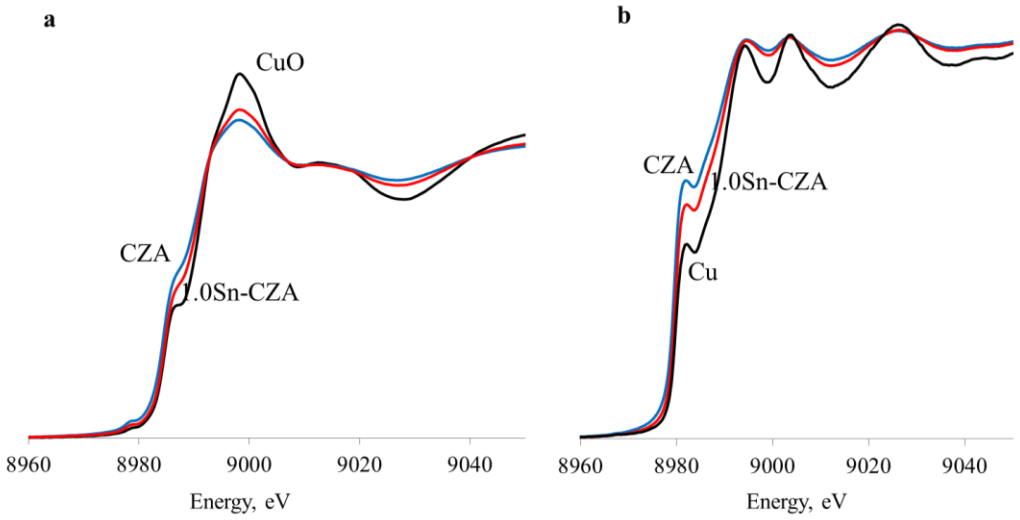

Figure. 6-7. In situ XANES spectra of catalysts CZA and 1.0Sn-CZA before (a) and after reduction (b) in hydrogen in comparison with CuO and Cu foil reference compounds.

Figure. 6-7b presents the Cu K-edge spectra of in-situ reduced catalysts in comparison with Cu foil. Cu foil shows the absorption edge at 8979 eV and two resonance features at 8993 and 9003 eV. The absorption at the edge at 8979 eV corresponds to 1s to 4p electronic transitions [20]. The XANES shapes for reduced samples CZA and 1.0Sn-CZA are similar to reference foil indicating the presence of mainly metallic Cu in the sample at the reaction conditions. However, the intensity of edge absorption at 8979 eV over reference copper foil is significantly lower than over CZA and 1.0Sn-CZA. The intensity decreases in the order CZA > 1.0Sn–CZA > Cu which can be attributed to the increase in the filling of unoccupied Cu 4p orbital [15]. In the case of CZA sample reduced Cu should be positively charged due to the strong interaction with oxides of $ZnO\text{-}Al_2O_3$ matrix in comparison with the reference Cu foil. The presence of Sn might lead to partial donation of electrons to 4p orbital with decrease of the transition from 1s to 4p.

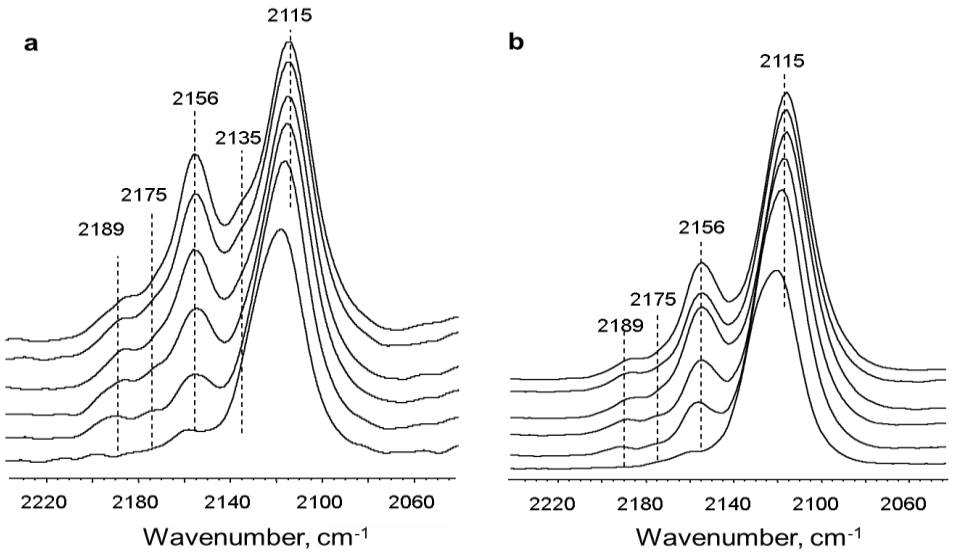

Figure. 6-8. FTIR spectra of low temperature CO adsorption over parent (a) and Sn promoted catalyst 1.0Sn-CZA (b).

FTIR spectroscopy yields valuable information about the interaction of Cu surface sites with adsorbed CO. Figure. 6-8 shows IR spectra measured during CO adsorption at low temperature over CZA and 1.0Sn-CZA catalysts after reduction with increase in CO pressure in the case of reduced catalysts. At low CO coverage both samples reveal the most intense band centered at 2120 cm^{-1}. The position of these peaks shifts to 2115 cm^{-1} with increase in CO pressure. This intense band has been earlier attributed over similar catalyst to the adsorption of CO over Cu^{+} cations or small clusters of metallic copper [21] and [22]. This band was very intense over both oxidized catalysts (not shown). Thus, taking also into account high stability of this carbonyl [23] most probably this band might be assigned to Cu^{+}-CO species. The shift of the band with increase of CO coverage has been explained by conversion between Cu^{+}–CO species and $Cu^{+}(CO)_2$ dicarbonyls [23]. CO adsorption over Cu^{+} species is significantly lower over tin promoted sample. Although, Cu^{+} species have not been observed by "bulk methods" like XRD and XANES, small amounts of Cu^{+} were identified in the catalysts from FTIR analysis of the bands of adsorbed of CO. Further increase in CO coverage leads to appearance of the bands at 2189, 2175 and 2156 cm^{-1}. The first two weak bands correspond to the vibrations of CO adsorbed over Lewis acid sites, Al^{3+} and Zn^{2+}, respectively [22]. The band at 2156 cm^{-1} is typical for the vibrations of hydrogen bonded CO, in particular, bonded with hydroxyl groups [21]. This is result of CO adsorption over hydroxyl groups of the $ZnO–Al_2O_3$ matrix and silanol groups of silica which has been used for dissolution of highly absorbing IR light Cu samples. Interestingly, the spectrum of

the parent reduced catalyst shows a shoulder at 2135 cm^{-1} which might be attributed to the presence of more positively charged cationic copper species. The band at 2135 cm^{-1} has been observed earlier during CO adsorption over Cu^{+} species in ion exchange position of zeolite ZSM-5 [24]. Isolated Cu^{+} species in zeolite should be more positively charged in comparison with Cu^{+} stabilized by $ZnO–Al_2O_3$ matrix. Note that this feature is absent in the FTIR spectra of CO adsorbed over the promoted catalysts.

To conclude, promotion of the CZA catalyst by tin leads to modification of the properties of both cationic and metallic copper species. Tin promotion leads to the decrease of ionic copper fraction (Cu^{+} and Cu^{2+}) in the reduced catalysts due to the strong interaction between copper and tin in the catalyst. At the same time, tin inhibits reduction of copper, decreases the surface area of metallic copper probably by formation Cu-Sn alloys and increases the electronic density on the metal.

6.2.2 DME synthesis and WGSR paths in the unpromoted and tin-promoted catalysts

The catalytic activities and selectivities in DME synthesis of the composite CZA/HZSM-5(45) and Sn-CZA/HZSM-5(45) catalysts are shown in Figures. 6-9, 6-10, 6-11 and Figure 6-12. The carbon monoxide conversions and selectivities are strongly affected by the presence of tin in CZA. The conversion decreases as a function of tin content in the catalysts and follows the following order (Figure. 6-9): CZA/HZSM-5 ≈ 0.1Sn-CZA/HZSM-5 > 0.2Sn－CZA/HZSM-5 > 0.5Sn－CZA/HZSM-5 > 1.0Sn－CZA/HZSM-5.

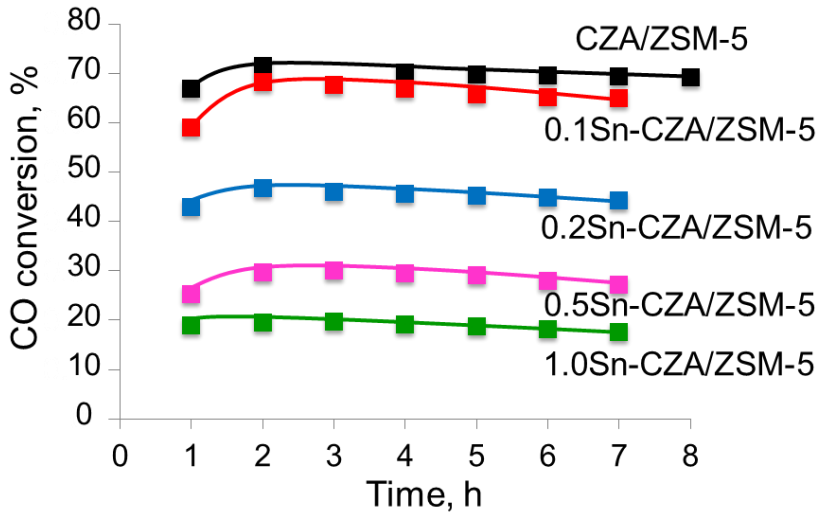

Figure. 6-9. CO conversion in time during DME synthesis over hybrid catalysts CZA/ZSM-5(45) with parent CZA and promoted by Sn. Conditions: T= 260 °C, P=20 bar, H_2 /CO=2, GHSV=3600 ml/(h•g_{cat}）

The observed phenomena might be explained by the lower activity of the formed Cu-Sn nanoparticles containing tin species in comparison with copper species in the parent CZA (Table 6-1). The decrease in the activity of the noble metals after doping by tin has been explained earlier by blocking of the surface sites by ligand effect and electronic effects [16]. The effect of change of catalytic performance during hydrogenation/dehydrogenation reactions by tin promotion has been explained by several authors by electronic interaction between tin and metal [25] and [26]. In the case of Pt the influence of tin as promoter has been assigned to donation of electrons to 5d band leading to deactivation of the active sites [25]. In the case of copper it should result in decrease of the participation of 3d electrons in bonding with exclusion of these sites from interaction with CO. The effect of tin as deactivating agent with inhibition of hydrogenolysis has been found to be similar to deactivation by coke deposition [26]. In both cases coke and tin selectively deactivated unselective Pt sites.

It is interesting to note (Figure. 6-9) that small amount of added Sn (0.1 %) almost does not affect the activity of the catalyst while the tin amount higher than 0.2 wt. % significantly reduces the catalytic activity. It indicates that Cu sites in the parent CZA samples might be not uniform. Indeed, FTIR spectra of adsorbed CO over in situ reduced CZA catalysts (Figure. 6-8) indicated the presence of Cu^{+} species in addition to copper metallic phase observed by in situ XRD (Figure. 6-6) and XANES (Figure. 6-7).

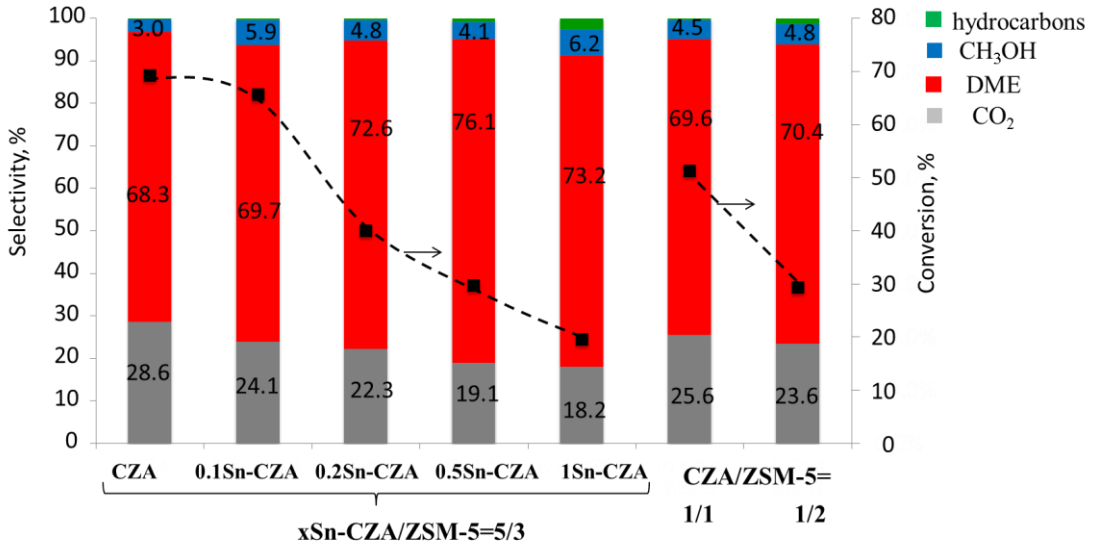

Figure. 6-10. Selectivity to main products during DME synthesis over hybrid catalyst CZA/zeolite with parent CZA and promoted by Sn with the weight ratio CZA to ZSM-5(45) equal to 5/3 and CZA to ZSM-5(45) equal to 1/1 and 1/2. Conditions: T= 260 °C, P=20 bar, H_2 /CO=2, SV=3600 ml/(h·g_{cat}）

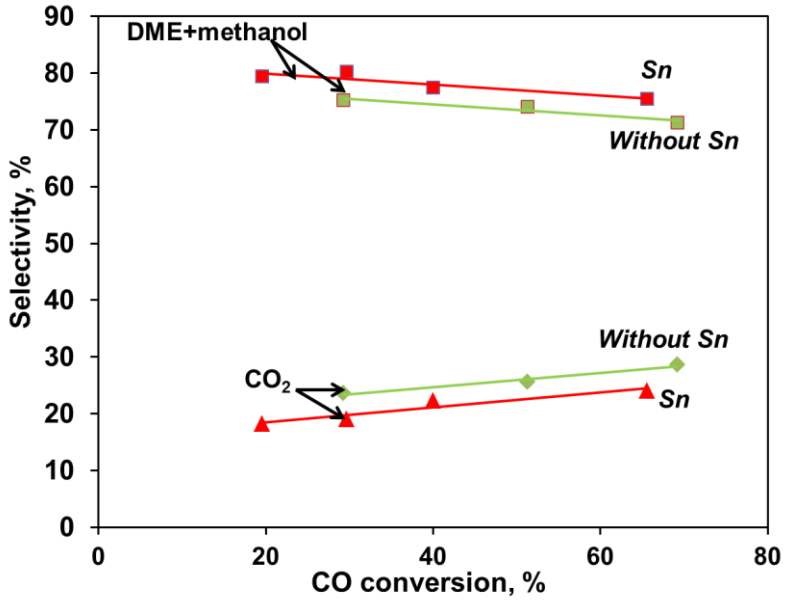

Figure. 6-11. Selectivity to DME+methanol and CO_2 over parent and tin promoted hybrid catalysts xSn-CZA/ZSM-5.

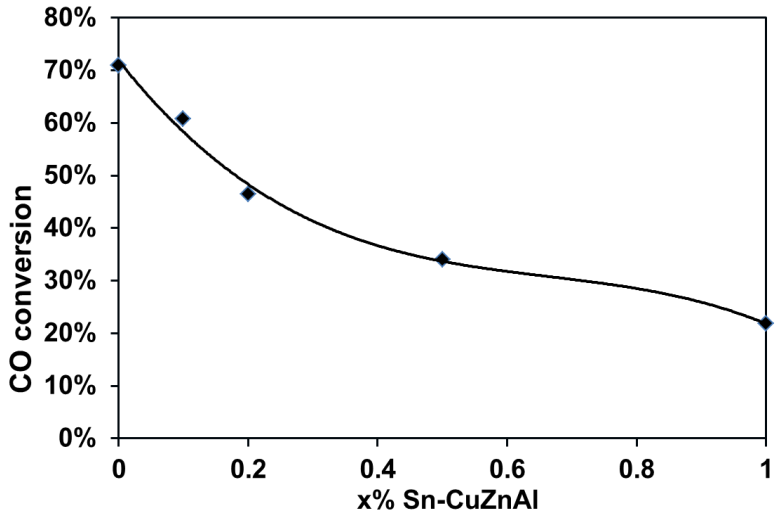

Figure. 6-12. CO conversion in WGS reaction depending on the Sn content in CZA catalysts. Reaction condition: P = 1 bar, T = 260 ^{o}C, GHSV=3600 ml/(g_{cat} h)

DME is the main product of the reaction with the selectivity in the range of 68-76 % (Figure. 6-10). The selectivity to methanol varies from 3 to 6 %. Methanol is the primary reaction product of DME synthesis. As expected for primary products, highest methanol selectivity is observed at low carbon monoxide conversions. Light hydrocarbons are produced with low selectivities (0.1-2.0 %). All the catalysts showed very significant selectivity to CO_2 which increases with carbon monoxide conversion. Carbon dioxide forms in WGSR. The ratio of DME to CO_2 selectivities over parent catalyst (2.3:1) is higher than

the theoretical ratio of 2:1. This suggests that part of water produced via methanol dehydration during DME synthesis does not participate in WGS reaction.

Higher tin content in the CZA catalyst results in the gradual increase in the selectivity to DME from 68 % over the parent CZA/ZSM-5 catalyst to 76 % over the tin promoted catalyst. Taking into account methanol, the combined selectivity to DME and methanol increases from 71 to 80 %. This effect is mainly the result of lower CO_2 selectivity which decreases from 28 to 18 %. The variation of the selectivity might be explained both by lower CO conversion in the tin-promoted catalysts and by the effect of tin on WGSR.

Tin was introduced by impregnation of the CZA catalyst. We assume that tin introduction selectively affects only the CZA catalyst. In order to further clarify the effect of tin on the DME selectivity, the tests have been conducted over the parent CZA/ZSM-5 catalytic systems with lower CZA content to simulate the lower activity of tin promoted Sn-CZA/ZSM-5. Figure 6-10 shows conversion of CO and selectivities over CZA/ZSM-5 with the ratio CZA/ZSM-5 in the catalyst equal to 5/3, 1/1 and 1/2. The conversion of CO decreases from 69.2 to 51.3 and 29.3 % as a function of CZA content in the bi-functional catalyst. Lower CO conversion coincides with the increase in DME selectivity from 68.3 to 69.6 and 70.4 %, respectively. Lower carbon monoxide conversion results in the lower CO2 selectivity similar to the tin promoted samples and might be explained by lower amounts of produced water in the system. Interestingly lower carbon dioxide and higher DME selectivities were observed at the similar conversions over the tin promoted catalysts compared to the parent catalyst (Figure. 6-10 and Figure. 6-11). Indeed, at the conversion of about 29 % over 0.5Sn-CZA/ZSM-5 and CZA/ZSM-5= 1/2 the selectivity to DME is 6 % higher over the tin promoted catalyst. The selectivity to CO_2 is lower by approximately 5 % over promoted systems in comparison with parent catalyst at the same conversions (Figure. 6-11). In the case of mild promotion (0.1 and 0.2 wt. % Sn) higher methanol selectivity is also observed which might be explained by higher water content in the reactor with its significant adsorption over acid sites of ZSM-5 which explains lower activity in dehydration of methanol to DME. The selectivity to hydrocarbons has been also slightly increased with higher amount of tin. This effect is due to the lower conversion of CO and might be observed also over CZA/ZSM-5 with higher zeolite fraction in the catalyst (Figure. 6-10).

One of the possible explanations of these observations can be related to the selective effect of tin addition on WGSR in comparison with CO hydrogenation to methanol. The most interesting effect in terms of the catalyst selectivity is observed over mildly promoted CZA catalysts (0.1Sn-CZA). Indeed, almost at the same conversion of CO the combined selectivity

to DME and methanol increases from 71 to 76 %.

Higher CO_2 and lower DME selectivities in the parent CZA/HZSM-5 catalyst might be explained by the presence of the sites in the CZA catalyst more active in WGS reaction in comparison with tin-promoted catalysts. Probably these are the $Cu^{\delta+}$ sites more positively charged in ZnO-Al_2O_3 matrix shown by FTIR (Figure. 6-8). Earlier investigations of the WGS reaction over Cu catalysts doped by oxides (ZrO_2, CeO_2) have shown that Cu sites interacting with O vacancy with easy redox Cu^{2+} to Cu^{+} pairs are responsible for high WGS activity [27] and [28]. The presence of tin might result in the preferably reduction of these Cu^{+} sites with formation of Cu-Sn alloy with increase of the selectivity to DME. This assumption is supported by the fact that the selectivity to CO_2 over promoted catalysts is always lower by 5 % in the whole conversion range in comparison with the un-promoted system (Figure. 6-11). This means that deactivation of most part of unselective sites take place already at low amount of added tin. Further increase in the amount of tin leads to the decrease in the fraction of the active surface metallic Cu and lower reaction rate in carbon monoxide hydrogenation (Table 6-1). To provide further insights into the effect of tin, the transformation of CO in the presence of water has been studied over the promoted catalysts. Figure. 6-12 shows CO conversion of versus tin content in the CZA catalysts. The main reaction products were CO_2 and H_2. The conversion of CO significantly decreases with the increase in Sn content. The presence of 0.1 wt. % of Sn results already in decrease in the conversion of CO from 71 to 60 %. The conversion drops to 23 % at higher tin content. Thus, indeed, the effect of tin over the CZA catalyst might be explained by lower rate of the WGS reaction. Small amounts of tin introduced to the CZA catalyst can principally deactivate the sites active in WGS reaction. Consequently lower CO_2 and higher DME selectivity are observed on the tin-promoted catalysts.

Most of previous research in the field of DME synthesis has addressed the catalyst promotion in order to decrease hydrocarbon selectivity. For example, promotion of zeolite by metal oxides (ZrO_2, MgO) resulted in increase in the selectivity to DME mainly due to suppression of hydrocarbons formation [29, 30]. The maximal selectivity to DME at the similar reaction conditions over CZA/ZSM-5 catalyst promoted by MgO was 64.5 % [29]. The neutralization of external acid sites of ZSM-5 performed in [19] significantly increased the stability of the catalyst with only slight increase of the selectivity to 69 % due to higher hydrophobicity of the catalyst and lower holdup of the water in the system. Application of zeolite-CZA capsule catalyst exhibited very high selectivity to DME due to suppression of further dehydration of DME to form alkane/alkene byproducts, although the activity of the

composite catalyst was very low [31]. It seems important to emphasize however those hydrocarbons are not the main side reaction products of carbon monoxide hydrogenation over bi-functional copper-zeolite catalysts with mild acidity. CO_2 is a major undesirable product which significantly reduces the carbon efficiency of the direct DME synthesis. Modification of the Cu based catalyst with tin provides new opportunities to increase the selectivity to DME by suppression of WGS.

6.3. Conclusion

The structure of copper species in Cu-Zn-Al catalyst has been shown to be significantly affected by the presence of tin as a promoter. TPR, XPS, in-situ XRD, in-situ XANES and FTIR measurements reveal the presence of the tin in reduced state and the presence of positively charged Cu^+ copper species in the parent catalyst. The presence of these copper species was indicated by FTIR.

The catalytic performance in direct DME synthesis from syngas of hybrid CZA/ZSM-5 depends on the amount of tin. An increase in the amount of the promoter results in the decrease in the catalyst activity which is accompanied by the increase of the DME selectivity. The presence of tin suppresses the WGS reaction and consequently reduces CO_2 production. The optimum amount of tin in the catalyst has been found to be 0.1 wt.%. At this tin content, almost no effect on the carbon monoxide hydrogenation rate was observed and the combined selectivity to DME and methanol increased by 5 % relative to the un-promoted catalyst.

6.4. References

[1] K. Sun, W. Lu, F. Qiu, S. Liu, X. Xu, Appl. Catal. A 252 (2003) 243-249.

[2] Z. Li, J. Li, Ch. Yang, J. Wu, J. Natur. Chem. 21 (2012) 360-365.

[3] X.-J. Tang, J.-H. Fei, Zh.-Y. Hou, X.-M. Zheng, H. Lou, Energ. Fuel 22 (2008) 2877-2884.

[4] J.-H. Fei, X.-J. Tang, Zh.-Y. Huo, H. Lou, X.-M. Zheng, Catal. Comm. 7 (2006) 827-831.

[5] M. Toba, S.-I. Tanaka, S.-I. Niwa, F. Mizukami, Z. Koppany, L. Guczi, K.-Y. Cheah, T.-S. Tang, Appl. Catal. A 2 (189) 243-250.

[6] R. Gavagnin, L. Biasetto, F. Pinna, G. Strukul, Appl. Catal. A 38 (2002) 91-99.

[7] S. Galvagno, Z. Poltarzewki, A. Donato, G. Neri, R. Pietropaolo, J. Mol. Catal. 35 (1986) 365-373.

[8] J.B. Ko, C.M. Bae, Y.S. Jung, D.H. Kim, Catal. Lett. 105 (2005) 157-161.

[9]. W.R.A.M. Robinson, J.C. Mol, Appl. Catal. 60 (1990) 73-86.

[10] P.D Zgolicz, V.I. Rodríguez, I.M.J. Vilella, S.R. de Miguel, O.A. Scelza, Appl. Catal. A 392 (2011) 208-217.

[11] W.L. Dai, Q. Sun, J.F. Deng, D.Wu, Y.H. Sun, Appl. Surf. Sci. 177 (2001) 172-179.

[12] P.H. Matter, D.J. Braden, U.S. Ozkan, J. Catal. 223 (2004) 340-351.

[13] L. Alejo, R. Lago, M.A. Pena, J.L.G. Fierro, Appl. Catal. A 162 (1997) 281-297.

[14] R. T. Figueiredo, A. Martinez-Arias, M. Lopez Granados, J. L. G. Fierro, J. Catal. 178 (1998) 146-152.

[15] J.H. Kim, S.M. Choi, S.H. Nam, M.H. Seo, S.H. Choi, W.B. Kim, Appl. Catal. B 82 (2008) 89-102.

[16] F. Coloma, A. Sepulveda-Escribano, J.L.G. Fierro, F. Rodrigueze-Reinoso, Appl. Catal. A 148 (1996) 63-80.

[17] E.B. Fox, S. Velu, M.H. Engelhard, Y.H. Chin, J.T. Miller, J. Kropf, C. S. Song, J. Catal. 260 (2008) 358-370.

[18] D. Gamarra, G. Munuera, A.B. Hungria, M. Fernandez-Garcia, J.C. Conesa, P. A. Midgley, X. Q. Wang , J. C. Hanson , J. A. Rodriguez , A. Martinez-Arias, J. Phys. Chem. C 111 (2007) 11026-11038.

[19] V.V. Ordomsky, M. Cai, V. Sushkevich, S. Moldovan, O. Ersen, C. Lancelot, V. Valtchev, A.Y. Khodakov, Appl. Catal. A 486 (2014) 266-275.

[20] Z. Sun, M. Meng, L. Zhang, Y. Zha, X. Zhou, Z. Jiang, S. Zhang, Y. Huang, Int.

J.Hydrogen Energy 37 (2012) 18860-18869.

[21] K.I. Hadjiivaniov, G.N. Vayssilov, Adv. Catal. 47 (2002) 307-511.

[22] G. Busca, U. Costantino, F. Marmottini, T. Montanari, P. Patrono, F. Pinzari, G. Ramis, Appl. Catal. A., 310 (2006) 70-78.

[23] K. Hadjiivanov, T. Tsoncheva, M. Dimitrov, C. Minchev, H. Knözinger, Appl. Catal. A, 241 (2003) 331.

[24] J. Szanyi, M.T. Paffett, J. Chem. Soc., Faraday Trans. 92(24) (1996) 5165-5175.

[25] G. Cocco, S. Enzo, J. Chem. Soc., Faraday Trans 81 (1985) 321.

[26] J. Völter, U. Kürschner, Appl. Catal. 8 (1983) 167.

[27] J.B. Ko, C.M. Bae, Y.S. Jung, D.H. Kim, Catal. Lett. 105 (2005) 157-161.

[28] K. Nishida, D. Li, Y. Zhan, T. Shishido, Y. Oumi, T. Sano, K. Takehira, Appl. Clay Sci, 44 (2009) 211-217.

[29] M. Dongsen, Y. Weimin, X. Jianchao, Zh. Bin, S. Qingying, Ch. Qingling, J. Catal. 230 (2005) 140-149.

[30] S.-H. Kang, J.W. Bae, K.-W. Jun, H.S. Potdar, Catal. Commun. 9 (2008) 2035-2039.

[31] G. Yang, N. Tsubaki, J. Shamoto, Y. Yoneyama,Y. Zhang, JACS 132 (2010) 8129-8136.

Charpter 7. General conclusions and perspectives

7.1 General conclusions

In this work, we have studied direct synthesis of dimethyl etherfromsyngas. The hybrid catalysts for direct DME synthesis from syngas contain metal for methanol synthesis and acidic catalystfor methanol dehydration to DME. The conventional bi-functional catalyst Cu-ZnO-Al_2O_3/ZSM-5 has been studied for DME synthesis in chapter 3. The results showed that the catalytic conversion in the direct DME synthesis over bi-functional catalyst was significantly higher than in the two steps synthesis. However, there are two main drawbacks: formation of CO_2 by WGS reaction due to the presence of water and deactivation of the catalyst during DME synthesis. The next step of this work in chapter 4 has been devoted to investigation of the deactivation during direct DME synthesis and development of stable catalyst. We have shown the catalytic performance of hybrid Cu–ZnO–Al_2O_3/ZSM-5 depends on the zeolite crystallite size and Si/Al ratio. Higher concentration of the zeolite Brönsted acid sites and smaller zeolite crystallite sizes favour higher DME productivity. The deactivation of the catalyst was a combination of several factors: copper sintering, copper oxidation, migration and ion exchange with hydroxyl groups in zeolite pores because of the detrimental interaction of CZA with zeolite ZSM-5. The contact of CZA particles with surface acid sites of zeolite particles leads to formation of ionic copper with high mobility on the surface with migration of ionic Cu inside of the pores of zeolite and segregation into largeparticles of metallic Cu. Deactivationof the Brönsted acid sites located on the external surface by silylation procedure of HZSM-5 was used to suppress the segregation of the Cu ions with the protons of HZSM-5 resulting in significant improval of the catalyst stability.

The effects of crystal size on the performance of various synthesized ZSM-5 zeolites in the direct dimethyl ether (DME) synthesis from syngas reaction were described in Chapter 5.

In chapter 5, a series of hybrid catalysts for DME synthesis were prepared using ZSM-5 zeolites with different crystallite sizes. The catalyst containing smaller individual zeolite crystallites showed higher carbon monoxide conversion rates and higher DME productivities. The observed effects have been attributed to the methanol transport phenomena in bi-functional hybrid catalysts from the copper catalyst to the zeolite acid sites. The methanol transport is enhanced in the catalysts containing smaller zeolite crystallites, while the

presence of crystallite intergrown agglomerates resultes in diffusion limitations. The effect of the sizes of zeolite particles on the catalytic performance is even more significant than the effect of total concentration of zeolite Brönsted acid sites.

In addition, the deactivation rate was correlated with the concentration of Brönsted acid sites on the external surface of zeolite crystallites. Lower concentration of Brönsted sites on the zeolite external surface leads to a less rapid deactivation and better stability of copper-zeolite hybrid catalysts. Smaller zeolite ZSM-5 crystallite size and lower concentration of Brönsted acid sites on the zeolite external surface seem to be beneficial for the design of active, selective and stable hybrid CZA-ZSM-5 catalysts for direct DME synthesis from syngas.

CO_2 is the major byproduct in this reaction which principally forms by WGS over CZA catalyst in the presence of water. To enhance the DME selectivity and decrease the production of CO_2, it is imperative to neutralize the unselective active sites for WGS reaction while keeping the methanol synthesis sites intact.

Chapter 6 described the effect of tin additive on the CZA-ZSM-5 hybrid catalysts for the direct DME synthesis from syngas. The tin promoted CZA catalysts were prepared by impregnation of tin over CZA catalyst. An increase in the amount of the promoter results in the decrease in the catalytic activity which is accompanied by higher DME selectivity. The presence of tin suppresses the WGS reaction and consequently reduces CO_2 production due to the deactivation of positively charged Cu species active in WGS reaction. The optimum amount of tin in the catalyst has been found to be 0.1 wt.%. At this tin content, almost no effect of the promoter on the carbon monoxide hydrogenation rate was observed and the combined selectivity to DME and methanol increased by 5 % relative to the unpromoted catalyst.

7.2 Perspectives

Despite remarkable progress, some unsolved problems still remain in direct DME synthesis reaction. First of all, the selectivity to byproduct CO_2 is very high and the lifetime of the catalyst is short. Therefore, developing novel highly active, selective and stable bi-functional catalysts is currently indispensable for the direct DME synthesis. Two active components in the bi-functional catalysts should be finely dispersed and maintain a close contact, and consequently exhibit a high degree of ‘synergistic effect’, which facilitates the formation of DME. At the same time, these compounds should not interact with each other

due to deactivation of the catalyst in this case.

New composite for DME synthesis prepared by microemulsion method would be a good way to finely mix the two functional catalysts with close distance but without interaction with each other.

Increase of the selectivity to DME would be possible by isolation of Cu based catalyst from the contact with water or in-situ removal of water from the reaction zone by membrane or adsorption. It would result in significant increase of the selectivity to DME but with partial decrease of the activity due to less favorable thermodynamic conditions.

DME can be also directly produced from CO_2. The process for methanol synthesis from syngas is currently close to the industrial implementation. Development of bifunctional catalysts for direct DME synthesis from CO_2 could be also an important challenge to address in the near future.

About the author

Mengdie Cai was born in July 19, 1987 in Hubei Province, China. After obtaining her Bachelor degree in department of Chemical and Environmental Engineering from Yangtse University in 2009, she continued her study in department of Chemical Engineering at Sichuan University, Chengdu, under the guidance of Prof. Wei Chu. She obtained her master's degree in 2012. From 2012 to 2015, she worked as a PhD student in the laboratory of Unité de Catalyse et Chimie du Solide in Université de Lille 1, France, under the supervision of Prof Andrei Khodakov, and Dr Vitaly Ordomsky. Her PhD project, described in this thesis, focused on the development of hybrid catalysts for direct DME synthesis from syngas.

List of papers published during my thesis

Journal papers

1. V.V. Ordomsky, **M. Cai**, V. Sushkevich, S. Moldovan, O. Ersen, C. Lancelot, V. Valtchev, A.Y. Khodakov, The role of external acid sites of ZSM-5 in deactivation of hybrid CuZnAl/ZSM-5 catalyst for direct dimethyl ether synthesis from Syngas, **Applied Catalysis A: General**, 2014, 486: 266-275.
2. **M. Cai**, V Subramanian, V.V. Sushkevich, V.V Ordomsky, A.Y. Khodakov, Effect of Sn additives on the CuZnAl-HZSM-5 hybrid catalysts for the direct DME synthesis from syngas, **Applied Catalysis A: General,** 2015, 502: 370-379.
3. **M. Cai**, A. Palčić, V. Subramanian, S. Moldovan, O. Ersen, V. Valtchev, V.V. Ordomsky,and A. Y. Khodakov, Submitted, 2015

Conference papers:

Mengdie Cai, Vitaly Ordomsky, Vijayanand Subramanian, Ana Palcic, Valentin Valtchev, Simona Moldovan, Ovidiu Ersen, Andrei Khodakov, Influence of Zeolite Crystallite Size on the Activity and Stability of Hybrid Copper-Zeolite Catalysts for Direct Synthesis of Dimethyl Ether, **24th North American Catalysis Society Meeting**, Pittsburgh, PA, 2015, O-Tu-403-2, oral presentation

Mengdie Cai, Vitaly Ordomsky, Andrei Khodakov, Development of stable hybrid catalyst CuZnAl/ZSM-5 catalyst for Dimethyl ether synthesis from syngas, **Groupe d'étude en catalyse (GECat 2014)** 2014, France, OIII-13, oral presentation

Acknowledgement

I am so grateful to all the people, whose assistance was indispensable to the completion of this research project.

First, I would like to express my sincere gratitude to my supervisors, Dr. Andrei Khodakov and Dr.Vitaly Ordomsky, for their guidance, kindness and understanding during my PhD study and research, they were always ready for helping me out and providing instruction on the direction of my research. More importantly, I am deeply affected by their scientific method and attitude. It's a great honor to be one of their students.

I would especially like to acknowledge the collaboration with Prof. Ovidiu Ersen, and Dr. Simona Moldovan in IPCMS- CNRS, who performed the TEM investigations presented in this thesis; Prof. Valentin Valtchev, and Dr. Ana PALCIC in LCS for the supply of synthesized zeolite for catalytic tests and the aid in analysis of zeolites, and Prof Cuong Pham-Huu, in ICPEES for discussion during the whole project.

My special thanks to Dr. Vijayanand Subramanian for his help, valuable discussions and advice both academically and personally during the course of my PhD research.

Many thanks to the "Unité de catalyse et de chimie du solide" (UCCS), USTL, Ecole Centrale de Lille and Hall Pilote in France for affording a good scientific and experimental platform. It is impossible to complete the work without the help of the whole team. I would also like to thank Laurence. Burylo, Martine Trentesaux, Olivier. Gardoll, Gerard. Cambien, Wouter Van Beek, the following people for their help with conventional X-ray diffraction, X-photoelectron spectroscopy, TPR measurements, N_2 physisorption and synchrotron experiments, respectively.

I am grateful to the Chinese Scholarship Council (CSC) for the financial support during my stay in France and the other staffs from Education Service of Embassy of China for their kind attention.

Thanks to the colleagues and friends of UCCS for a memorable experience: Tong, Fangli, Mengnan, Chang, Kang, Cathy, Remy, Anita, Maha, Zhiping, Xiaofeng, Samadhan, Jorge, Guillaume, Majid, Marine, Mirella, Wenhao, Lei, Jie, Hao, Yaqian, Haiqin, Georgette, Sylvain, Jesus, and Helo.

Acknowledgement

Most importantly, I would like to thank my family: my parents and brother for their support, encouragement and love throughout my life.

Lastly, I offer my regards and blessings to all of those who supported me in many different ways during the period I spent working on this project.